Metamaterial design principles for mitigating low-frequency traffic-induced soil vibrations

Exploring spatial gradients and impact-based resonators for enhanced performance

Astrid Kleijnen

movares smart urban engineering

TU Delft

Metamaterial design principles for mitigating low-frequency traffic-induced soil vibrations

Exploring spatial gradients and impact-based resonators for enhanced performance

Astrid Kleijnen
5085365

Supervisors:

Dr. ir. A.B. (Andrei) Fărăgău	TU Delft, Chair
Dr. ir. K.N. (Karel) van Dalen	TU Delft, Committee Member
Prof. dr. A. (Andrei) Metrikine	TU Delft, Committee Member
Ir. A.J. (Arnold) Robbemont	Movares, Company Supervisor

July 18, 2025

Preface

With this thesis, my academic journey at TU Delft comes to an end. It has been an incredible experience, full of highs and only a few lows. I've had the opportunity to explore the field of Civil Engineering, create wonderful memories, and build lasting friendships. I look back on this time with nothing but positive feelings.

This thesis addressed a fascinating topic, and I never expected to enjoy doing research as much as I did. This would not have been possible without the invaluable support of my committee. I would like to sincerely thank Andrei Faragau, my daily supervisor, for always helping out, for thinking along with me, and for your constant positive encouragement.

My thanks also go to Arnold for making it possible to carry out this thesis in collaboration with a company, which gave me a more practical perspective on the project and allowed me to meet new people at Movares. I am also grateful to Karel van Dalen and Andrei Metrikine for their critical yet constructive feedback, their positivity, and their inspiring lectures, which sparked and sustained my interest in the dynamics track.

Thank you all for making this such a rewarding journey.

Summary

As rail and traffic travel increase, often intertwining with urban areas, infrastructure and buildings face growing challenges from ground-borne vibrations. Traditional mitigation methods, using heavy masses or stiff trenches, often struggle with low frequencies due to their large wavelengths. This report investigates a novel approach: the use of metamaterials. In this study, the metamaterial consists of mass-spring systems with a small amount of viscous damping. Through local resonance, these metamaterials can absorb low-frequency propagating waves using relatively small masses. This research explores the behavior of various metawedges to identify the most effective design and to develop relevant design criteria. These criteria simplify the derivation of metamaterial parameters, offering a solid foundation for a metawedge design. Additionally, it investigates the potential for increased energy dissipation when using an impact-based resonator. Our research provides a thorough analysis of different metawedges, enabling quicker future design iterations. Furthermore, a new approach for additional energy dissipation is investigated to determine its feasibility.

This research focuses on a target frequency of 10 Hz, characteristic of vibrations in soil generated by trains and traffic. For an initial analysis, three metawedge types – uniform, wave conversion, and rainbow trapping – were examined with different configurations at this target excitation frequency. The most effective configuration of each metawedge was then tested across various frequencies. This evaluation concluded that the wave conversion metawedge offers the most effective wave mitigation at the surface. However, the rainbow trapping metawedge has a better impact on the surrounding environment because it focuses on energy dissipation instead of redirection.

The analysis of the most effective metawedge yielded several design criteria for its parameters. The first criterion is that the exact spacing of the resonators is not critical, as long as they are positioned relative to the wavelength and enable local resonance. Thus, the metawedge can be made as compact as possible. A second criterion states that low frequencies are inherently more challenging to mitigate than higher ones. Assuming a linear gradient between the eigenfrequencies of the resonators, this difference should be smaller when targeting a lower frequency range. The specific range of eigenfrequencies depends on the target frequency and the number of resonators present. This relationship is captured by the relative resonator bandwidth ($RRBN$):

$$0.025 < RRBN = \frac{f_{high} - f_{low}}{f_{center} \cdot N} < 0.030 \tag{1}$$

This formula operates on the premise that the targeted frequency range should be maximized. Increasing N will result in greater dissipation through viscous damping. The third design criterion illustrates the effect of different masses on the metawedge's performance.

Understanding that higher frequencies are generally easier to mitigate, this research further investigates a method to enhance resonator efficiency using an impact-based resonator. This thesis examines enhanced viscous damping due to impact. When impact occurs, various frequencies are excited. Viscous damping, being frequency-dependent, is more effective at absorbing energy from higher frequencies. This principle is confirmed through a 2-degree-of-freedom system, on which a parametric study has also been performed. In addition to energy dissipation through viscous damping, the soil more rapidly dampens higher frequencies, further reducing energy. However, these expectations are not confirmed by numerical simulations of a metawedge employing impact-based resonators on a soil domain. In fact, this mitigation strategy leads to an amplified response at the receiver. This counterintuitive outcome demands further analysis to explain the discrepancy between expectations and results, as well as to optimize the impact-based resonator design.

Contents

1 Introduction

With rising city populations and increasing globalization [10], both car use and the more sustainable option of trains have grown. Ongoing developments in railways and highways lead to increased speed and usage [14], significantly contributing to ground-borne vibrations. However, as cities expand and urban development accelerates, tackling the problem of ground-borne vibrations becomes ever more pressing. These vibrations can lead to discomfort and dissatisfaction among residents [19], and in some cases, may even cause structural damage to surrounding buildings and infrastructure. Therefore, mitigating these vibrations is essential for a sustainable and healthy built environment.

Conventional methods for mitigating ground-borne vibrations include constructing stiff in-filled trenches to create barriers. These trenches rely on their mass to block or dissipate vibrations, which can be effective for higher frequencies, but they frequently prove inadequate at mitigating lower frequencies, a common issue stemming from insufficient mass or poor damping properties [1], [2]. Another approach involves using vibration isolation pads or mats made from materials like rubber or elastomers, which are placed beneath railway tracks or roads. While these pads can reduce the transmission of vibrations, their effectiveness diminishes at very low frequencies, where energy absorption becomes less efficient.

An alternative and potentially more effective solution involves employing metamaterials [13]. These materials, when designed in the shape of a metawedge, leverage their unique properties and complex geometry to target and mitigate specific frequencies, which may also include the low frequencies. The metamaterial consists of multiple resonators with specific damping and stiffness coefficients [18], allowing it to perform beyond the limitations of conventional strategies.

This thesis will examine and take into account three types of metawedges and evaluate their potential for mitigating ground-borne vibrations.

The first method utilizes a metamaterial in which all resonators share identical parameters, making it highly effective at mitigating a specific frequency since all resonators resonate simultaneously. This configuration is known as the uniform metawedge.

The second method leverages the phenomenon of elastic rainbow trapping, where vibrations are confined and attenuated between resonators of varying properties within the metawedge. This approach is particularly effective in designs that employ the classic metawedge.

The third method addresses ground vibrations through wave-mode conversion, where incoming Rayleigh waves are accelerated by the metamaterial, causing them to transform into body waves that are redirected into the ground. This mechanism is predominantly observed when an inverse metawedge is implemented.

The effectiveness of metawedges relies on the specific tuning of their internal mass-spring systems. These systems work best when vibrated at their natural frequency. However, this frequency dependence means they can only block a limited number of vibrations. Introducing nonlinearity to the resonator could expand this range [9], as it would cause the resonator's behavior to depend on the vibration's strength instead of its frequency.

1.1 Literature review

Some research has been conducted on using metawedges to mitigate ground-borne vibrations. Alessandro Bracci [1] investigated conventional approaches, such as stiff trenches, for vibration reduction. He also modelled a metawedge design, demonstrating how it could transform Rayleigh waves into body waves.

To gain a deeper understanding of metamaterials, Nicolás Contreras [5] provides an accessible

review. Local resonant metamaterials rely on mass-spring systems that resonate at the frequency of incoming vibrations, creating band gaps. These metamaterials aim to achieve negative effective mass and stiffness values, leading to band gaps. The nonzero imaginary parts of the dispersion curve define the boundaries of these band gaps.

Sjoerd van Gaal [13] investigated the fundamental physics of metamaterials, particularly their behavior when modeled as part of an Euler-Bernoulli beam system. His research analyzed three types of metawedges: uniform, classic, and inverse. The classic metawedge induces "elastic rainbow trapping," where the phase velocity decreases, shortening the wavelength and trapping waves between resonators. The inverse metawedge facilitates "wave-mode conversion," increasing phase velocity, elongating wavelength, and transforming surface waves into body waves. Van Gaal also conducted a 2.5D study on wave behavior at low frequencies and small incidence angles.

A promising avenue for mitigating problematic low-frequency vibrations lies in the use of metamaterials equipped with a nonlinear softening spring. The fundamental advantage of a softening spring is that its stiffness effectively reduces with increasing displacement. This nonlinearity fundamentally alters the system's dynamics: rather than possessing a single, fixed natural frequency, the system's resonant behavior becomes dependent on the amplitude of the vibration. This amplitude-dependent response allows the metamaterial to achieve a wider band of effective vibration mitigation, particularly beneficial for low frequencies which are often difficult to control with traditional linear systems. This innovative approach is exemplified by the work of J. Lou [23], who further enhanced this capability by integrating the nonlinear softening spring with an inerter, a component known for its ability to amplify inertial forces, thereby enabling the mitigation of even ultra-low frequencies.

The overview of A. Saeed [25] highlights the potential of impact-based resonators. It starts by outlining the drawbacks of traditional tuned-mass dampers, then proposes potential solutions to these issues. Two different impact-based resonator (IBR) designs are presented, and their respective advantages are detailed. The impact-based resonator is capable of mitigating a broad frequency band. For large-scale structures, the single-sided impact-based resonator is noted as the most efficient.

Building on the concept of targeted energy transfer, A. Vakakis's research [30] focuses on Nonlinear Energy Sinks (NES). This includes not only the study of nonlinear springs but also vibro-impact NES. A clear demonstration of an impact-based NES shows its effectiveness in mitigating high-amplitude energy.

1.2 Problem Statement

Metawedges have shown considerable potential in mitigating ground-borne vibrations, and research continues to seek ways to enhance their performance and broaden their applicability.

While metamaterials are well understood within the academic community, translating these concepts into real-world engineering practice requires a shift toward more pragmatic, application-driven research. Developing clear design criteria, performance benchmarks, and implementation guidelines is essential to make these materials accessible to practicing engineers. At present, however, no standardized guidelines exist to assist engineers in selecting and designing the key parameters of a metamaterial for civil engineering applications.

Next to that, the effectiveness of locally resonant metamaterials is fundamentally tied to the eigenfrequencies of their resonators, which limits the range of frequencies that can be attenuated. This highlights the need for innovative design approaches, such as graded, multi-resonator, or nonlinear configurations, to extend the operational bandwidth and make these materials more versatile for real-world vibration mitigation challenges.

1.3 Aim of the Thesis

The main goal of this project is to understand the mechanisms and evaluate the performance of the different metawedges. This knowledge will inform the development of more general design criteria for metawedges. These criteria aim to create metawedges that mitigate the broadest possible range of frequencies, while ensuring the metamaterial behaves as expected. The focus is on mitigating low-frequency vibrations, such as those from rail or traffic, with a target frequency of 10 Hz.

In addition to its main objective, this report explores the potential of a novel approach to metawedge resonator design. By introducing contact between the resonators, energy absorption efficiency is expected to improve significantly. This modification is anticipated to create a broader bandgap within the metamaterial by introducing an amplitude-dependent response alongside the typical frequency dependence. Subsequently, this innovative design will be compared to the established 'traditional' metawedges, which operate solely based on frequency dependence.

Local resonance is utilized in this research because, unlike Bragg scattering, it does not rely on the targeted wavelength. In Bragg scattering-based designs, the metamaterial size is directly dependent on the wavelength of the target frequency. Since low frequencies correspond to large wavelengths, a Bragg scattering-based metamaterial would require substantial dimensions. By employing local resonance, the overall size of the metamaterial can be significantly reduced while maintaining effective vibration mitigation.

Passive control is preferred over active control in civil engineering applications due to the large scale of these systems and their exposure to environmental conditions. Active control mechanisms often fail over time due to external influences, whereas passive control provides a more robust and reliable solution that is easier to implement in long-term applications.

Ground vibrations can originate from various sources, but this research will specifically focus on traffic-induced vibrations, such as those generated by railways and road traffic.

This project aims to answer the following research questions. To get an understanding of the problem, an analytical model will be developed and analyzed.

1. **Which metawedge design provides the most effective solution for mitigating ground-borne vibrations?**

   This question is further explored through the following subquestion:

   - How do variations in mass, damping, and stiffness of the resonators influence vibration mitigation performance?

   These questions are addressed by conducting a numerical analysis in Abaqus, which is validated against an analytical model. The numerical model offers additional insights beyond the analytical model. Furthermore, the most efficient metawedge design will be identified for use in the subsequent phases of the project.

2. **How do design parameters such as target frequency, resonator spacing, number of resonators and resonator mass influence the effectiveness of metamaterials in mitigating ground-borne vibrations? Can these components be captured in design criteria?**

   The design criteria are based on statements derived from insights gained by addressing the first research question. These criteria are validated through numerical analysis.

3. **What is the effect of an impact-based resonator and how does incorporating an impact-based resonator influence the performance of a metawedge for wave mitigation?**

The impact-based resonator is first analyzed using a two-degree-of-freedom system. Subsequently, multiple resonators are modelled in series within a soil domain. Together, these analyses evaluate the resonator's potential.

1.4 Thesis overview

This thesis is structured into several chapters, with each one building on the last. Chapter 2 covers the fundamental principles of metamaterials on a beam. Chapter 3 dives into various metawedge designs. Chapter 4 then introduces nonlinearity into a specific resonator design.

Chapter 2 is all about developing a beam model featuring a metamaterial. This model is solved semi-analytically to identify its bandgaps. Through this model, the impact of changes in mass, stiffness, and damping are explored. The use of inerters is also examined.

Chapter 3 starts by researching relevant target frequencies. Next, a metamaterial is modelled on a soil block to understand the distinct mechanisms of different metawedges. This newfound understanding of metawedges allows for the creation of design criteria, which capture the design of various parameters in different formulas. Finally, the design is tested in a case study, exciting the metamaterial with a real signal.

Chapter 4 starts the process of adding nonlinearity to the design to more effectively mitigate transient vibrations. This nonlinearity comes in the form of an impact-based damper. This damper is first analyzed in a simple design, then tested on a soil domain in series.

2 Analysis of parameter effects of metamaterial on shear beam

This chapter investigates the behavior of a metamaterial-based design leveraging local resonance, conducted on a shear beam. This theoretical study aims to examine how variations in model parameters influence the system's response.
The metamaterial is initially analysed on a beam before being studied in soil. Introducing soil complexities from the outset would hinder a clear analysis of parameter influences. In a shear beam, the propagating wave affects every node uniformly, making it ideal for research purposes, and the model is computationally efficient. A shear beam is selected over other beam types because its governing equation involves only a second spatial derivative instead of a fourth, which simplifies the analysis. Additionally, the shear beam allows vertical motion, making it well-suited for studying the behavior of the mass-spring systems.
The model consists of a shear beam supported by distributed springs and dashpots (k_s and c_s). This dispersive system simulates the soil. On top of the beam, continuously distributed mass-spring systems (m_m and k_m) represent the metamaterial.
Let $w_1(x,t)$ represent the downward displacement of the beam, and $w_2(x,t)$ the motion of the metamaterial. The beam is excited by a harmonic frequency $F(t)$, with an excitation frequency Ω.

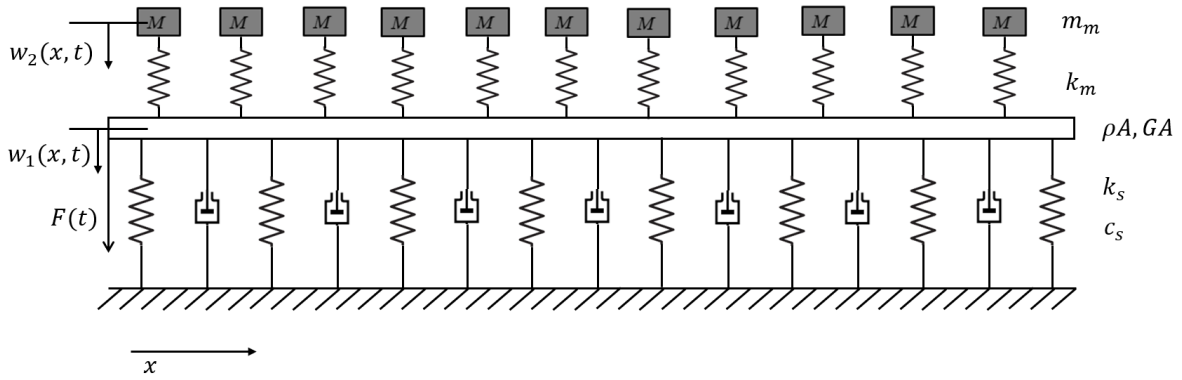

Figure 2.1: Schematic representation of a shear beam with metamaterial on top

The equations of motion are as follows:

$$\rho A\frac{\partial^2 w_1}{\partial t^2} - GA\frac{\partial^2 w_1}{\partial x^2} + c_s\frac{\partial w_1}{\partial t} + k_s w_1 = k_m(w_2 - w_1) \tag{2.1}$$

$$m_m\frac{\partial^2 w_2}{\partial t^2} + k_m(w_2 - w_1) = 0 \tag{2.2}$$

In Equation 2.1, ρ denotes the mass density of the beam, G is the shear modulus, and A is the cross-sectional area of the shear beam.

Assuming wave propagation, the solution is sought in the following form, where B_1 and B_2 are unknown constants, ω denotes the angular frequency (in rad/s), and k is the wavenumber (in rad/m):

$$w_1(x,t) = B_1 e^{i(\omega t - kx)} \tag{2.3}$$

$$w_2(x,t) = B_2 e^{i(\omega t - kx)} \tag{2.4}$$

The assumed solutions are substituted into the equations of motion. In the following solution, B_2 is expressed by B_1:

$$B_2 = \frac{k_m B_1}{-m_m \omega^2 + k_m} \tag{2.5}$$

Substituting this into the equation of motion for the shear beam:

$$-\rho A\omega^2 + GAk^2 + i\omega c_s + k_s = k_m \left(\frac{k_m}{-m_m \omega^2 + k_m} - 1 \right) \tag{2.6}$$

To simplify this equation (2.6), the term 'effective mass' is introduced. This term represents the beam's mass as perceived by the propagating wave. It's equation reads as follows:

$$m_{\text{eff}}(\omega) = -\rho A - \frac{k_m}{\omega^2} \left(\frac{k_m}{-m_m \omega^2 + k_m} - 1 \right) \tag{2.7}$$

By the introduction of the effective mass, the final dispersion curve can be written in a familiar form in the following equation:

$$m_{\text{eff}}(\omega)\omega^2 + GAk^2 + i\omega c_s + k_s = 0 \tag{2.8}$$

This equation can be used to derive the wavenumbers k.

$$k_1, k_2 = \pm \sqrt{\frac{-m_{eff}\omega^2 - i\omega c_s - k_s}{GA}} \tag{2.9}$$

By now, the only unknown is B_1, from which its value can be determined from the boundary condition at $x = 0$. The shear beam is excited here with a harmonic forcing $F = F_0 cos(\omega t)$.

$$GA\frac{dw_1}{dx} = F_0 Re(e^{i\omega t}) \tag{2.10}$$

Leading to the following solution of B_1:

$$B_1 = \frac{-F_0}{ikGA} \tag{2.11}$$

All unknowns are determined, enabling the calculation of the dispersion curve and the beam's response. This provides deeper insights into the beam's behavior.

2.1 Response of beam with metamaterial

The response of the shear beam is derived and now plotted using Python. The properties of the beam and metamaterial are presented in Table 2.1.

A clear way to determine whether waves will propagate through the medium or decay is by examining the dispersion curve, which shows the relationship between ω and k as expressed in Equation 2.8. The dispersion curve of the shear beam without the metamaterial is presented in Figure 2.2a, while the dispersion curve for the shear beam with metamaterial is illustrated in Figure 2.2b.

In these figures, two lines are shown: the blue line, representing the real part of the dispersion curve, corresponds to frequencies that can propagate through the beam, while the red dotted line, representing the imaginary part, corresponds to frequencies that decay within the material.

Symbol	Value	Units
ρ_A	100	$\mathrm{kg\,m^{-1}}$
GA	1×10^7	N
c_s	10	$\mathrm{N\,s\,m^{-1}}$
k_s	10000	$\mathrm{N\,m^{-1}}$
m_m	10	kg
k_m	100000	$\mathrm{N\,m^{-1}}$

Table 2.1: Parameters of the shear beam with metamaterial

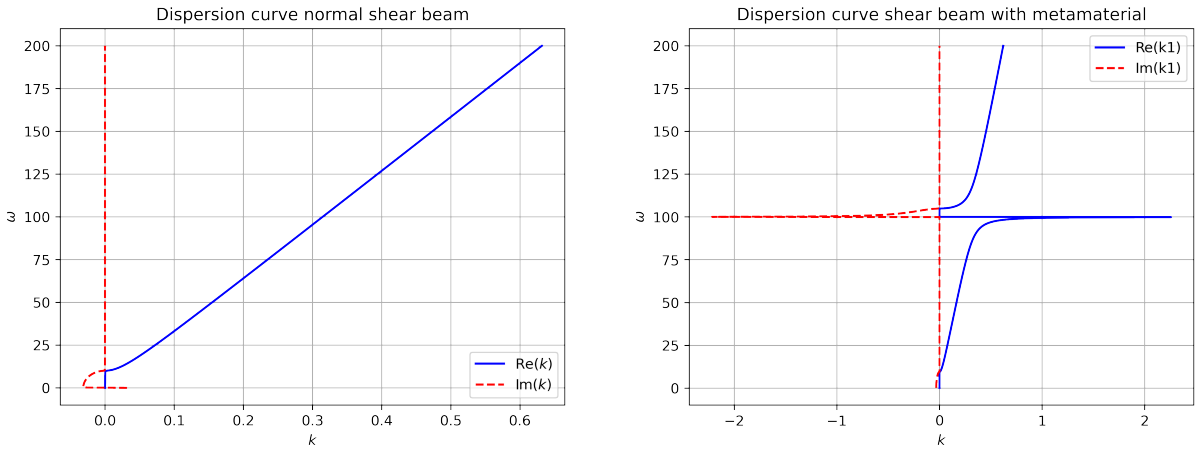

(a) Without metamaterial

(b) With metamaterial

Figure 2.2: Dispersion curves of the shear beam on elastic foundation with and without metamaterial. Re(k) is the real part of the wavenumber k, Im(k) is the imaginary part.

In the case of a shear beam without metamaterial, for excitation frequencies below $\omega = 10$ rad/s, the imaginary part is non-zero, indicating that these frequencies do not propagate. Consequently, the system exhibits a cut-off frequency at $\omega = 10$ rad/s. However, this behavior does not reflect reality, as the soil is modelled as a half-space and therefore should not possess a cut-off frequency.

The material properties of the resonators were selected so the metamaterial's resonance frequency is at $\omega = 100$ rad/s. In the case of the shear beam with metamaterial, this results in a stopband at that frequency on the dispersion curve, indicated by the imaginary part becoming very large and the real part approaching zero. Within this stopband, waves will not propagate.

Figure 2.3 displays snapshots of the shear beam's movement when excited at $\omega = 100$ rad/s (2.3a) and at $\omega = 100.1$ rad/s (2.3b). When the excitation frequency deviates only slightly, the metamaterial does not mitigate the propagating waves effectively. This shows the limitation of the locally-resonant metamaterial. Its performance is fully dependent on the eigenfrequency of the resonators. Mitigating a large amount of frequencies without having too much resonators is challenging due to this fundamental principle.

The wavenumber is given by the dispersion relation, $k = 0.312 - 0.000136i$. The wavelength can be computed using the following equation:

$$\lambda = \frac{2\pi}{|k|} = 20.14\,\mathrm{m} \tag{2.12}$$

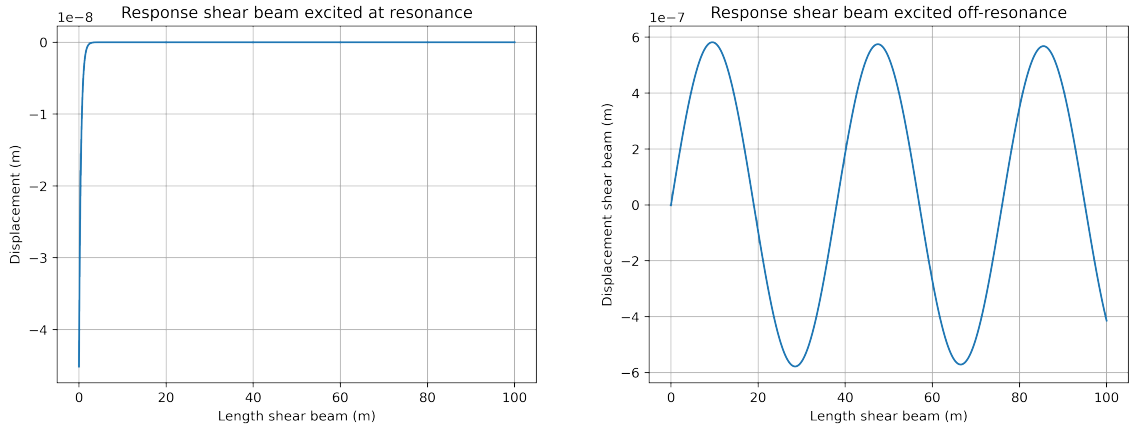

(a) Response system at excitation frequency $\omega = 100$ rad/s (resonance)

(b) Response system at excitation frequency $\omega = 100.1$ rad/s

Figure 2.3: Response of a shear beam on elastic foundation with metamaterial on top excited at a resonant and off-resonant frequency

This wavelength is observable in the plot of the propagating wave (Figure 2.3b). This wavelength is relatively long; therefore, selecting a locally resonant metamaterial over a Bragg scattering metamaterial is appropriate. Bragg scattering requires a structure spanning several wavelengths to be effective, whereas a locally resonant metamaterial operates efficiently even at sub-wavelength scales [8]. Within urban areas, the amount of space is a limiting factor.

Increasing both mass and stiffness while maintaining the same resonance frequency results in a wider bandgap, shifting towards higher frequencies. When the system is being excited with the resonance frequency of the resonators, Figure 2.4a shows the dispersion curve in the case when the mass of the resonators m_m is increased to 30 kg and Figure 2.4b shows the case where m_m is 3 kg. In the case of a large mass, the real part is 0 for a larger amount of frequencies than in the case of a small mass.

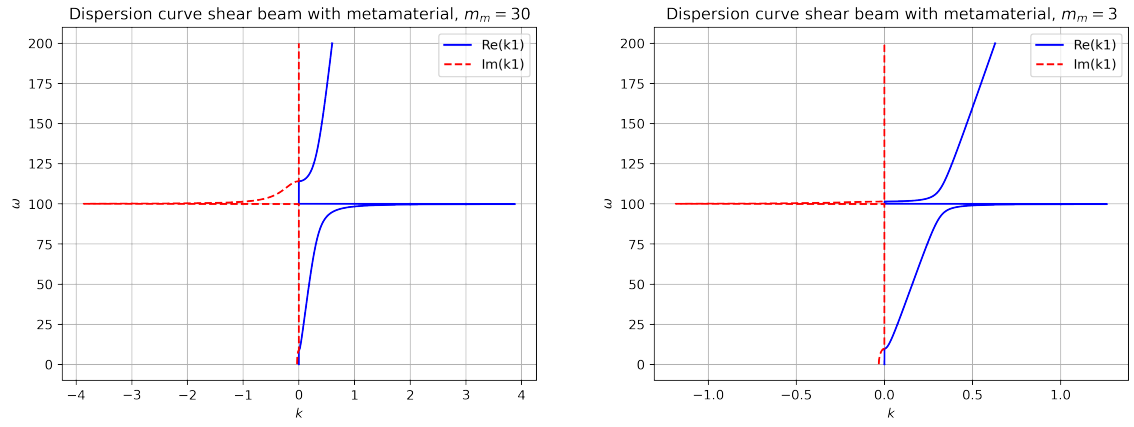

(a) $m_m = 30$ kg

(b) $m_m = 3$ kg

Figure 2.4: Dispersion curve for different resonator's mass, having same eigenfrequency $\omega_n = 100$ rad/s.

2.2 Metamaterial with damping

Adding damping (c_m) to the metamaterial at the top of the beam changes the dispersion curve, as shown in Figure 2.5.

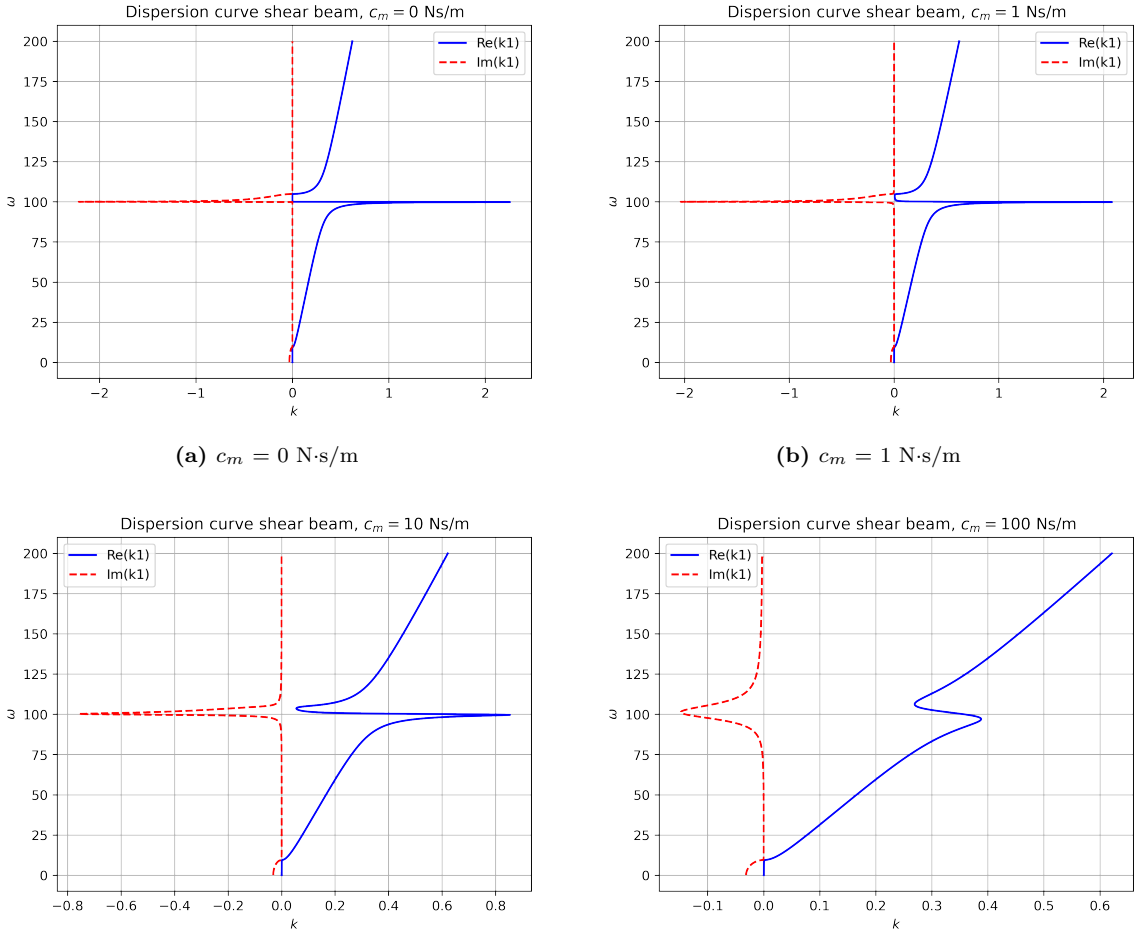

(a) $c_m = 0$ N·s/m **(b)** $c_m = 1$ N·s/m

(c) $c_m = 10$ N·s/m **(d)** $c_m = 100$ N·s/m

Figure 2.5: Dispersion curve with increasing viscous damping (c_m) of the metamaterial

Increasing the metamaterial's damping coefficient affects the resulting bandgap. The real part of the response remains nonzero across the bandgap, while the imaginary part broadens along the y-axis but decreases in amplitude. This suggests a trade-off: higher damping coefficients lead to a wider bandgap, but the metamaterial's overall performance diminishes, even at the targeted frequency. The bandgap itself expands towards both higher and lower frequencies.

2.3 Metamaterial with inerters

An inerter is a mechanical device that produces a force proportional to the relative acceleration between its two connected points [27]. Its behavior is characterized by the following relation:

$$F = b(\ddot{x}_1 - \ddot{x}_2) \tag{2.13}$$

Where F is the force generated by the inerter, b is the inertance (with units of kg), and $\ddot{x}_1$, $\ddot{x}_2$ are the accelerations of the two connected points.

Although inerters can be physically lightweight, they effectively behave as if they add mass to the system, this is a concept known as effective mass. This added dynamic inertia can significantly

alter the wave propagation characteristics of a metamaterial, in particular by shifting the location and width of bandgaps. The bandgap, which is a frequency range where wave propagation is suppressed, may move to lower frequencies as the effective inertia of the unit cell increases. This property is particularly useful in the design of low-frequency vibration isolation systems using mechanical metamaterials.

$$m_{\text{eff}} = \frac{b}{\omega^2} \tag{2.14}$$

$$\omega = \sqrt{\frac{k}{m}} \tag{2.15}$$

When the effective mass increases, the natural frequency of the resonator will decrease. When applying this to the shear beam in an analytical manner, the dispersion curve of a metamaterial with different values for the inertance can be found in Figure 2.6.

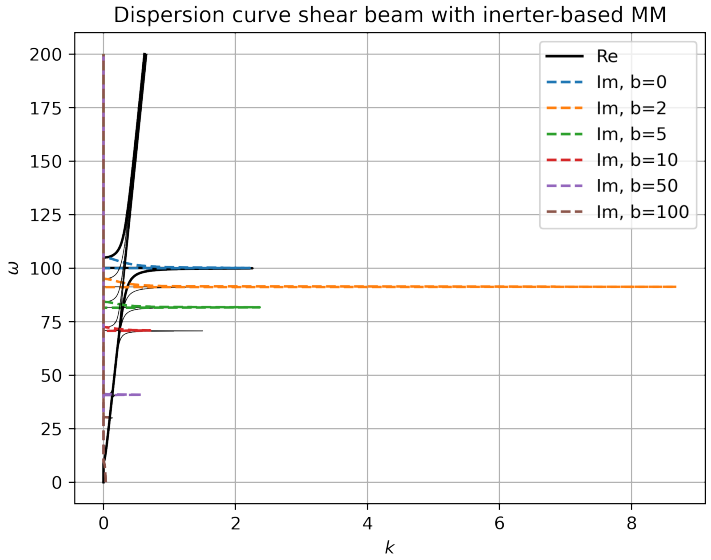

Figure 2.6: Dispersion curve of the shear beam with inerter-based metamaterial

The analytical model shows that increasing the inerter value b shifts the bandgap to lower frequencies. However, this comes with a trade-off: the bandgap becomes slightly narrower, and the attenuation performance diminishes as the imaginary part decreases. Notably, the imaginary part only increases when $b = 2$.

Incorporating inerters into the metamaterial design lowers the eigenfrequency. However, as the performance of the metamaterial deteriorates at lower eigenfrequencies, this trade-off does not yield a significant improvement. Therefore, the use of inerters is not pursued further in this research.

2.4 Interpreting different numerical analyses using Abaqus

The analytical results provide valuable insight into the theoretical behaviour of the metamaterial. However, to model more complex systems, the finite element software Abaqus will be employed. In this section, different Abaqus simulations are validated against the analytical results to ensure a correct interpretation of the numerical models. This validation builds confidence that more complex models can also be accurately analysed and interpreted using Abaqus.

In this case, a Timoshenko beam is modelled in 2D, since a shear beam is not possible within

Abaqus. As well as in the analytical model, there is a harmonic load applied at the start of the beam. The beam is supported by distributed springs and dashpots, and the metamaterial on top of the beam consists of multiple mass-spring systems with the same properties.

An implicit dynamic analysis and a steady-state analysis were conducted. The results from both analyses are discussed in the subsequent section.

2.4.1 Dynamic, Implicit analysis

With the implicit dynamic analysis, the problem is solved in the time domain. The time step used is 0.005 seconds and the total time is 2 seconds. The Nyquist frequency is equal to 628 rad/s. The acceleration data from a node before the metamaterial and a node after the metamaterial are taken and converted to the frequency domain.

The frequency-domain response for the node located behind the metamaterial is presented in Figure 2.7. The figure shows the frequency domain responses for two cases: the response with and without any transient vibrations.

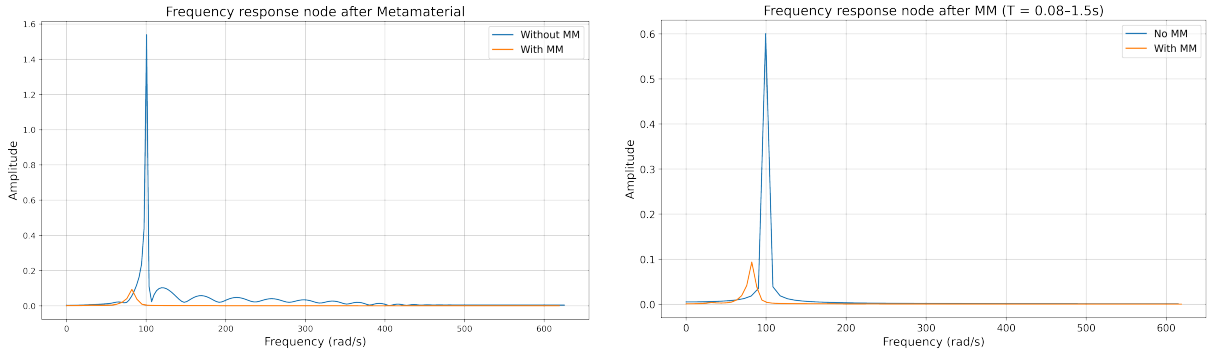

(a) With transient vibrations

(b) Without transient vibrations

Figure 2.7: Frequency domain from accelerations

The metamaterial in this case leads to a decrease in peak amplitude from 0.6 to 0.1. This is a decrease of 83 percent. When looking at the transient domain, this leads to an even higher decrease.

The response is not a perfect harmonic force at 100 rad/s, as multiple peaks are present in Figure 2.7a. This occurs due to the transient vibrations caused by the system's initial excitation. Data collection began at 0.8 seconds to largely remove these transient vibrations. Figure 2.7b shows the responses of both nodes, using data taken after 0.8 seconds. In these filtered results, peaks at frequencies other than 100 rad/s are much smaller.

In an analytical analysis of this model, a sharp peak would appear at 100 rad/s. However, because this is a numerical model with harmonic forcing applied over a finite time window, the peak is not confined exactly to 100 rad/s, it spreads slightly to neighbouring frequencies.

When looking at the same 10 nodes after the metamaterial ends, the result is plotted in Figure 2.8. It can be seen that the metamaterial leads to a wave mitigation of almost 90%. When the metamaterial is introduced, two other peaks become more prominent than before adding the metamaterial. While the metamaterial can damp certain frequencies, it can amplify other frequencies. Therefore, the design of the metamaterial must be carefully analysed prior to installation.

2.4.2 Steady-state analysis

Steady-state analysis provides an assessment of the beam's behavior across various excitation frequencies, excluding transient effects. This approach offers a straightforward method to evaluate

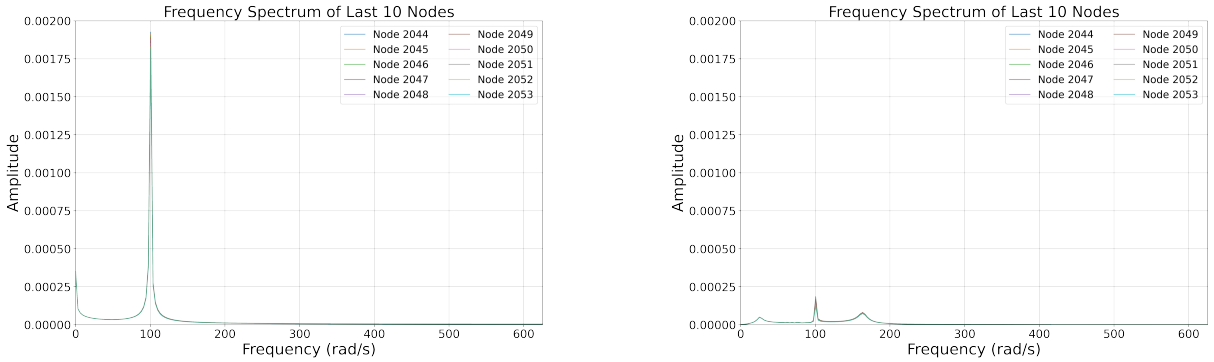

(a) Without metamaterial

(b) With metamaterial

Figure 2.8: Frequency response nodes after metamaterial

the metamaterial's effectiveness.

A stop band is anticipated at 100 rad/s, which corresponds to 15.9 Hz. Next to the bandgap where the acceleration is exactly 0 m/s^2, between 15.9 and 32 Hz, there is significant wave attenuation. The acceleration is very close to zero in this region.

Figure 2.9 illustrates the acceleration response of the node positioned beyond the metamaterial. The second subplot within this figure presents a binary representation: a value of 0 indicates the absence of acceleration, while a value of 1 represents the presence of some acceleration. The peak observed in the response occurs at a frequency of 15.9 Hz, which precisely aligns with the resonance frequency of the metamaterial.

While this metamaterial's theoretical bandgap is at $\omega = 15.9$ rad/s, significant wave attenuation occurs for excitation frequencies between 15.9 and 32 Hz. This is evident from the flat line in Figure 2.9a. Although the acceleration within this range is not perfectly zero, preventing it from being a pure bandgap, its relatively small magnitude allows it to be considered an effective bandgap.

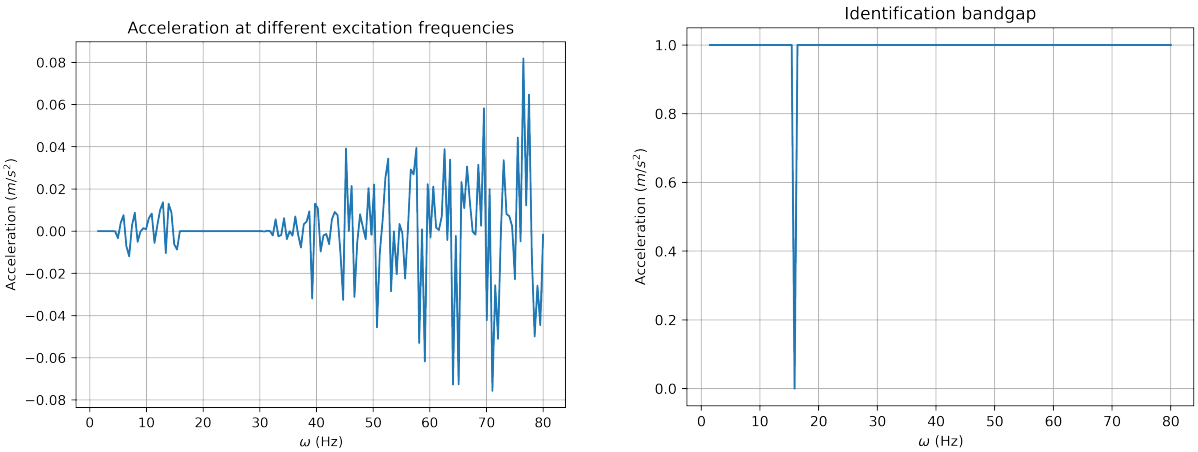

(a) Acceleration vs Frequency (Hz)

(b) Acceleration vs Frequency (Hz) in 0 or 1 block

Figure 2.9: Frequency response node after metamaterial

3 Metawedge on soil

This chapter explores various metawedge configurations, each engineered to attenuate multiple frequency components. The arrangement of resonators significantly influences the metamaterial's behavior and determines its effectiveness in wave propagation. Metawedges are specifically employed to enhance the bandgap of frequencies that a metamaterial can mitigate. They achieve this by arranging resonators with specific eigenfrequencies, which in turn alter wave properties, causing the propagating wave to change speed. This is used to mitigate the incoming waves.

The primary goal of this chapter is to analyze three distinct metawedge types, identifying which is most effective. This analysis leads to the development of clear design criteria, outlining the principles behind metawedge construction. Subsequently, these criteria are used for designing a metawedge in a case study.

The models discussed here are numerical simulations developed using the Abaqus software. Incorporating a soil layer into these models enhances their realism, providing a more accurate representation of physical behavior.

3.1 Target Frequency

To design the most efficient metawedge, the main frequency that needs to be mitigated must be identified. This is achieved by conducting a brief literature review on the most dominant frequencies originating from both traffic and railway tracks. All frequency spectra can be found in Appendix A.

3.1.1 Frequencies from Railway

The research conducted by Sinan Al Suhairy [28] involved various measurements of trains passing over soft soil in Sweden, leading to the development of frequency spectra. Different types of trains were tested, including freight trains, X2000, and Intercity trains, with measurements taken at various distances from the tracks. The results indicated that lower frequencies were more dominant at a distance, with peaks observed at 5 Hz and 12.5 Hz.

Xiaojing Sun [29] focused specifically on freight trains, as they contribute most significantly to lower frequencies that can travel far. This research identified two peaks: one below 25 Hz and another between 45 and 63 Hz. The second peak attenuated more rapidly than the first but remained observable at some distance.

Paul de Vos [31] examined the different causes of these frequencies and summarized them in a table. The findings suggest that the faster the moving load, the higher the frequencies generated.

Cao [3] investigated the measurement of vibrations around a high-speed railway viaduct. Measurements were taken at different distances from the viaduct, and various train speeds were tested. This study concluded that vibrations between 8 Hz and 50 Hz decay the slowest.

3.1.2 Frequencies from Traffic

Zdeněk Kaláb [17] conducted measurements capturing the frequencies generated by road traffic at two different locations. At both locations, the highest frequency observed was around 10 Hz.

Measurements taken by Zonneveld, which will be used in the Case Study in this report, also indicate that the dominant frequencies for road traffic are around 10 Hz.

Zhe Li [22] conducted research on the prediction of ground-borne vibrations from traffic. To validate the model with real data, he performed measurements at a distance of 100 meters from the source. These measurements revealed a clear frequency spectrum with a peak at 10 Hz.

3.1.3 Design Frequencies

Based on this literature review, the design frequency for this study is set at 10 Hz. This decision is justified by the consistent peak around 10 Hz for traffic in all cases. Although the frequency spectrum for trains is broader, every study reviewed indicates a peak around 12.5 Hz, which is close to 10 Hz. Additionally, vibrations between 8 Hz and 50 Hz decay the slowest and thus have the most significant environmental impact. In general, low frequencies are more challenging to mitigate, making it unnecessary to select a higher design frequency.

3.2 Modelling of soil domain

Understanding the mechanics of the metamaterial, specifically its ability to redirect and trap waves, hinges on a realistic model of the soil. This section will cover the modelling and validation process for a plain soil domain.

To simulate a model of a metamaterial on a soil domain, a 2D model is created in Abaqus. This model has properties described in Figure 3.1. A harmonic force is placed on the center of the surface of the soil to simulate the forcing due to trains or traffic passing by. The railway track or road can be imagined running perpendicular to the 2D model's surface.
The infinite characteristic of the soil is modelled through infinite boundaries at the outer planes of the soil which consist of plane strain solid continuum infinite elements (CINPE4). With these elements, infinite boundaries are approximated, so only a small part of the energy is reflected. In this way, a half-space is approached.

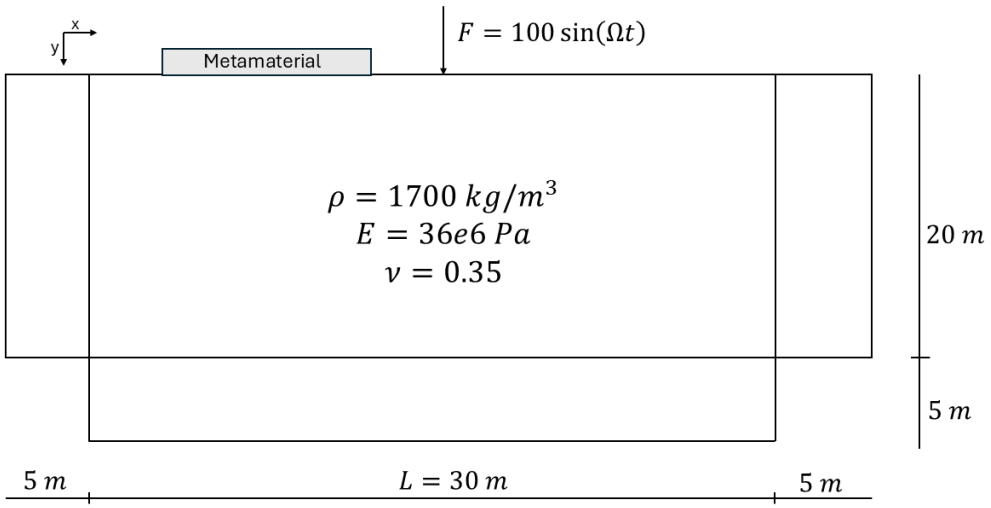

Figure 3.1: Schematic illustration of soil domain with metamaterial

Without a metamaterial, the harmonic forcing results in the displacement shown in Figure 3.2a. This is a snapshot of the displacement field at $t = 5$ seconds. The force is applied on the center of the model, and the figure displays the displacement of the surface to the left of the forcing location.

The mesh of the model consists of elements of 2.5 centimeters by 2.5 centimeters. The frequency spectrum of the last 40 surface nodes aligns with the 10 Hz excitation frequency, as depicted in Figure 3.2b.

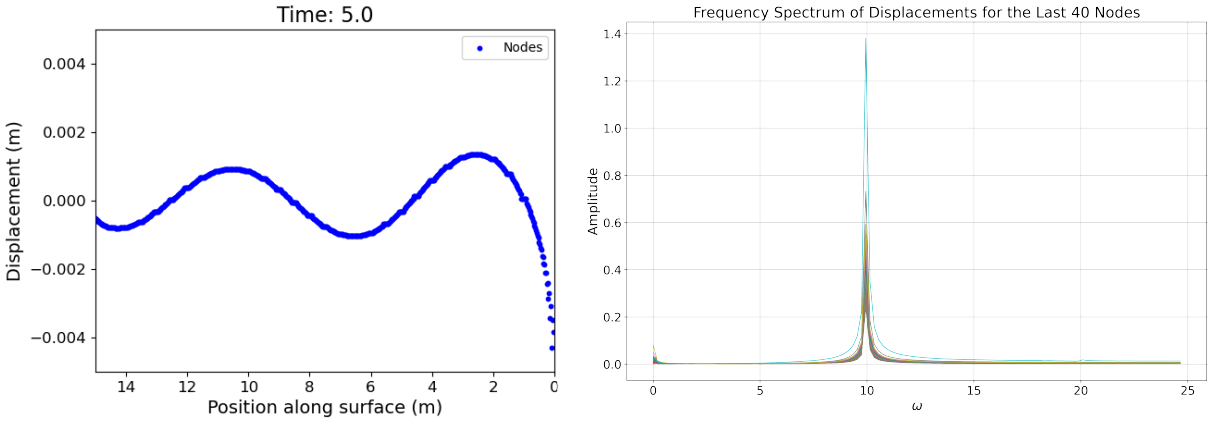

(a) Displacement response at $t = 5$ seconds

(b) Frequency response last 40 surface nodes

Figure 3.2: Response surface of soil domain without metamaterial

3.2.1 Validation of the soil domain

To validate whether the infinite boundary conditions for wave propagation are functioning correctly, the maximum amplitude of the soil is plotted.

If the soil truly had infinite boundaries, the maximum amplitude would exhibit a smooth and gradually decaying profile which follows this function [26]. u_z is the vertical displacement of the soil, which depends on the distance (x) at the surface with respect to the applied force.

$$u_z(x) = \frac{1}{x} \tag{3.1}$$

The corresponding results are shown in Figure 3.3.

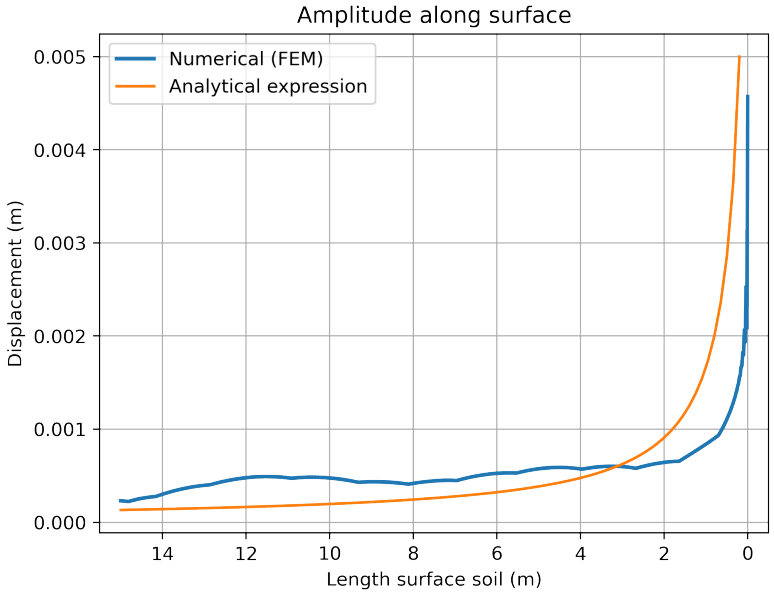

Figure 3.3: Maximum amplitude surface of the soil domain, numerical vs. analytical solution

The graph indicates that the decay of the wave amplitude is not entirely smooth. As expected, the highest amplitude occurs at the point where the force is applied. A general decay follows, although it is not perfectly uniform. Notably, a small peak appears around 12 meter, which is relatively far from the source. This suggests that while most of the propagating wave energy is

absorbed by the infinite boundary, a minor portion is reflected.

Ideally, zero reflection would provide a clearer result. However, since the observed reflection is minimal, the model remains suitable for analysis.

3.2.2 Results plain soil domain

The model of the soil domain acts as a baseline against which other models will be compared. This comparison will be conducted using two methods.

The primary component of the analysis involves the energy flux around the excitation force. This energy flux facilitates a clearer understanding of the metamaterial's behavior and effectively highlights differences between metamaterial designs. The secondary component is the displacement of the soil behind the metamaterial, which provides a more practical assessment of the metamaterial's performance.

To study the energy flux, a half-circle is computed with its center located at the node where the force is applied, as shown in Figure 3.4. The metamaterial is positioned to the left of this point. The red line in the figure indicates the nodes used to calculate the energy transmitted across the boundary. These results provide insight into the wave-manipulation behavior of the metamaterial. The blue part at the left of the metamaterial is the 1 meter surface area that is taken for analysing the displacement of the nodes.

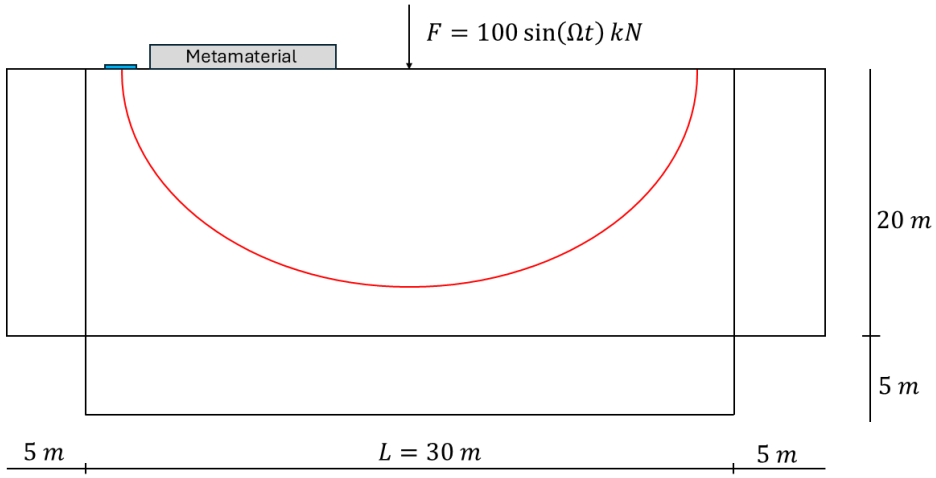

Figure 3.4: Schematic illustration of the soil domain with energy flux boundary

The energy flux E is calculated by evaluating the stresses and velocities at each node along the energy flux boundary (L). The corresponding formulas are provided below. In these formulas, σ_{xx} and σ_{yy} are the normal stresses in the x- and y-directions, respectively. σ_{xy} is the shear stress acting on a plane whose normal is in the x-direction, with the stress itself acting in the y-direction. Conversely, σ_{yx} is the shear stress on a plane with a normal in the y-direction, and the stress acts in the x-direction. Finally, v_x and v_y denote the velocities of the nodes in the x- and y-directions, respectively.

$$S_x = \sigma_{xx} v_x + \sigma_{xy} v_y \tag{3.2}$$

$$S_y = \sigma_{yx} v_x + \sigma_{yy} v_y \tag{3.3}$$

$$\vec{S} = \boldsymbol{\sigma} \cdot \vec{v} \tag{3.4}$$

$$E = \int \vec{S} \cdot \vec{n} \, dL \tag{3.5}$$

To compute the second evaluation component —the normalized energy flux— the input energy must first be determined. As the metamaterial is located 3 meters from the point of force application, there is a possibility that it influences the input energy. The input energy is calculated by multiplying the external force with the velocity at the node where the force is applied.

$$E_{input} = \int_{-\infty}^{\infty} F(t)v(t)dt \tag{3.6}$$

Figure 3.5 shows the energy flux in the case where no metamaterial is applied.

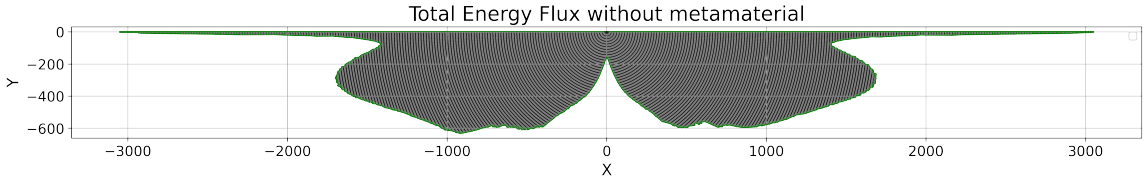

Figure 3.5: Energy flux in soil domain without metamaterial

A significant amount of energy is observed at the surface, primarily due to Rayleigh waves excited by the applied force. Another prominent concentration of energy appears at approximately 45 degrees within the soil, corresponding to the P and S waves propagating at an angle. Directly beneath the force, the energy flux is relatively low.

The symmetry of the energy flux distribution on both sides aligns with the physical configuration. Li Xiao et al. [32] presented a similar analysis in this report, utilizing the concept of energy flux. The figures within his report illustrate bulk energy fluxes that correspond to the retrieved energy flux shown in Figure 3.5.

To obtain the normalized energy flux, the total energy flux values are divided by the input energy. Finally, these normalized values are multiplied by a factor of 1000 to enhance their visibility in the results (Figure 3.6).

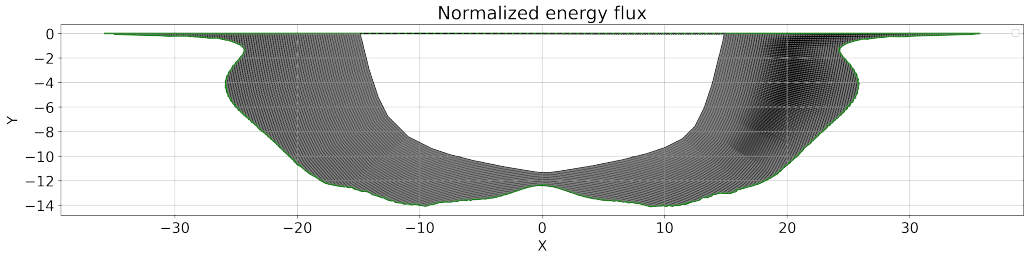

Figure 3.6: Normalized energy flux Baseline model

The maximum soil displacement is observed at the nodes located on the left side of the model. These nodes are positioned left to where the metamaterial will eventually be placed. Figure 3.7 depicts the maximum displacement observed in the plain soil model.

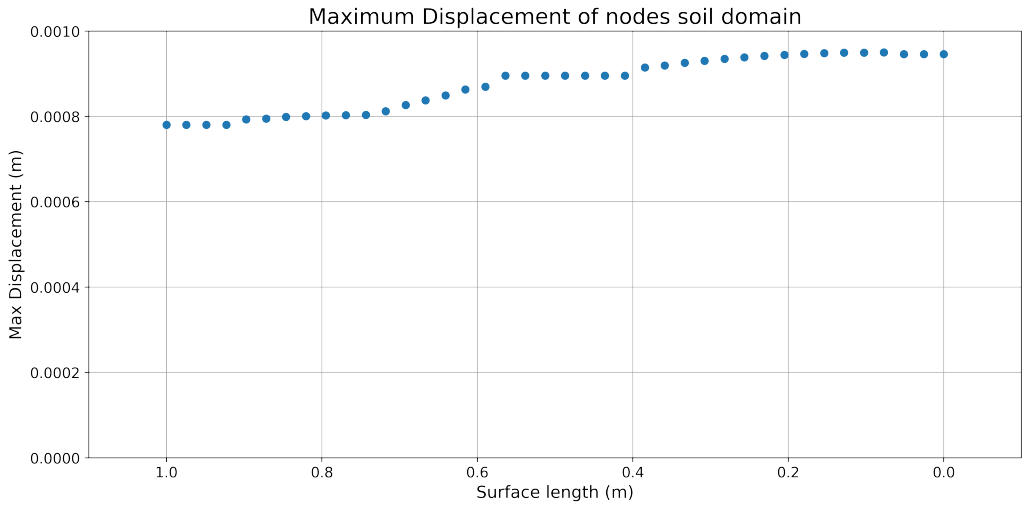

Figure 3.7: Maximum displacements nodes of soil surface without metamaterial at a 15 meter distance from the source

3.3 Metawedges

The metawedge types considered in this report are explained in this section. An overview of current research will allow for the prediction of how each metawedge behaves when placed on a soil model. The goal of this section is to model all three metawedges and compute results which will allow identification of the most effective design when varying the design parameters and excitation frequency.

To be able to mitigate vibrations in the soil, there are three different metawedges which work in different manners [12], [13]. Figure 3.8 shows the three different metawedges.

The first type is the uniform metawedge, which is characterized by resonators that all share the same resonance frequency. This design allows for highly precise targeting of a specific frequency. Chapter 2 provides the analytical model for this metawedge. The resonators, when excited, will resonate at their designed frequency, absorbing energy from the soil.

The second type is the classic metawedge, which will be named rainbow trapping metawedge in this report. In this case, the resonance frequency of the resonators gradually decays. This causes the wave to slow down until it reaches a resonator where the wave's frequency matches the resonator's fundamental frequency. This point is referred to as the turning point, where the wave trajectory diverges and 'trapped' between the resonators and eventually is dissipated via the viscous damping [4]. At different resonators, different frequencies are stuck in the metamaterial. In literature, this is referred to as 'elastic rainbow trapping'.

The third type is the inverse metawedge, which will be named the wave conversion metawedge. In this design, the resonators' eigenfrequencies gradually increase, causing the wave to undergo wave-mode conversion [24], [11]. The Rayleigh wave accelerates, resulting in an increased wavelength, and is subsequently converted into an S-wave. This S-wave decays more rapidly within the soil due to its three-dimensional propagation characteristics.

By utilizing a rainbow trapping or wave conversion metawedge, multiple frequencies can be targeted, allowing for manipulation of waves across a broader frequency range.

The metawedges used in this research are designed with a key constraint: they interact primarily with the vertical component of Rayleigh wave motion. Rayleigh waves exhibit an elliptical particle motion, in which the vertical displacement is slightly greater than the horizontal. The metawedge leverages this dominant vertical motion to maximize its effectiveness in attenuating

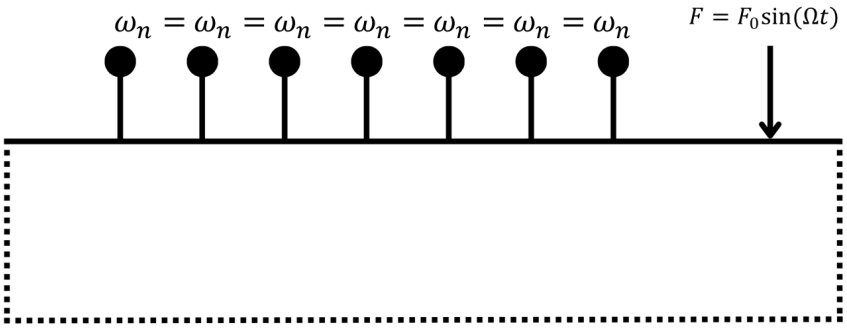

(a) Uniform metawedge

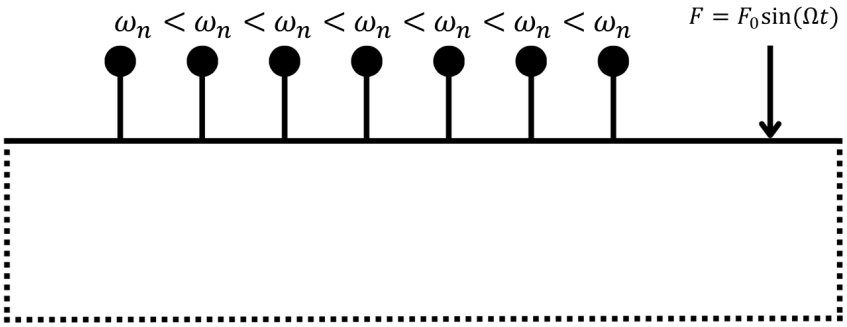

(b) Rainbow trapping metawedge

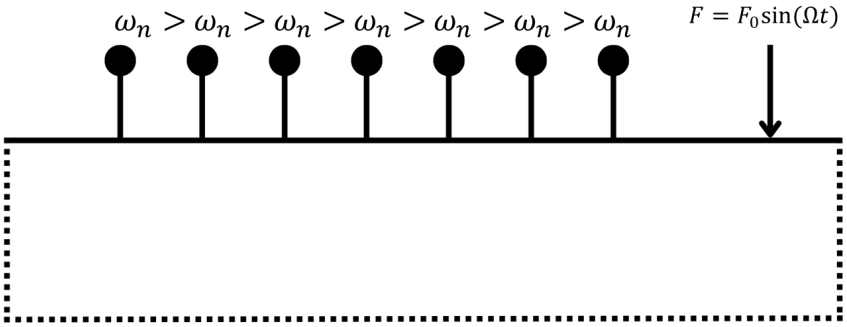

(c) Wave conversion metawedge

Figure 3.8: Schematic illustrations of three different metawedges

the wave.

In designing the metawedges for this study, the masses were limited to a maximum of 200 kg to demonstrate the effectiveness of using relatively small masses in metamaterials compared to the much larger masses typically employed in conventional approaches. This upper limit was also selected based on practical considerations.

3.3.1 Frequency range of resonators

For the design of an elastic rainbow or wave-converting metawedge, all resonators must exhibit distinct eigenfrequencies. To assess whether the eigenfrequency bandwidth of the resonators is suitable for the desired metamaterial performance, the relative resonator bandwidth (RRB) is calculated for each configuration. Hussein et al.[16] used the normalized bandwidth to investigate its dependence on the damping ratio.

In this report, we propose using the normalized bandwidth as a starting point for the metamaterial design. The RRB is defined as shown in Equation 3.7, where f_{high}, f_{low}, and f_{center} denote the highest, lowest, and central eigenfrequencies of the resonators, respectively:

$$\text{RRB (Relative Resonator Bandwidth)} = \frac{f_{\text{high}} - f_{\text{low}}}{f_{\text{center}}} \tag{3.7}$$

This metric provides an initial indication of the allowable variation in the resonators' eigenfrequencies while still enabling the metawedge mechanism to operate effectively. At lower frequencies, mitigation becomes more challenging; therefore, for the same number of resonators, the relative resonator bandwidth should be smaller. The RRB does not explicitly account for the number of resonators; however, for a fixed number of resonators, the RRB should remain approximately constant for a high-performing metawedge. Based on this research, metawedges demonstrate optimal performance when the RRB coefficient is between 0.5 and 0.6.

Here, the eigenfrequency of the resonators is assumed to follow a linear gradient. Adding more resonators could expand the bandwidth while maintaining consistent metawedge behavior. This formula, with its constants between 0.5 and 0.6, is only applicable for cases involving 20 resonators with roughly equivalent masses.

3.3.2 Uniform metawedge design

The uniform metawedge consists of identical resonators, each designed with an eigenfrequency matching the target frequency of 10 Hz. The design parameters for the uniform metawedge are listed in Table 3.1.

Parameter	**Value**
Eigenfrequency (f_n)	10 Hz
Mass (m)	200 kg
Stiffness (k)	790 000 N m^{-1}
Damping coefficient (c)	1 N s m^{-1}
Number of resonators	20
Spacing between resonators	0.5 m

Table 3.1: Parameters of resonators of Uniform metawedge

The energy flux for the model with the uniform metawedge is shown in Figure 3.9 in the color grey. The energy flux is compared to the energy flux from the case in which there is no metamaterial applied, which has the blue color.

The energy flux on the left side of the model, where the uniform metawedge is located, is

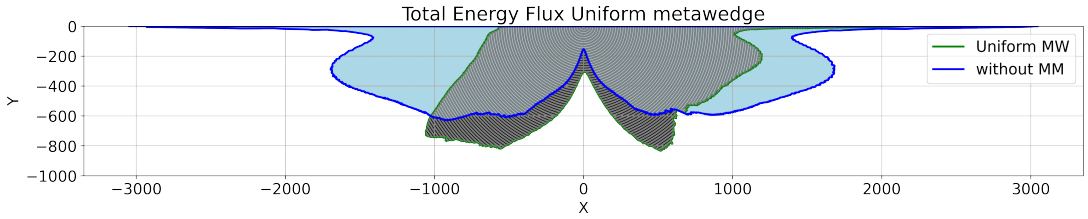

Figure 3.9: Energy flux uniform metawedge (without MM represents the case without metamaterial, Uniform MW represents the case with a uniform metawedge)

significantly reduced as expected. This reduction occurs because the metamaterial absorbs, damps, and redirects the propagating waves traveling in that direction.

The mitigation of wave energy results from both damping within the system and reflections. Evidence of reflection appears as an increased energy flux at approximately a 45-degree angle beneath the surface. The damping effect is indicated by a generally lower overall energy level.

The total energy flux throughout the system is also decreased, which can be attributed to energy absorption by the metamaterial, since the reduction in input energy is negligible.

On the right side, the energy flux is notably lower compared to the case without the metamaterial, despite the metamaterial being positioned on the left of the input force. This reduction of energy flux on the right side is likely caused by the metamaterial altering the content of input force, resulting in a greater proportion of P- and S-waves instead of surface waves.

The model has an energy input of 141786 J. Figure 3.10 displays the normalized energy flux. For better visualization, the values have been multiplied by 1000.

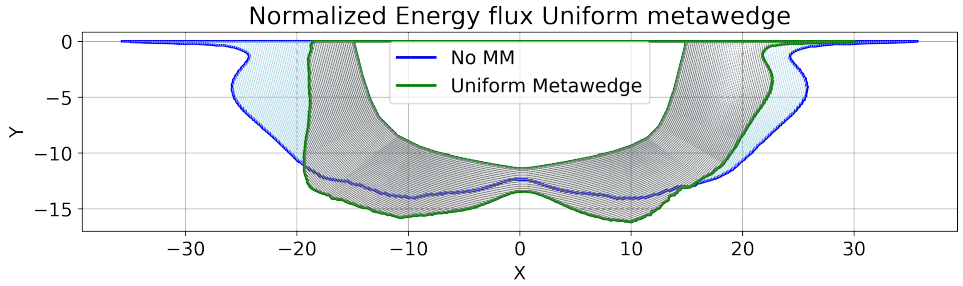

Figure 3.10: Normalized energy flux Uniform metawedge

3.3.3 Rainbow trapping metawedge designs

This section will analyse the RRB factor, which serves as an indicator of the effectiveness of the metawedge, across various designs of the rainbow trapping metawedge. A rainbow trapping metawedge is formed by a specific arrangement of resonators, creating a "wedge" in terms of their eigenfrequencies. This analysis aims to identify the most effective design for a rainbow trapping metawedge, prioritizing the largest possible bandgap.

The rainbow-trapping metawedge is designed to gradually slow down incoming waves and effectively "trap" them at the position where the resonators' eigenfrequency matches the frequency of the incident wave. Consequently, we anticipate observing increased energy absorption and a reduced energy flux along the energy flux boundary.

Three different versions have been created, each with distinct parameters, as listed in Table 3.2. All versions include 20 resonators spaced 0.5 meters apart. The first resonator is positioned 3 meters from the source of excitation, and a damping ratio of 0.001 is used for all cases.

Parameter	Version 1	Version 2	Version 3
Bandwidth resonators	14 - 8 Hz	12 - 6 Hz	15 - 8 Hz
Relative resonator bandwidth	0.55	0.67	0.61
Relative resonator spacing	0.0275	0.335	0.305

Table 3.2: Resonator configurations across three versions of the rainbow trapping metawedge

Appendix B shows the parameters of m, k and c for every resonator from every version. k and m are tuned such that the gradient of the eigenfrequencies of the metawedge is linear.

The masses were selected to be practical to handle and relatively low, in order to demonstrate the potential of the metawedge. Additionally, the masses were chosen such that the resulting stiffness k does not exceed 1.000.000 N/m. This ensures that the design remains feasible for fabrication using materials such as rubber components or metal strings.

The first version employs a metawedge designed with a resonator bandwidth ranging from 14 to 8 Hz, corresponding to a relative bandwidth of 55 percent. Figure 3.11 displays the resulting energy flux. It is evident that the energy flux is significantly reduced compared to the scenario without a metamaterial. The reduction is more pronounced on the left side, where the metawedge is located. This asymmetry is due to the metawedge altering the propagation of energy at the surface. While not all surface energy on the left side is blocked, a noticeable decrease in flux is observed, indicating effective energy manipulation by the metawedge.

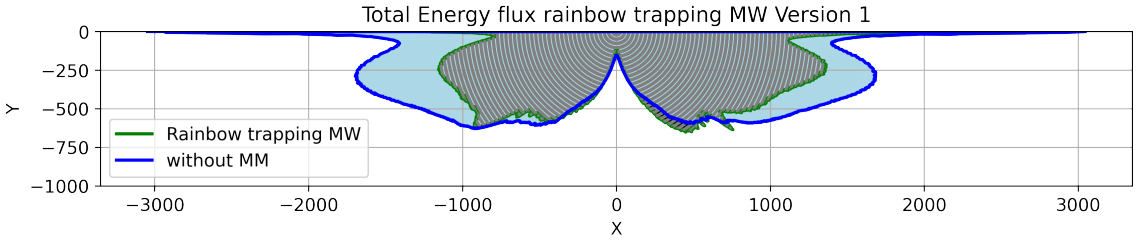

Figure 3.11: Energy flux rainbow trapping metawedge 14 - 8 Hz

To investigate whether increasing the relative resonator bandwidth improves performance, the bandwidth was adjusted to 12–6 Hz. While keeping the same absolute frequency gap, the relative bandwidth becomes 67 percent. Figure 3.12 illustrates the energy flux for this second version. A significant amount of wave reflection is observed on the right side of the figure. This behavior deviates from what is typically expected from a rainbow trapping metawedge. It is likely that the large gap in eigenfrequencies between adjacent resonators causes excessive contrast in stiffness, leading to reflection rather than gradual wave slowing.

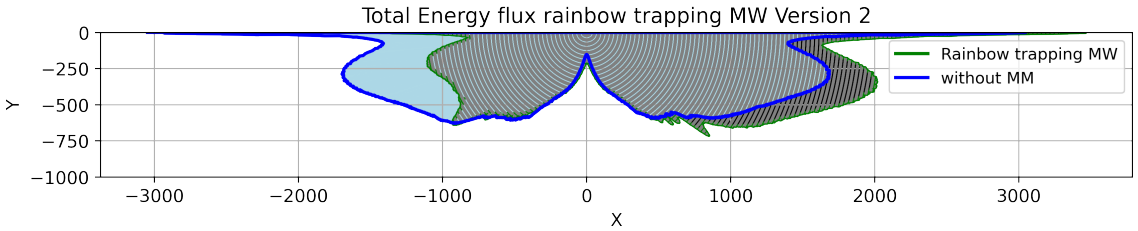

Figure 3.12: Energy flux rainbow trapping metawedge 12 - 6 Hz

The final version of the energy flux (Figure 3.13) has a relative resonator bandwidth of 61 percent, which falls between that of the first and second versions, spanning from 15 to 8 Hz.

This configuration still results in energy dissipation, though less than in Version 1, as expected due to the larger relative bandwidth. Compared to Version 2, there is noticeably less reflection, which can be explained by its smaller relative resonator bandwidth reducing stiffness contrasts between resonators.

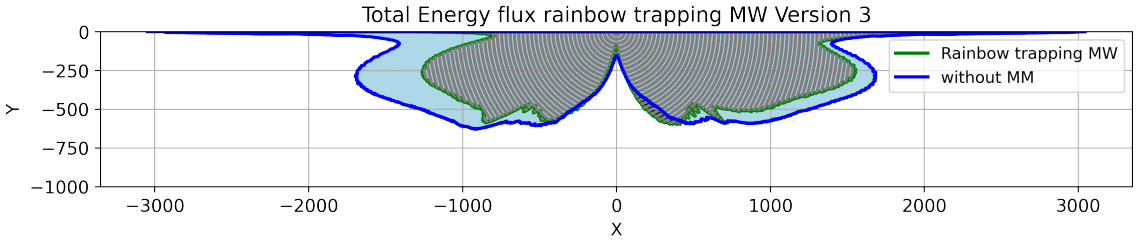

Figure 3.13: Energy flux rainbow trapping metawedge 15 - 8 Hz

The input energies for the three versions are 145375 J for version 1, 146406 J for version 2, and 147223 J for version 3. The differences compared to the input energy in the case without a metamaterial are negligible; therefore, the normalized energy flux will not be considered.

For metawedge designs with an RRB below 0.5, the targeted bandwidth is covered by a larger number of resonators, making the rainbow-trapping metawedge resemble a more uniform design. While the overall dissipation is expected to increase slightly, this approach results in more resonators than necessary. Since the goal of this report is to maximize the bandwidth without significantly compromising performance, designs with $RRB < 0.5$ are avoided.

3.3.4 Wave conversion metawedge designs

The wave conversion metawedge consists, as well as the rainbow trapping metawedge, of a configuration of different resonators. These can be found in Appendix C. In this case, the natural frequency of resonators increases. To be able to create an effective design of the wave conversion metawedge, different configurations have been made. In Table 3.3 the two different versions can be found.

Parameter	Version 1	Version 2
Bandwidth resonators	9 - 13 Hz	8 - 14 Hz
Relative resonator bandwidth	0.36	0.55
Relative resonator spacing	0.018	0.0275

Table 3.3: Comparison of configurations of the wave conversion MW

The first configuration is one with a relatively small bandgap (9 - 13 Hz), which gives a relative resonator bandwidth of 36 percent. In Figure 3.14 the energy flux can be found.

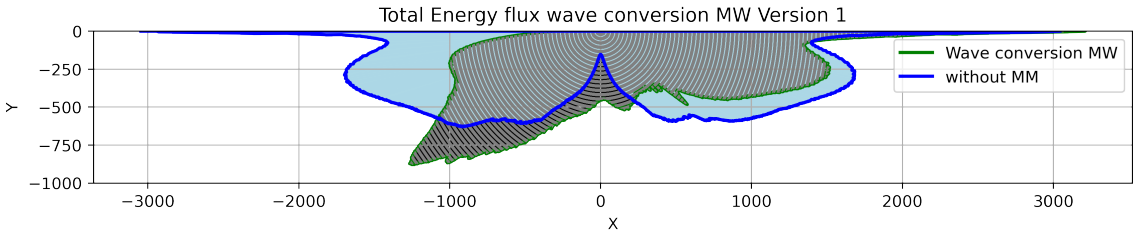

Figure 3.14: Energy flux wave conversion metawedge 9 - 13 Hz

A significant amount of reflection is expected due to the conversion of surface waves into S waves caused by the metawedge. However, in the first version, substantial absorption is observed instead. This can be attributed to the narrow relative resonator bandwidth, with many resonators

having eigenfrequencies clustered around 10 Hz. The damping within the resonators allows them to resonate effectively at the frequency of the incoming wave, dissipating energy through viscous damping, consistent with the behavior of a uniform metawedge. Additionally, the small bandgap may prevent the waves from accelerating enough to transform into S waves.

In the second design, the resonator bandwidth is increased to span 8–14 Hz, corresponding to a relative bandwidth of 55 percent. As shown in the energy plot (Figure 3.15), significant reflection occurs. The energy flux on the left side of the metamaterial is greatly reduced, but much of this energy appears to be reflected to other areas, resulting in a higher energy flux at the right side compared to the case without the metamaterial. This behavior aligns with what is expected from an wave conversion metawedge.

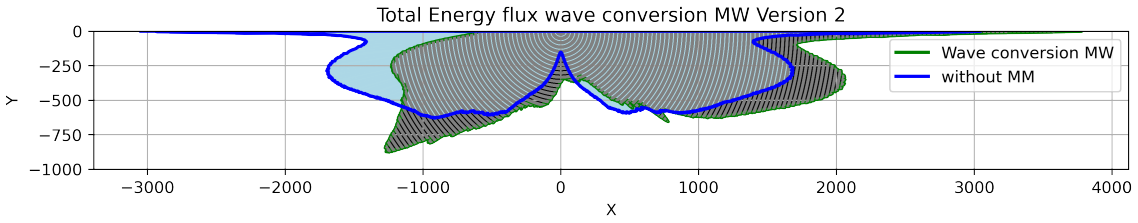

Figure 3.15: Energy flux wave conversion metawedge 8 - 14 Hz

The input energies for Version 1 and Version 2 are 148483 J and 147623 J, respectively. These values differ only slightly from the input energy of the model without metamaterial, so it is assumed that the normalized energy graph would not provide any additional insights.

Of course, the metamaterial's efficiency can be further expanded by increasing the number of resonators and by increasing the mass, but for this research, the possibilities of a small mass and a practical amount of resonators are shown.

3.3.5 Maximum displacements after metawedge

The performance of the metawedge can be considered through the energy flux, but the maximum displacement after the metawedge at the surface should also be taken into account. The goal of applying a metawedge in this case is to protect buildings from incoming waves. Figure 3.16 shows the displacements of the surface nodes behind the metamaterial.

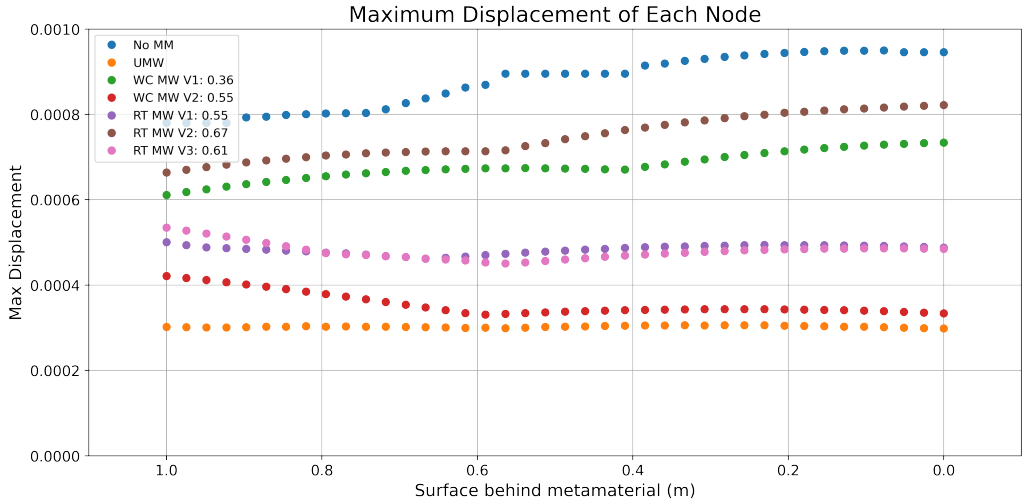

Figure 3.16: Displacements nodes behind metawedge, UMW being the uniform metawedge, WC MW being the wave conversion metawedge and RT MW being the rainbow trapping metawedge. The RRB coefficient per version is seen in the legend.

The excitation frequency in this case is 10 Hz, which results in the uniform metawedge exhibiting a very low maximum displacement, as it is tuned to this frequency. Similarly, metawedges with an RRB coefficient between 0.5 and 0.61 also show relatively low displacements. In contrast, metawedges with an RRB coefficient outside this range exhibit significantly higher maximum displacements.

3.3.6 Metawedges for further analysis

The wave conversion metawedge design chosen for further analysis in this report is Version 2. This design exhibits the expected behavior of a wave conversion metawedge and maintains a moderate relative resonator bandwidth. The resonator bandwidth for this version spans from 8 to 14 Hz, which is identical in range to the rainbow trapping metawedge but is ordered inversely. This mirrored configuration provides the opportunity to compare and better understand the performance differences between the rainbow trapping and wave conversion metawedge designs.

The optimal design out of the three tested designs for the rainbow trapping metawedge is Version 1. This is a design which has the best effect on the energy mitigation and has the same displacements as Version 3. The bandwidth of 14 - 8 Hz covers the most critical frequencies.

3.4 Metawedges at different frequencies

In reality, incoming waves almost never consist of only one single excitation frequency, therefore it is valuable to investigate the response of the metawedge across a range of frequencies, building upon the results obtained from the 10 Hz excitation. This will provide deeper insights into the performance of the various metawedge designs. For this analysis, the most effective design from each distinct metawedge type will be selected and evaluated at these different frequencies.

When choosing the optimal design for the metawedge, this is assessed by looking at two components.

- **Energy Flux**: This component is used to measure the total energy received beyond the metawedge and to determine whether the metawedge functions primarily through dissipation or reflection.
- **Displacements after metamaterial**: The primary design objective is to minimize displacements beyond the metamaterial in order to protect nearby structures.

The metawedge designs which will be tested at different frequencies are in Table 3.4.

Metawedge	Version	Bandgap	RRB
Uniform metawedge	Version 1	10 Hz	-
Rainbow trapping metawedge	Version 1	14 - 8 Hz	0.55
Wave conversion metawedge	Version 2	8 - 14 Hz	0.55

Table 3.4: Metawedge designs for analysis on different frequencies

3.4.1 Optimal uniform metawedge

The uniform metawedge has only one design capable of targeting the design frequency of 10 Hz. This design is therefore used in the subsequent analysis.

The model is excited with a harmonic force at 12 Hz, and the resulting energy flux is shown in Figure 3.17. In this figure, the blue line represents the energy flux without a metamaterial, the green line corresponds to the uniform metawedge excited at its tuned frequency of 10 Hz, and the red line shows the response of the same metawedge when excited at 12 Hz.

On the left side of the figure, the propagating waves are still partially mitigated at 12 Hz, although the effect is noticeably weaker than at the optimal 10 Hz excitation. This residual

damping is likely due to resonator damping slightly broadening the effective bandgap, which provides limited attenuation outside the tuned frequency. Nevertheless, the reflections observed throughout the domain indicate that a significant portion of the wave energy is being reflected by the metawedge rather than absorbed or transmitted. As a result, the energy flux increases in many directions due to this reflected energy.

It is important to note that while 12 Hz is only slightly offset from the tuned 10 Hz frequency, the mitigation performance already deteriorates noticeably. At frequencies with larger deviations from 10 Hz (greater than approximately 2 Hz), the performance is expected to diminish even further.

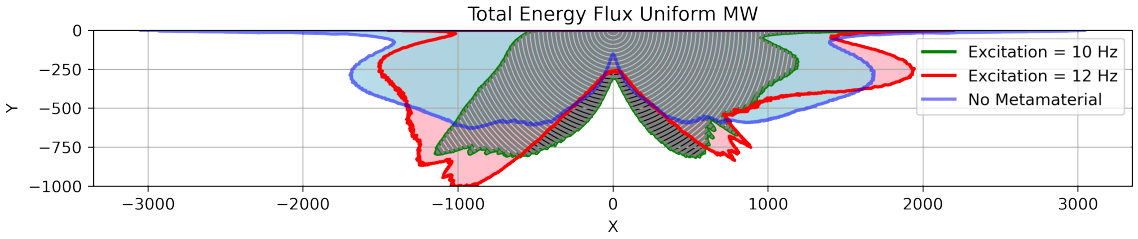

Figure 3.17: Energy flux Uniform metawedge, excitation frequency = 12 Hz

3.4.2 Optimal rainbow trapping metawedge

To be able to see the performance of the rainbow trapping metawedge Version 1 at other frequencies, the excitation frequency will be set at 8 Hz and 14 Hz. The results will be provided below.

When the harmonic excitation is 8 Hz, the metamaterial is excited at a frequency corresponding to a resonator located at the end of the metamaterial's bandwidth. Figure 3.18 displays the energy flux for this scenario. While P/S-waves are significantly attenuated, the surface waves are not as effectively mitigated. Although all wave types on the left side are weaker than in the case without the metamaterial, the 10 Hz waves show better mitigation than the 8 Hz waves. This aligns with expectations, as the metamaterial's performance diminishes for frequencies at the edge of the resonator's effective bandwidth.

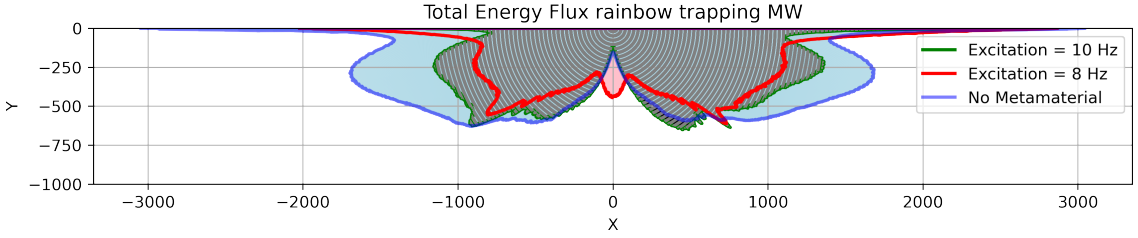

Figure 3.18: Energy flux rainbow trapping metawedge, excitation frequency = 8 Hz

With an excitation frequency of 12 Hz (Figure 3.19), which falls closer to the center of the resonator's bandwidth, a more effective mitigation of surface waves was anticipated. The experimental results, represented by the red line, confirm this expectation, demonstrating significant surface wave mitigation on the left side of the tested area. This mitigation at 12 Hz proved to be even more substantial than that observed in the 10 Hz case. Since 12 Hz is higher than 10 Hz but still within the middle range of the resonators' eigenfrequencies, it is assumed that this frequency is mitigated more effectively.

Figure 3.20 illustrates the energy flux resulting from soil excitation at 14 Hz. This frequency, being at the start of the resonator's bandwidth, makes wave mitigation challenging and causes

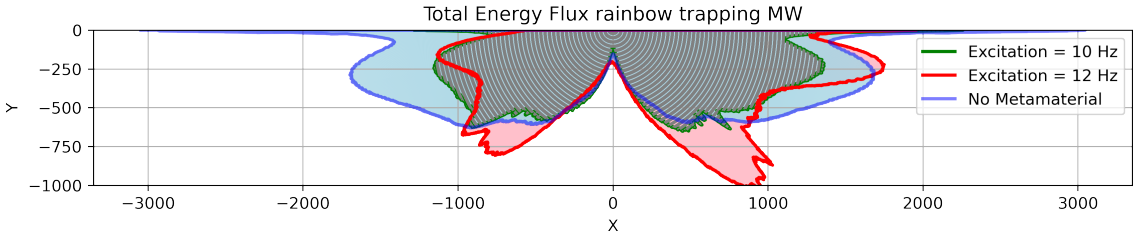

Figure 3.19: Energy flux rainbow trapping metawedge, excitation frequency = 12 Hz

significant wave reflection at the base of the half-circle. Consequently, when the wave encounters the metamaterial, it is redirected predominantly downwards and slightly towards the right surface. Nevertheless, the left side experiences less energy flux than in the case without any metamaterial.

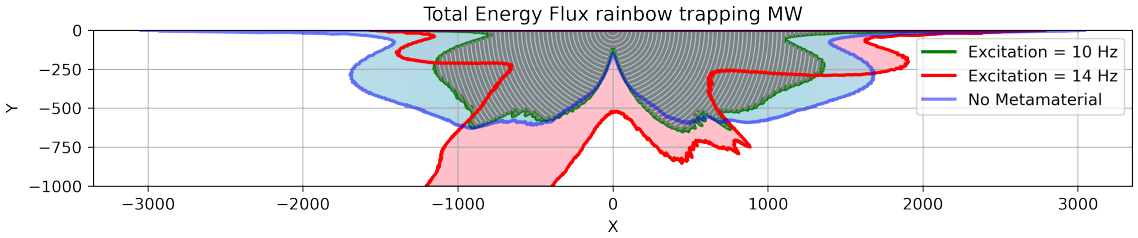

Figure 3.20: Energy flux rainbow trapping metawedge, excitation frequency = 14 Hz

3.4.3 Optimal wave conversion metawedge

The wave conversion metawedge Version 2 was tested at the same excitation frequencies as the rainbow trapping metawedge: 8, 12, and 14 Hz.

For an excitation at 8 Hz, surface wave mitigation was not as effective as in the case of 10 Hz excitation. This observation mirrors the results from the rainbow trapping metawedge version, and the explanation is that the excitation frequency is very close to the boundary of the resonators' bandwidth, making mitigation challenging. Figure 3.21 illustrates the energy flux at an 8 Hz excitation frequency. On the right side of the graph, some reflection is present. This reflection appears to be less pronounced than that observed with a 10 Hz excitation frequency. This could be because the surface waves are not as effectively mitigated at 8 Hz, leading to less energy available for reflection.

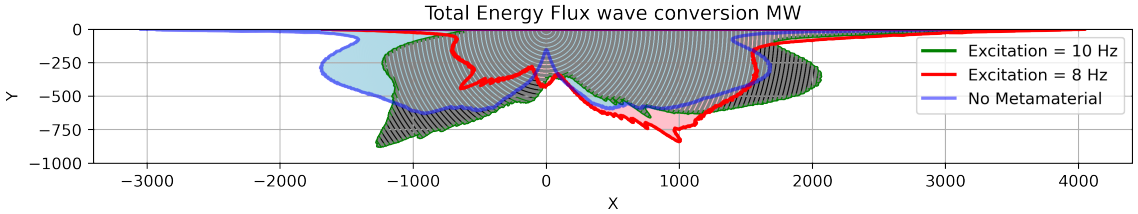

Figure 3.21: Energy flux wave conversion metawedge, excitation frequency = 8 Hz

The energy flux when the excitation frequency is 12 Hz is shown in Figure 3.22. These results show a good mitigation of surface waves at the left side of the graph and show quite a lot of reflection in all other parts of the graph. This is an indication the wave conversion metawedge works.

When the soil is excited with 14 Hz, the results show a very large energy flux. The surface waves are almost not mitigated and the energy flux at the right side of the forcing increases

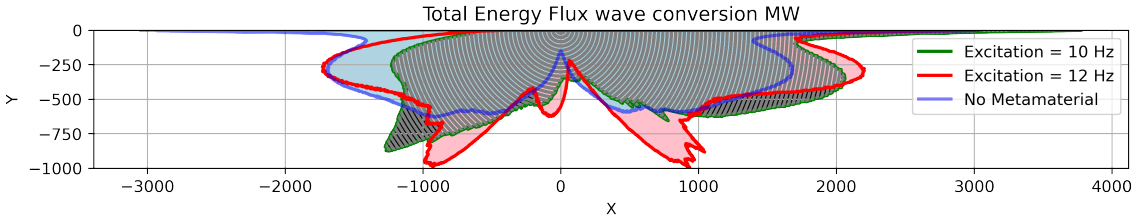

Figure 3.22: Energy flux wave conversion metawedge, excitation frequency = 12 Hz

significantly. The excitation frequency is equal to the eigenfrequency of the resonators at the end of the metamaterial.

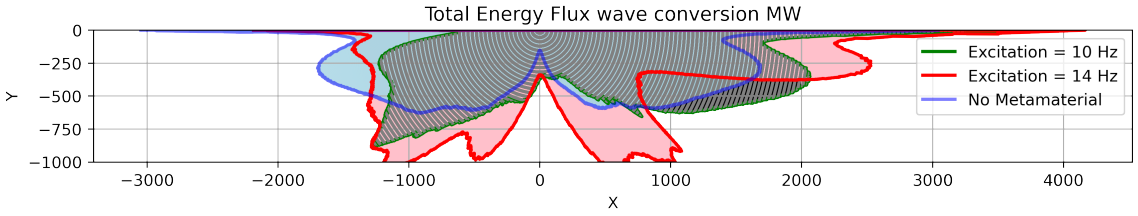

Figure 3.23: Energy flux wave conversion metawedge, excitation frequency = 14 Hz

3.4.4 Energy dissipation surface

The most important objective for a metamaterial is the decrease of response of the surface behind the metamaterial. To assess this criteria, the surface node behind the metamaterial on the left side is taken and the results on different excitation frequencies and different metawedges are plotted in Figure 3.24.

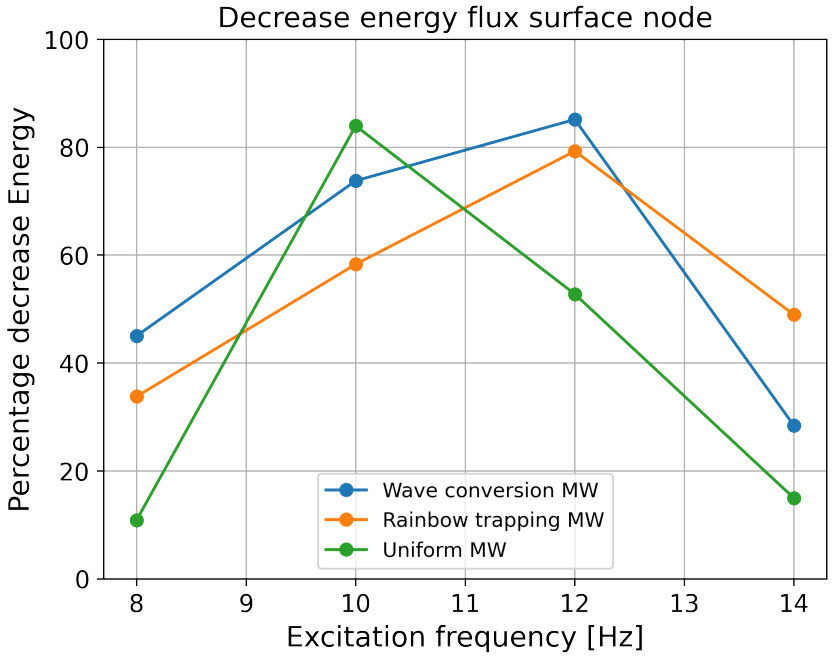

Figure 3.24: Percentage of decrease surface node with different metawedges

The uniform metawedge performs well at the excitation frequency of 10 Hz, but when the excitation frequency differs, the reduction of energy flux at the surface is very small.

Both the rainbow trapping and wave conversion metawedges effectively mitigate excitation

frequencies that fall within the middle of the resonators' eigenfrequency bandwidths. Frequencies on the higher end of this middle range show the best mitigation.

The rainbow trapping metawedge generally shows consistent performance, with a noticeable drop at an excitation frequency of 8 Hz. This is likely because the rainbow trapping metawedge slows down waves, but waves at 8 Hz may not be slowed further due to co-alignment with the last resonator, leading to reduced performance.

The wave conversion metawedge performs well when the excitation frequency aligns with the frequencies in the middle of the resonators' bandgap. There's a clear drop in performance at an excitation frequency of 14 Hz. This is because the wave-mode conversion mechanism works by speeding up waves, but at 14 Hz, the waves cannot be sped up significantly, which leads to a considerable reduction in performance.

3.4.5 Mechanisms behind metawedges

The rainbow trapping and wave conversion metawedges exhibit distinct energy flux performances, despite having identical resonator bandgaps. This indicates that each metawedge operates through a different mechanism. To observe and validate the performance of these different metawedge configurations, the energy dissipated through viscous damping (E_{VD}) is calculated using the following formula:

$$E_{VD} = \int c_m(v_s - v_r)^2 dt \tag{3.8}$$

Here, c represents the viscous damping coefficient of the resonator, v_s is the velocity of the soil, and v_r is the velocity of the resonator's mass.

For the rainbow trapping metawedge, the amount of viscous energy dissipation is computed for every excitation frequency (Figure 3.25a).

The energy dissipation per resonator of the wave conversion metawedge is shown in Figure 3.25b.

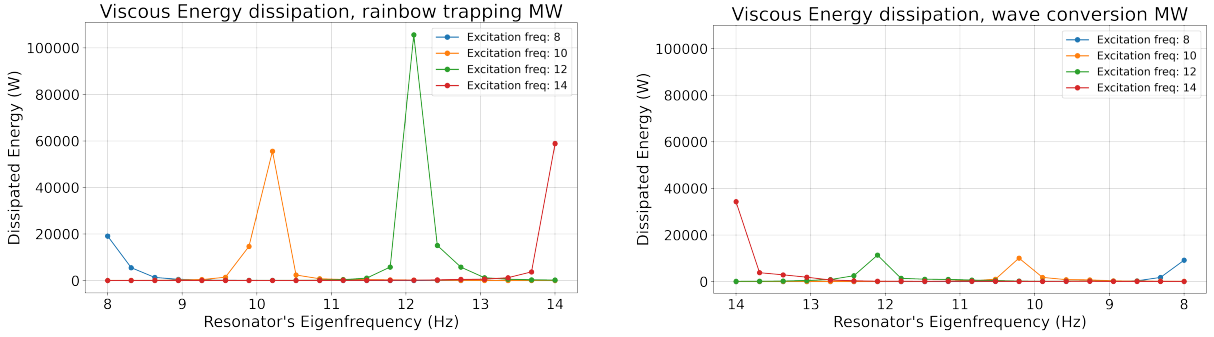

(a) Rainbow trapping metawedge

(b) Wave conversion metawedge

Figure 3.25: Viscous energy dissipation of rainbow trapping and wave conversion configurations.

In both metawedge configurations, a peak in energy dissipation via viscous damping is observed, centered around the excitation frequency. The resonators operating near this frequency exhibit the highest energy dissipation. The resonator with a slightly higher frequency than 10 Hz demonstrates optimal performance, as the small amount of viscous damping contributes to a slight upward shift in the resonator's bandgap.

It is notable that the amount of viscous energy dissipation is highest in the middle area of the resonator's bandwidth. Here, the propagating waves are trapped within the metamaterial and taken up by the metawedge. When the excitation frequency aligns with the start or end of the resonator's bandwidth, the amount of viscous dissipation is much less.

The rainbow trapping metawedge is expected to dissipate energy through viscous damping. This is attributed to the mechanism by which the metawedge slows down the waves, causing them to be trapped within the metawedge structure, where they are then dissipated by the viscous damping or the damping present in the soil.

Conversely, the wave conversion metawedge operates by redirecting waves into the soil. As a result, it's expected to have less energy dissipation from viscous damping than the rainbow trapping metawedge. That aligns with the results in Figure 3.25a and 3.25b. This does not say that the wave conversion metawedge is more robust, since it is still dependent on the resonance properties of the system.

Table 3.8 presents the total viscous energy dissipation for both models in Watt, clearly indicating that the rainbow trapping metawedge exhibits considerably more dissipation than the wave conversion metawedge.

Excitation Frequency (Hz)	Dissipated energy RT MW	Dissipated energy WC MW
8	27605	11869
10	77897	16377
12	137107	21202
14	66189	45359

Table 3.5: Total energy dissipation at different excitation frequencies

3.5 Design criteria metawedges

To design a metawedge more quickly, some design criteria will be proposed in this section of the report. These criteria are based on different physical assumptions and are validated by numerical results. It is impossible to capture all the physics of the metamaterial in simple design criteria, but these criteria aim to capture the most important features.

The underlying principle of these assumptions is that the bandgap of mitigated frequencies should be as large as possible while using as few resonators as possible.

Statement 1: Spacing of resonators has very little effect on performance

When using local resonance, the mechanism does not rely on the wavelength of the incoming waves. Therefore, the spacing between the different resonators has little effect on the performance of the metawedge.

To demonstrate this, the rainbow trapping metawedge Version 1 was constructed with three different resonator spacings: 0.5 m, 0.25 m, and 0.1 m. In each configuration, the resonators were positioned starting at 3 meters from the source, extending to the left. This positioning can be found in Figure 3.26.

Figure 3.27 shows the energy flux of the two different cases and the results are almost the same. There is a slight increase in energy flux on the right side. The small difference can be explained by a slight change in characteristics of the input force, because there are more resonators close together. It is not due to the transient response, because the same result is derived when using the energy flux after the transients are dissipated.

Since the spacing between the resonators has little impact on the effectiveness of the mitigation mechanism, the design can be made highly compact with minimal loss of performance. This underscores one of the key advantages of the concept: efficient use of space while preserving the desired attenuation characteristics.

It should be noted that when the resonators are placed very far apart, the mechanism will

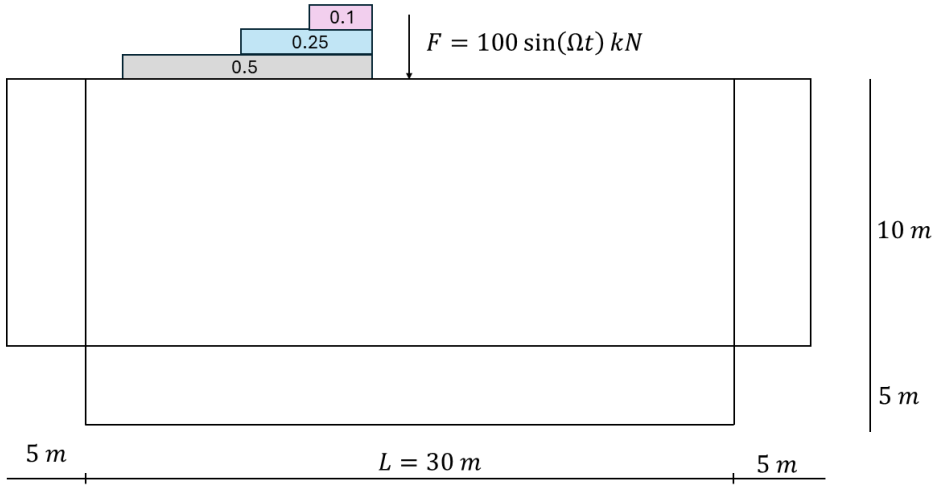

Figure 3.26: Positioning 20 resonators with the distance between each resonator in different cases

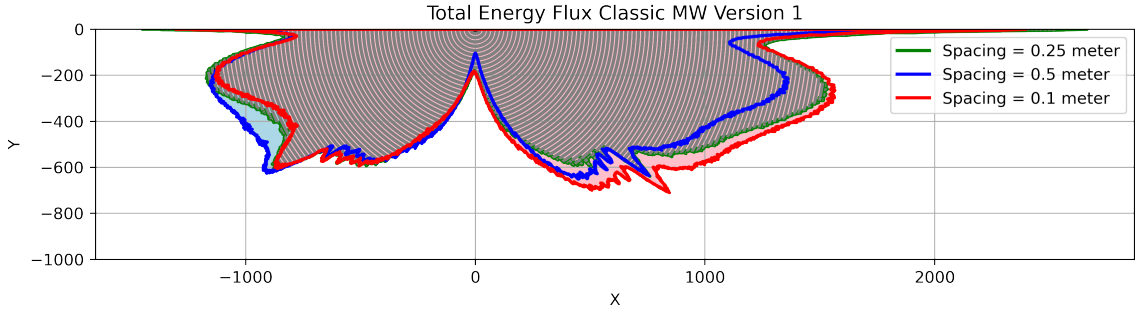

Figure 3.27: Energy flux rainbow trapping metawedge, spatial difference resonators

not function properly, and the resonators will behave as individual units. Therefore, the placement of resonators should be relative to the wavelength, as local resonance operates based on semi-wavelength.

Statement 2: Gap between eigenfrequency resonators is dependent on the target frequency

The RRB coefficient used in this report is only applicable for comparing different metawedges that have the same mass and number of resonators. The aim of this section is to generalize this coefficient so that it can be used to compare metawedges with different numbers of resonators.

Since low frequencies are harder to mitigate than high frequencies, the allowable difference in bandgap for low target frequencies must be smaller than for high frequencies. In addition to the target frequency, the number of resonators also influences how wide the resonator bandwidth can be.

The generalized formula for the relative resonator bandwidth is proposed as follows:

$$RRBN = \frac{f_{high} - f_{low}}{f_{center} \cdot N} \tag{3.9}$$

The assumption is that both the metamaterial's performance and its bandwidth are optimized when this value falls within the range of 0.025 to 0.03. This considers that achieving a broader

bandwidth requires more resonators, with a greater number being necessary for lower-frequency bandgaps compared to higher-frequency ones. Furthermore, this formula is predicated on maximizing the resonators' bandwidth while maintaining a reasonable number of resonators.

Adding more resonators than necessary causes the RRBN value to drop below 0.025. This results in increased viscous damping, as the metawedge's behavior begins to resemble that of a uniform metawedge. Consequently, increasing the number of resonators N enhances the total viscous energy dissipation. However, increasing N also raises the total mass of the system, which in turn requires more energy to activate the mechanism. This added inertia negatively impacts the performance of the metawedge.

Incorporating the target frequency into the design criteria is now essential. Energy dissipation is understood to peak close to the center of the resonator's bandwidth. To allow for design adaptability, a frequency band is established within which the target frequency should fall. As low frequencies prove more difficult to mitigate, opting for a target frequency closer to the upper limit of this band yields marginally higher energy dissipation than selecting one near the lower limit. The target frequency's bandwidth is set within the middle third of the resonator's total bandgap.

$$f_{target} > f_{center} - \frac{f_{high} - f_{low}}{6} \tag{3.10}$$

$$f_{target} < f_{center} + \frac{f_{high} - f_{low}}{6} \tag{3.11}$$

To be able to prove that the formula of RRBN leads to the metawedge utilizing the mechanism which is expected, the following case has been tested. The configuration can be found in Table 3.6.

Bandwidth eigenfreq (Hz)	**RRB**	**RRBN**	**Amount of resonators**
9–13	0.36	0.028	13

Table 3.6: Bandgap characteristics and corresponding resonator parameters

A wave conversion metawedge featuring 13 resonators, each with a mass between 100 and 150 kg, was tested. The resonator's bandwidth was narrowed to 9 - 13 Hz. In Figure 3.14, this design was evaluated using a 10 Hz excitation frequency and 20 resonators. This setup resulted in partial energy redirection and partial dissipation. This occurred because the resonators behaved partly as a wave conversion metawedge and partly as a uniform metawedge. The eigenfrequencies were very close together, leading to many resonators around the 10 Hz excitation frequency. However, this report shows that the metawedge achieves optimal performance, with minimal use of resonators, when the RRBN value lies between 0.025 and 0.03. For the wave conversion metawedge, the anticipated outcome is the redirection of the waves propagating leftward.

The upper boundary of the target frequency is chosen, so the excitation frequency is 11.67 Hz. Since this frequency is slightly larger than the model with 10 Hz, comparison might not be fully fair. Examining the energy flux along the entire boundary (Figure 3.28) reveals the expected behavior of a wave conversion metawedge, namely the redirection of surface waves into body waves.

When examining the energy flux results at the surface node behind the metamaterial, three models were created using an wave conversion metawedge. These three cases feature different resonator eigenfrequency bandwidths, leading to varying RRB values. The number of resonators used is determined by the RRBN formula, with this value remaining consistent across all resonators.

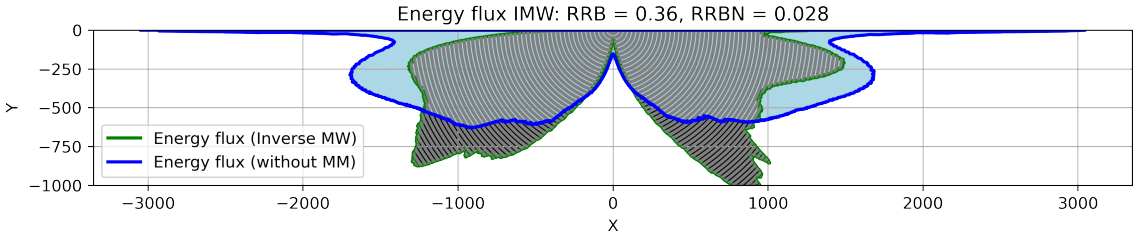

Figure 3.28: Energy flux wave conversion metawedge, excitation frequency = 11.67 Hz

Bandgap (Hz)	RRB	RRBN	Low-frequency	High-frequency	Amount resonators
8–14	0.55	0.0278	10.33 Hz	11.67 Hz	20
9–13	0.36	0.0280	10 Hz	12 Hz	13
7–15	0.72	0.0280	9.67 Hz	12.33 Hz	26

Table 3.7: Different models with their coefficients

The three different models are excited at the upper and lower boundary (stated in formula 3.11). The RRB is different, but the RRBN is kept equal. The results are plotted in 3.29.

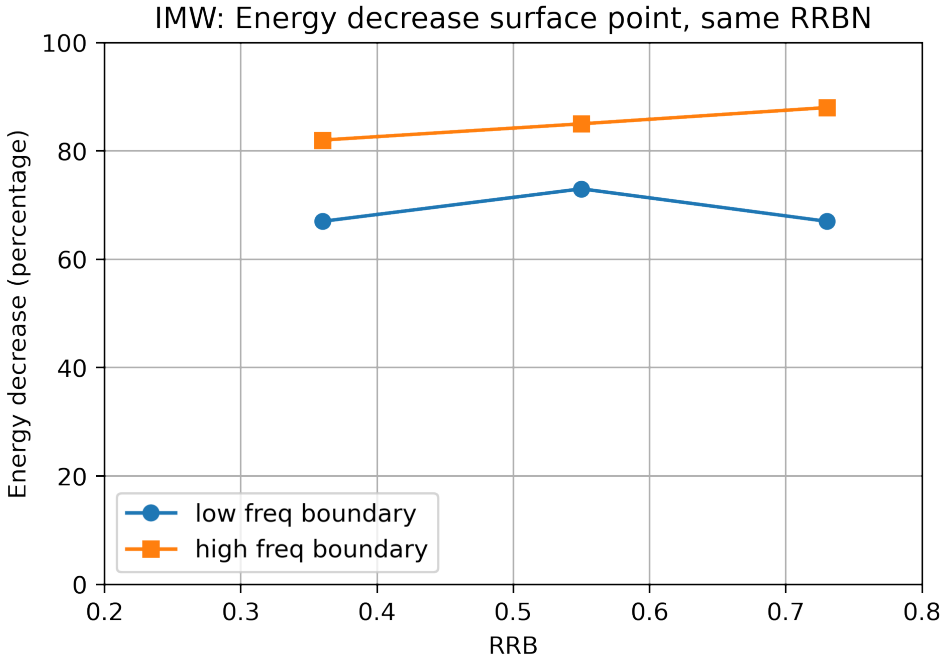

Figure 3.29: Energy decrease surface node, RRBN = 0.028

The results show that the upper and lower boundaries remain relatively constant across the different RRB values. This suggests that the RRBN provides a reliable indication of the maximum achievable bandgap, while maintaining performance and optimizing the number of required resonators. Since the RRBN is more general and applicable to a wider range of cases, this coefficient appears to be superior to the RRB.

Statement 3: There is an optimum for the amount of mass that has to be used

The amount of mass significantly influences a metawedge's performance. Too little mass prevents sufficient energy transfer from the system, while excessive mass requires too much energy to move, also hindering optimal performance.

Initial research focused on the rainbow trapping metawedge due to its reliance on viscous damping, providing a good starting point. The primary findings from this involved viscous damping and the reduction of energy behind the surface. Masses of 10 kg, 50 kg, 100 kg, 200 kg, and 500 kg were used in these investigations. These numerical results are obtained with a model containing 20 resonators.

The decrease in energy flux at the surface behind the metamaterial was evaluated. The number of resonators and the damping ratio ($\xi = 0.001$) were kept constant. This implies that as mass increases, viscous damping also increases, leading to higher damping per meter for larger masses. This assumption might not reflect reality, as the damping coefficient can be designed to be independent of mass.

When selecting the appropriate mass, a trade-off between cost and resources is necessary. Figure 3.30a illustrates the decrease in energy flux for various masses. The figure indicates that increasing the mass up to 100 kg substantially improves results. Beyond 100 kg, the energy flux decrease continues, but at a reduced rate. Considering resources and cost, the optimal mass lies between 100 kg and 200 kg.

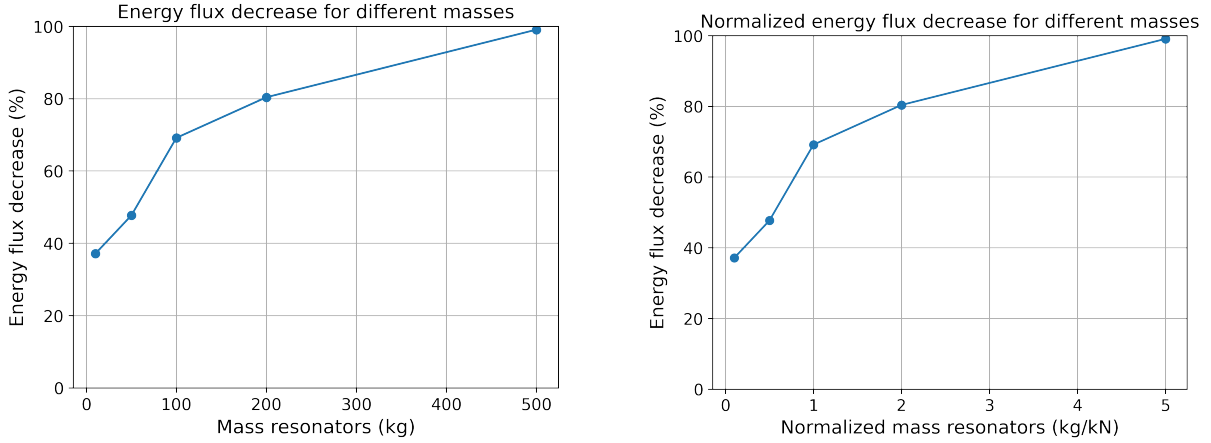

(a) Decrease of energy flux for different masses

(b) Normalized decrease of energy flux for different masses

Figure 3.30: Energy decrease for different masses

Figure 3.30a shows a significant decrease in energy flux when each resonator has a mass of 500 kg. This is a relatively large mass. Observing the full energy flux around the harmonic forcing (Figure 3.31) reveals that this flux includes both dissipation and reflection. This substantial mass creates a hybrid effect, combining characteristics of a metawedge with the conventional method of using a large mass. This combination leads to a very high reduction in energy flux, but this decrease isn't solely attributable to the metawedge's function.

The ideal mass size depends on the input force's amplitude and potentially on the soil's properties. To make the mass values more generalizable, it would be better to normalize this graph to the input force's amplitude (Figure 3.30b).

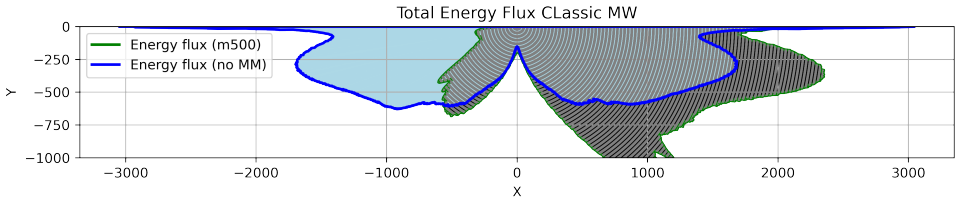

Figure 3.31: Decrease energy flux for different masses

3.6 Design of a resonator

Now the parameters of the metawedge are clear, but these parameters have to be transferred to a design. For this design, the parameters of the rainbow trapping metawedge version 1 are taken.

The masses differ from 50 to 200 kg. Since the resonators are 0.5 meter apart from each other, the masses, which are assumed to be squared, cannot be larger in geometry than 0.25 x 0.25 x height. Structural steel has a density of 7850 kg/m^3. For the different masses used in the metawedge, the following geometry can be used when using structural steel.

Assumed is that the width of the mass should be 0.2 meters, because that fits within the geometry of the whole metawedge. The depth is chosen to be 0.3 meters and the height differs, depending on how much the weight of the resonator should be. The height is rounded, so the actual mass might differ a bit from the targeted mass.

Target mass (kg)	**Height resonator (m)**	**Actual mass (kg)**
50	0.11	51.8
100	0.22	103.6
150	0.32	150.7
200	0.43	202.5

Table 3.8: Total energy dissipation at different excitation frequencies

When translating the parameters of stiffness k and viscous damping c into materials which have these properties, the following materials can be looked at to represent the spring and damper in the design of a metamaterial.

The stiffness of a material is determined by the following formula. In this formula, A represents the area of the material, L represents the height and E is the Young's modulus.

$$k = \frac{EA}{L} \tag{3.12}$$

The range of stiffness used in the most metamaterials designed is between $k = 200.000$ and $k = 1.000.000$ N/m. Since the stiffness is dependent on the size of the material, assumed is that area of the spring is equal to $A = 0.2 \cdot 0.3 = 0.06$ m^2. This is the same area as assumed for the mass. Table 3.9 offers a preliminary look at some materials that could potentially be used to create a resonator. These materials were chosen to provide a broad conceptual overview for the design. For a finalized resonator design, more in-depth research will be necessary.

Category	E	L **for** $k = 2 \times 10^5$	L **for** $k = 1 \times 10^6$	**Viscous Damping** c
Soft Foam	1×10^6 Pa	30 cm	6 cm	5 - 40 Ns/m
Rubber	2×10^6 Pa	60 cm	12 cm	20 – 50 Ns/m
Hard Foam	5×10^6 Pa	150 cm	30 cm	5 – 15 Ns/m

Table 3.9: Various materials with their properties and geometries used to represent spring and damper behavior through material selection

3.6.1 Spatial design possibilities

This research focuses solely on the vertical motion component of Rayleigh waves. This section explores several conceptual spatial designs tailored to mitigate this vertical motion.

The first conceptual design, illustrated in Figure 3.32a, presents a relatively simple setup. It features a rubber or foam component functioning as both a spring and a damper, topped by a

mass. This mass is designed to undergo vertical motion, facilitated by a rolling or sliding system on its sides. A rolling system would likely face rapid fatigue, while a sliding system would require regular maintenance to ensure low friction. This design can either be placed on the soil surface or embedded within it.

Figure 3.32b depicts a second design, where a mass is suspended by four strings that act as a spring. These strings contribute to stiffness in both the vertical and horizontal directions. Damping can be integrated directly into the metal strings. A potential drawback of this design is that large vertical displacements of the mass could lead to fatigue issues in the strings over time.

The third design, shown in Figure 3.32c, utilizes a pendulum. This system can be created beneath the soil surface and connected to it. The pendulum comprises a mass, and its string can incorporate viscous damping. The length of the string dictates the system's stiffness and eigenfrequency, making it relatively straightforward to implement. This design can be excited by both vertical and horizontal ground motion. However, the attachment points may experience fatigue due to extensive swinging during operation.

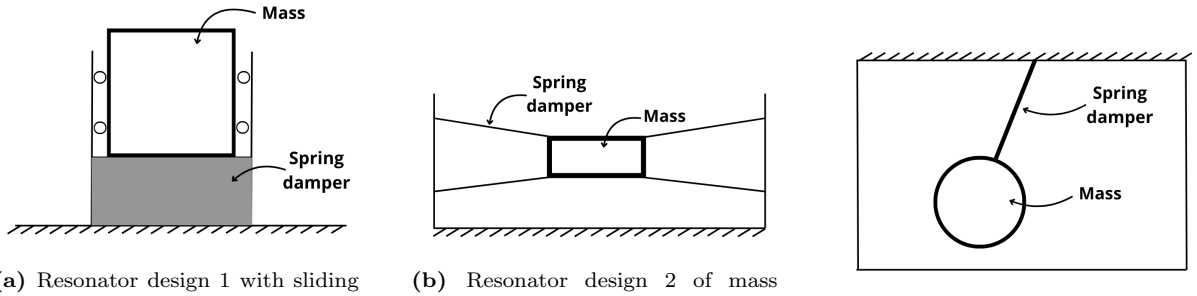

(a) Resonator design 1 with sliding or rolling mechanism

(b) Resonator design 2 of mass attached to horizontal strings

(c) Resonator design 3 of a pendulum

Figure 3.32: Conceptual spatial designs of a resonator with vertical motion

3.7 Case study Wageningen

This report has so far explored the metamaterial's response to various pure harmonic excitations, establishing an understanding of its behavior and outlining design criteria. Now, the metamaterial will undergo a case study to evaluate its reaction to the combined transient and harmonic vibrations generated by a passing truck. It's crucial to observe how it performs under this more realistic vibrational scenario.

The aim of this chapter is to analyze the metamaterial's behavior when subjected to a real-world signal containing multiple frequencies.

The specific case study involves a new building at the University of Wageningen, which will house a laboratory with highly sensitive equipment. Vibrations from a nearby road are interfering with measurements conducted in the lab, necessitating minimal vibration levels.

Movares, a company specializing in such analyses, previously measured the vibrations emanating from this road. For this particular case study, their measurements of a passing truck are utilized.

Figure 3.33 shows the map of the environment in Wageningen. The blue part between points A, B, C and D represents the spot of the new building. The road to the right of the building is the Bornestraat and is the main source of vibrations. The smallest distance between the new building and the road is 20 meters. This is the distance between point A and E.

For this case, 20 meter is taken as the maximum distance for the metamaterial. To keep the possibility for a realistic design, the miminum distance between the resonators is taken as 0.5 meter.

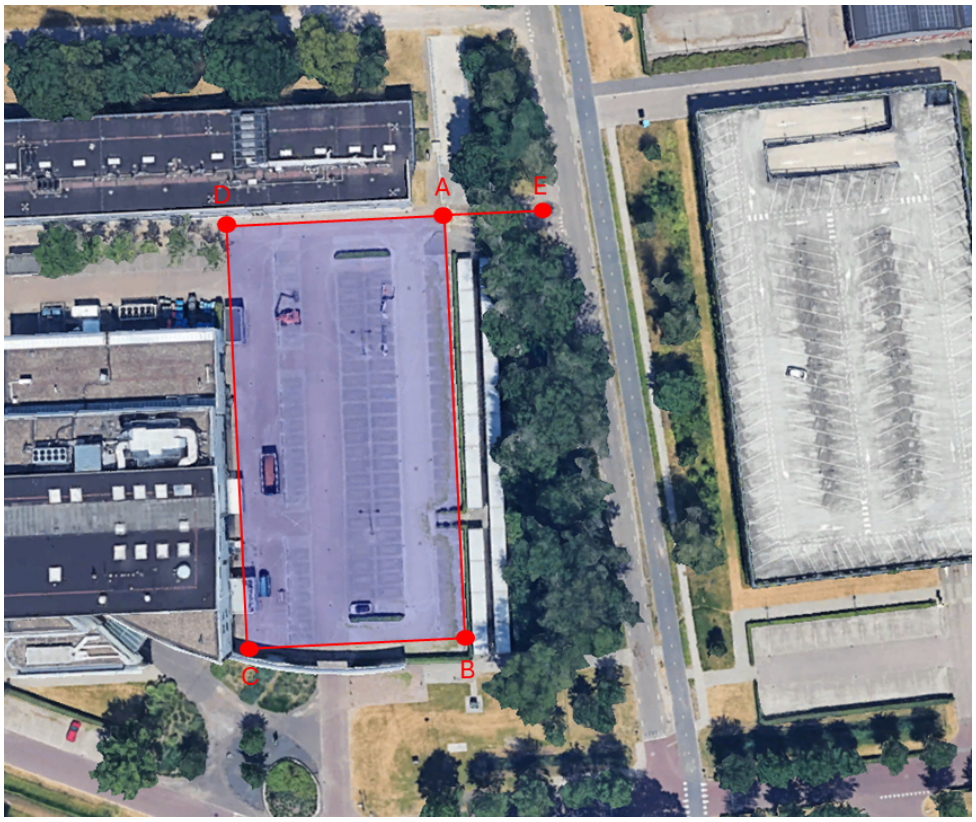

Figure 3.33: Outline new laboratory building Wageningen

At the location, measurements have been taken. One of the measurements consist of a large truck passing by. This measurement will be taken as the critical point to which the metawedge has to be designed.

The signal is shown as a time signal in Figure 3.34a and a frequency domain signal in Figure 3.34b. The signals are measured in x-, y- and z-direction.

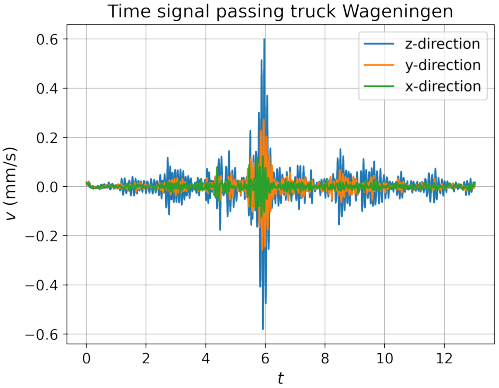

(a) Time domain signal

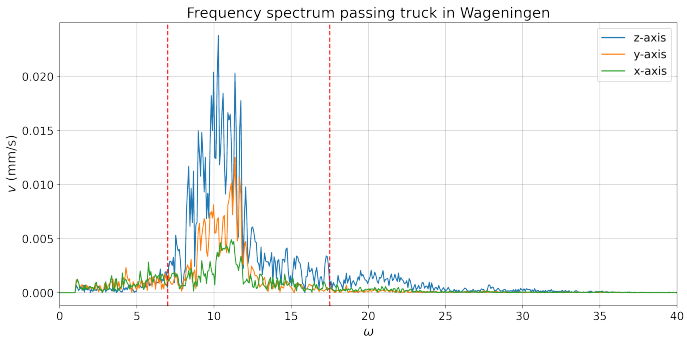

(b) Frequency domain signal with most critical frequencies within the red dotted lines

Figure 3.34: Time and frequency domain signals of passing truck

The z-direction is the dominant direction for the signal. Therefore, orienting the metawedge's resonators vertically will extract the most energy. The highest energy concentration is at 10 Hz, with significant energy also present in frequencies around this point. Figure 3.34b illustrates this with two vertical red dotted lines, indicating the range where most energy is contained. Consequently, the metawedge will be designed to mitigate frequencies between 7 and 17.5 Hz as

broadly as possible.

The velocities in the y- and z-direction are applied to the model.

3.7.1 Design parameters of metawedge

Since the focus is on the new building, and the other buildings in the environment do not have to be free of vibrations, the use of the wave conversion metawedge has been chosen. This works best for mitigating energy at the surface, but since the mechanism works on redirecting, there is a possibility that the surrounding environment experiences somewhat higher levels of energy.

Since the distance between the building and the local road is 20 meters, it is assumed that there is 15 meters space to place the metamaterial. This means that there will be 31 resonators. The target frequency is 10 Hz, because of analysis of the frequency response function of the velocity.

The most critical frequencies lie between 7 and 17.5 Hz, which can be seen in Figure 3.34b. While keeping the target frequency of 10 Hz in the middle third bandwidth of the eigenfrequencies of resonators, the RRBN value should be kept between 0.025 and 0.030.

To meet both design criteria, the bandgap of eigenfrequencies is taken from 7 to 16 Hz, because the lower frequencies are more crucial to mitigate. This leads to a value of RRBN of 0.0252. The middle third bandgap is 10 to 13 Hz. This configuration leads to satisfaction of the design criteria.

The design of the parameters is chosen such that the mass is between 100 and 200 kg, since this region is the most impactful in terms of resources. By varying the mass m, stiffness k can be managed to stay somewhat in the same range, such that the material that will be used can be the same for every resonator. The input force is applied on a node as a prescribed velocity. This is done by a factor of 1000 to be able to have more clear results.

In addition to the design based on the specified criteria, two metawedges with narrower bandwidths were constructed. The resonators of the rainbow trapping metawedge have eigenfrequencies decreasing from 11 Hz to 9 Hz, while those of the wave conversion metawedge increase from 9 Hz to 11 Hz. This configuration exhibits behavior characteristic of a uniform metawedge.

3.7.2 Results Case study

The results of the metawedge are assessed by comparing the frequency response in the vertical direction of 40 nodes on the surface behind the metamaterial, contrasting the cases where the metamaterial is present versus absent.

Figure 3.35a displays the frequency spectrum of vertical displacement, comparing scenarios with and without the metawedge. The region between the two black dotted lines indicates frequencies that align with the eigenfrequencies of the metawedge's resonators. While the metawedges with a large bandwidth show some influence on frequencies excited by the passing truck, their overall effect is not substantial.

For the metawedges with small bandwidth, the effect on the incoming frequencies is quite a lot. This bandwidth focuses on the largest peak in energy, which can be mitigated quite well. The large bandwidth metawedges focus on some frequencies with less energy and their effect is much less.

The limited impact likely stems from the truck's excitation primarily consisting of transient vibrations, with a relatively small harmonic component, especially for frequencies higher than 13 Hz. This means the mass-spring systems of the metawedge do not have sufficient time to fully engage with the harmonic frequency and, consequently, does not reach a significant amplitude in resonance.

The results shown in Figure 3.36 indicate a minimal decrease of maximum 25 percent in

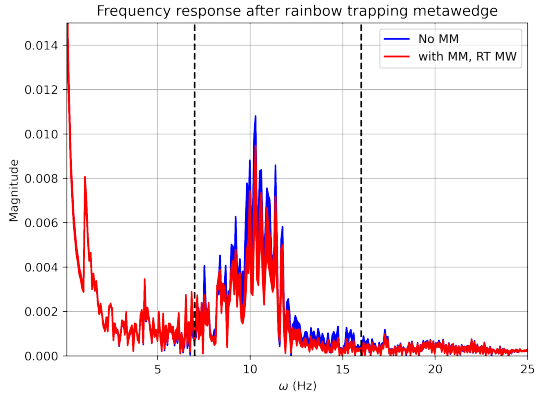

(a) Frequency spectrum z-direction, rainbow trapping metawedge

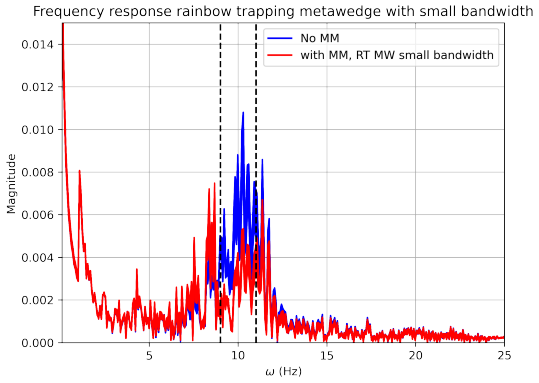

(b) Frequency spectrum z-direction, rainbow trapping metawedge with small bandgap (11–9 Hz)

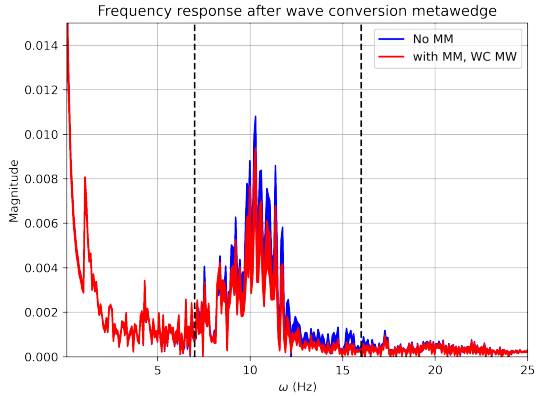

(c) Frequency spectrum z-direction, wave conversion metawedge

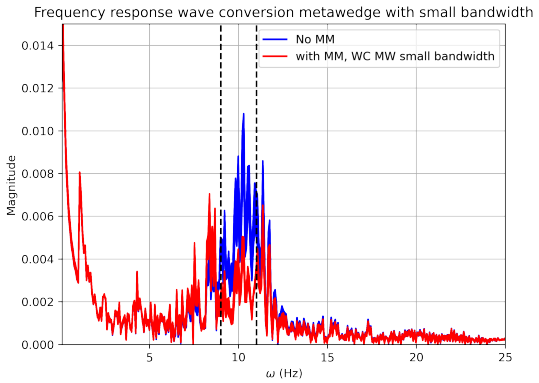

(d) Frequency spectrum z-direction, wave conversion metawedge with small bandgap

Figure 3.35: Comparison of frequency spectra in the z-direction for different metawedge designs.

displacement of the nodes after the metamaterial. This raises doubts about the practicality of using this kind of metamaterial for the intended purpose.

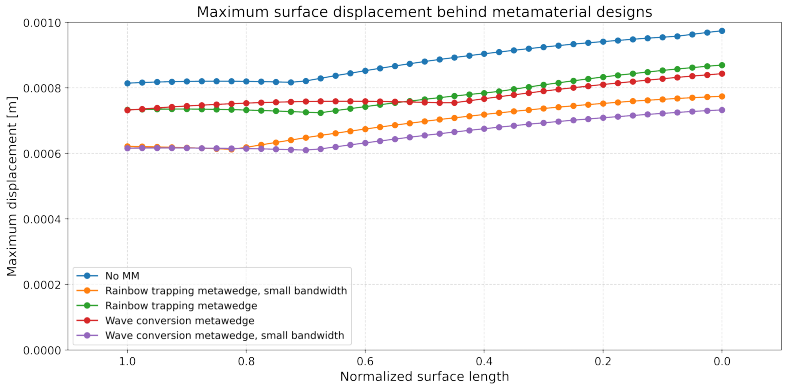

Figure 3.36: Displacement surface behind metamaterial in case study

When looking at the time signal, between 5.5 and 6.5 seconds, the highest amplitude is reached and this is the time where the truck passes the measurement design. This one-second interval corresponds to about 10 cycles of the dominant frequency. To show that the metamaterial needs more time to get to resonance / a significant amplitude, the case is tested with a harmonic excitation of 5 seconds.

Figure 3.37 shows the displacement of 6 masses closest to the input force when they are excited at their resonance frequency. After 2 seconds, the masses appear to reach their maximum displacement, which is influenced by the level of viscous damping. From this point onward, they extract the most energy, and the metawedge operates at peak effectiveness.

The graph shows that the displacement of the masses is not fully symmetric. In addition, the masses appear to be affected by another frequency. This could be due to residual transients remaining in the system, as the infinite boundaries are not perfectly effective.

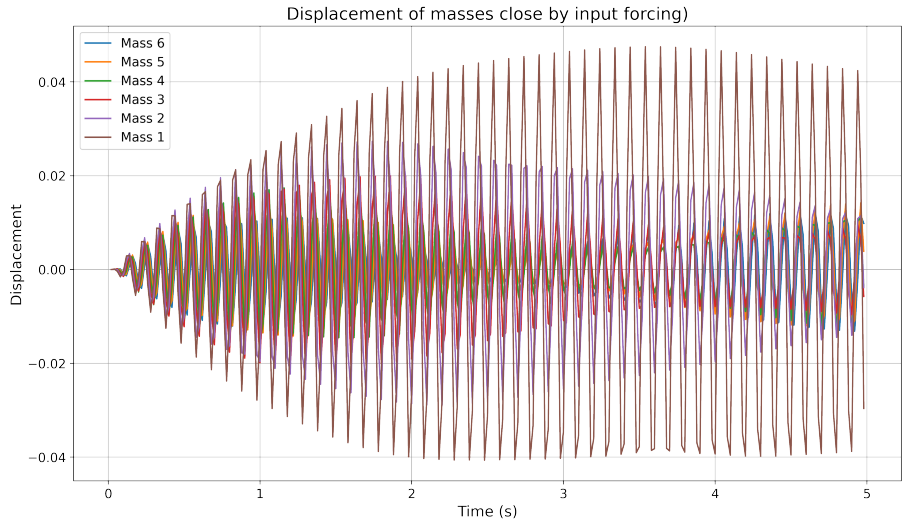

Figure 3.37: Displacement masses throughout metamaterial

When an ideal undamped system is in resonance, its amplitude increases linearly over time [15]. This is illustrated by the red line in Figure 3.38a, showing a linear growth in amplitude. To achieve a faster response from the metamaterial, an exponential increase in amplitude would be more advantageous. This would necessitate the resonator behaving as an unstable system [20], with its amplitude depicted in Figure 3.38b.

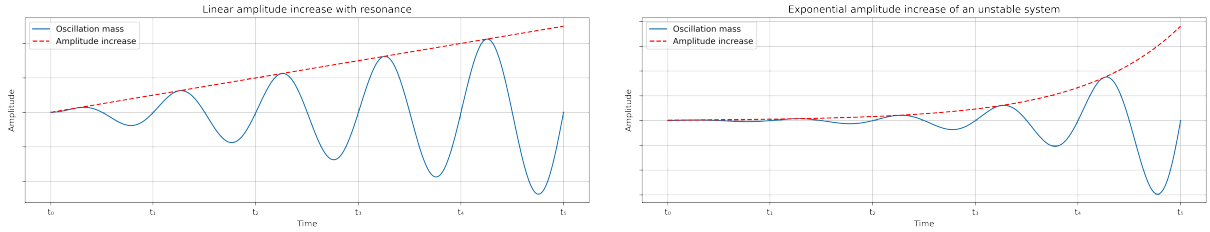

(a) Resonant regime

(b) Unstable regime

Figure 3.38: Amplitude increase resonant versus unstable regime

This indicates that the metawedge requires several seconds of input excitation to achieve significant displacement, during which it effectively extracts energy from the soil and dissipates it through viscous damping. Consequently, the initial few seconds of the input signal pass through the metamaterial with minimal attenuation and reach the receiver almost unaltered. This delay in response represents a limitation inherent to purely local resonance-based metamaterials.

4 Impact-based resonator

In the previous chapters, tuned mass-spring-dampers (TMDs) are used in the design of the metamaterial. The effectiveness of TMDs is frequency dependent, meaning they mitigate certain frequencies, often in a narrow frequency band. The most optimal design of a metamaterial in this research is capable of mitigating harmonic frequencies between 8 and 14 Hz. This makes them ineffective for wideband excitations, since the frequencies excited by trains and traffic contain many different frequencies and are partly transient.

An alternative approach, which relies more on input energy for its effectiveness, is using impact-based dampers. This is inspired by the literature on Nonlinear Energy Sinks (NES) [30], [25], [7]. The NES can absorb energy across different frequencies, but it requires a certain amount of energy such that it passes the threshold of activation.

Drawing from Li [21], this chapter first explores the concept of an impact-based damper. Subsequently, its potential integration into metamaterial applications is discussed.

A new resonator design must satisfy several requirements. Initially, the resonator should be relatively lightweight concerning the primary structure. The impact-based damper should also demonstrate effectiveness across a broad spectrum of excitation frequencies. Furthermore, the impact-based damper needs to maintain robustness despite minor system variations.

An impact-based damper was selected as the energy sink for this research. This mechanism operates by dissipating energy once a specific input energy threshold is reached, with this threshold being frequency-dependent. Impact-based resonators, while possessing a relatively high energy threshold, offer a very quick reaction time. This characteristic makes them particularly well-suited for mitigating shock impacts and absorbing seismic waves. This study will investigate the suitability of this type of resonator for integration into a metamaterial designed to mitigate vibrations originating from traffic or railway systems.

The impact-based resonator operates with non-smooth stiffness. The hard boundaries can be seen as nonlinear springs that are activated when the two parts collide with each other. Between the impacts, the system behaves linearly, but at each inelastic impact, the nonlinearity acts up. New initial conditions are established to be used in the next linear part of the movement.

Energy dissipation via the impact-based damper occurs through two main mechanisms. When the contact happens, energy is lost in the contact in the form of heat, sound and deformation. This energy dissipates from the whole system, so the total energy in the system drops. The second mechanism is the viscous damping. Through the contact, there is a redistribution of energy to higher structural modes. Viscous damping is dependent on the frequency, so with higher frequencies, the viscous dissipation will be higher. Since higher frequencies can be mitigated quicker, this could potentially increase the amount of energy dissipation.

Adnan Saeed's review paper [25] indicates that impact-based dampers appear to offer straightforward implementation, rapid response, and sustained high performance across a broad frequency range.

The review paper indicates that an impact-based resonator can function through two primary mechanisms:

- Double-sided impact-based resonator (DSVI NES)
- Single-sided impact-based resonator (SSVI NES)

The DSVI NES is more extensively researched and is typically implemented in small-scale structures. The SSVI NES is researched more recently and seems to be more efficient than the DSVI NES. It is more used in large-scale structures.

A key challenge of the impact-based resonator is its analytical complexity. Solving this system analytically often requires simplifications. In this research, mostly numerical methods will be used to solve the problem with new resonator.

4.1 Basic resonator

To be able to understand what different parameters can be tuned and what their effect is, a very basic design of an impact-based resonator is made. From the literature [25], the single-sided VI NES is most effective, when designed correctly.

The resonator consists of two mass-spring-damper systems which are in series. $M_1 > m_2$ and the system is excited by a harmonic force on the start of the series. There is a hard boundary connected to M_1 which is installed such that m_2 can have impacts with the boundary. The space between the hard boundary and m_2 is e. A figure of the basic resonator can be seen in Figure 4.1.

Based on the works of Vakakis et al. [30] and Wenke Li et al. [21], a specific version of an impact-based resonator is analyzed. This same version will also be examined in the present research. It is chosen because it can be readily adapted to represent a resonator on soil, with the first mass-spring-damper system (M_1, k_1, and c_1) serving as a simplified model of the soil.

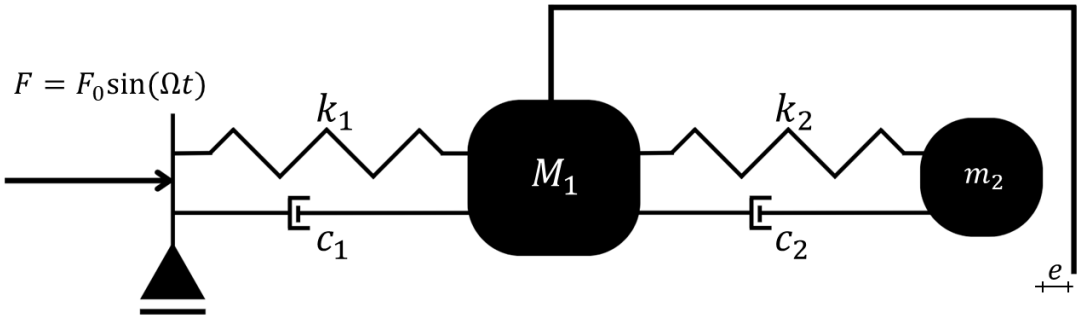

Figure 4.1: Basic impact-based resonator

The model parameters, presented in 4.1, were chosen partially based on A. Vakakis's report [30] and partially on a random basis.

Parameter	Value	Unit
M_1	1	kg
k_1	100	N/m
c_1	0.01	Ns/m
m_2	0.4	kg
k_2	40	N/m
c_2	0.1	Ns/m
e	0.01	m

Table 4.1: Parameter values for the basic impact-based resonator depicted in Figure 4.1

Equation of motion Mass 1:

$$m_1\ddot{u}_1 + k_1u_1 + c_1\dot{u}_1 + k_2(u_1 - u_2) + c_2(\dot{u}_1 - \dot{u}_2) - G(u_1, u_2) = F_0 \cos(\Omega t) \tag{4.1}$$

Equation of motion Mass 2:

$$m_2\ddot{u}_2 + k_2(u_2 - u_1) + c_2(\dot{u}_2 - \dot{u}_1) + G(u_1, u_2) = 0 \tag{4.2}$$

where

$$G(u_1, u_2) = \begin{cases} 0 & \text{if } u_2 - u_1 < 0 \\ k_c(u_1 - u_2)^x & \text{if } u_2 - u_1 \geq 0 \end{cases} \tag{4.3}$$

The hard boundary has a stiffness, which is expressed by the function $G(u_1, u_2)$. Since Abaqus works with a non-constant stiffness parameter x, the value of $G(u_1, u_2)$ cannot be derived analytically.

The equations of motion now consist of different forces, but they can be converted to an energy balance. By multiplying with the velocity, the power balance is obtained. When integrating over time, the energy balance is gotten.

For mass 1:

$$\frac{1}{2}m_1\dot{u}_1^2 + \frac{1}{2}(k_1 + k_2)u_1^2 + \int \left((c_1 + c_2)\dot{u}_1^2\right) dt - \int (k_2 u_2 \dot{u}_1)\, dt - \int (c_2 u_2 \dot{u}_1)\, dt = \int F_0 \cos(\Omega t)\dot{u}_1 dt \tag{4.4}$$

For mass 2:

$$\frac{1}{2}m_2\dot{u}_2^2 + \frac{1}{2}k_2 u_2^2 - \int (k_2 u_1 \dot{u}_2)\, dt + \int \left(c_2\dot{u}_2^2\right) dt - \int (c_2 \dot{u}_1 \dot{u}_2)\, dt + \int \left(G(u_1, u_2)\dot{u}_2\right) dt = 0 \tag{4.5}$$

Given the complexities of analyzing nonlinear systems analytically, energy balances will be used to track where energy in the system is directed. Abaqus provides several energy storage units, enumerated in the following list. Each analytical energy unit can be assigned to one of these Abaqus energy storage terms.

Energy Term	**Expression**
ALLKE (Kinetic Energy)	$\frac{1}{2}m_1\dot{u}_1^2 + \frac{1}{2}m_2\dot{u}_2^2$
ALLIE (Internal Elastic Energy)	$\frac{1}{2}(k_1 + k_2)u_1^2 + \frac{1}{2}k_2 u_2^2$ $- \int k_2 u_2 \dot{u}_1\, dt - \int k_2 u_1 \dot{u}_2\, dt$
ALLAE (Artificial Strain Energy)	$\int G(u_1, u_2)\dot{u}_2\, dt$
ALLVD (Viscous Damping Energy)	$\int (c_1 + c_2)\dot{u}_1^2\, dt + \int c_2\dot{u}_2^2\, dt$ $- \int c_2 \dot{u}_2 \dot{u}_1\, dt - \int c_2 \dot{u}_1 \dot{u}_2\, dt$
ALLWK (Work Done by External Forces)	$\int F_0 \cos(\Omega t)\dot{u}_1 dt$

The model presented in this chapter assumes no damping through contact. The total energy, constant at zero throughout the entire analysis, is constituted by the following factors.

$$E_{total} = E_{kinetic} + E_{internal} + E_{viscous} - E_{work} \tag{4.6}$$

When performing dynamic analyses in Abaqus, both the Implicit and Explicit solver can be employed. Regardless of the solver chosen, it's generally good practice to use small time steps at the beginning of an analysis for accuracy, as well as during moments of contact.

The implicit method solves the system by iterating to find an equilibrium at each time step. While it's unconditionally stable, meaning it can theoretically handle large time steps without

becoming unstable, smaller time steps are often needed to achieve sufficient accuracy. The solver uses the Newton-Raphson method to calculate equilibrium for every time step. This type of analysis is computationally expensive because it involves solving a large number of equations simultaneously, making it best suited for static or quasi-static problems where inertial effects are minimal.

In contrast, the Explicit analysis calculates accelerations based on the applied forces. From these accelerations, velocities and displacements are then determined. This method "explicitly" advances its solution forward in time using information from the previous increment, without iterating to find equilibrium within a time step. Because no equilibrium is calculated at each step, the explicit solver is conditionally stable; the time step used must be smaller than a critical value to maintain numerical stability. The solver is particularly well-suited for highly dynamic events.

For the nonlinear problems discussed in this chapter, which involve sharp discontinuities caused by contact, the explicit solver is often the more accurate and robust choice.

4.1.1 Energy dissipation through resonator

Two different mechanisms are representable for the damping when there is contact between the mass and the rigid boundary.

The first damping mechanism is viscous damping, which acts continuously throughout the motion of the system. It is possible that during an impact, the amount of energy dissipated through viscous damping increases due to the excitation of a broader frequency spectrum, although with lower amplitudes.

By expressing the viscous damping in the frequency domain and calculating the associated dissipated energy, the following energy expression is derived [6]:

$$E = \frac{c}{2\pi} \int_{-\infty}^{+\infty} \omega^2 \, \hat{v}(\omega) \, \hat{v}^*(\omega) \, d\omega \tag{4.7}$$

This equation indicates that energy dissipated through viscous damping increases quadratically with frequency. Theoretically, then, an impact exciting higher frequencies should lead to greater energy dissipation via viscous damping. However, because the amplitudes of these high-frequency components are typically lower, the actual increase in damping might not be as substantial as the frequency dependence alone implies. Given that higher frequencies are generally mitigated more effectively than lower frequencies, this mechanism shows promise and will be investigated further in this study.

The second damping mechanism arises from the impact during contact. When the mass collides with the boundary, a significant portion of kinetic energy is lost. This energy is dissipated through various channels, such as deformation, sound, and heat—each representing a form of energy loss due to impact. This report's analysis doesn't account for this potential energy loss.

If the impact force is sufficiently high to exceed the yield strength of either the mass or the boundary, permanent (plastic) deformation can occur. The associated energy loss, referred to as plastic work, is irreversible and contributes to additional damping. However, in this report, energy loss due to plastic deformation is not considered.

In certain contact scenarios, friction between surfaces may also contribute to energy dissipation. Nevertheless, for the purposes of this model, frictional effects are neglected.

4.2 Parameteric study

This report presents a preliminary study to assess whether the impact-based resonator has potential for mitigating a greater amount of energy. To gain a better understanding of the problem, an energy analysis was conducted using Abaqus. The base model is adopted from the literature, specifically from Vakakis [30] and Wenke Li [21]. Various model configurations are analyzed by examining their respective energy components and performing a time-frequency analysis.

The analysis is based on two key visualizations: a plot of the different energy contributions within the system, and a time-frequency representation. The energy plot provides insight into how much energy is dissipated through viscous damping. The time-frequency analysis reveals the range and distribution of frequencies that are excited as a result of the impact.

The sections below will give the results on changing different parameters. The system is excited with a harmonic force is 5 Hz in an analysis which also takes transients into account.

The eigenfrequencies of the linear system without the hard boundary can be derived with the equation of motions of the system without any external forcing. These are:

$$m_1\ddot{x}_1 + k_1x_1 - k_2(x_2 - x_1) = 0 \tag{4.8}$$

$$m_2\ddot{x}_2 + k_2x_2 - k_2x_1 = 0 \tag{4.9}$$

When computing an Eigenvalue problem, the determinant has to be set to zero.

$$\det\left(\begin{bmatrix} k_1 + k_2 - \omega^2 m_1 & -k_2 \\ -k_2 & k_2 - \omega^2 m_2 \end{bmatrix}\right) = 0$$

When solving this equation, the eigenfrequencies of the system are computed. For this system with parameters from Table 4.1, the eigenfrequencies are 2.17 Hz and 1.17 Hz.

Contact in Abaqus is done via the so-called penalty method. This assumes that the mass can penetrate into the beam. Then, an artificial spring pushes back the mass from the boundary.

4.2.1 Model without boundary

To be able to compare the effects of the contact, first the model without a boundary will be analyzed. The model of Figure 4.1 is taken, but the rigid boundary is taken away. This leads to a two-degree-of-freedom system which is harmonically excited.

The different energy components in this model are shown in Figure 4.2. Initially, there is a rapid increase in viscous damping during the first second, which then transitions to a linear trend toward the end of the simulation. At this stage, the system has reached a steady state, and the cumulative viscous damping increases linearly, as expected. In the system with contact, it is anticipated that the amount of energy dissipated through viscous damping will be even higher. The total energy (ETOTAL) equals zero, indicating that the system behaves as expected. A nonzero total energy would suggest an error in the modelling.

The time-frequency analysis provides insights into the system's dynamic response. Figure 4.3 presents the time-frequency analysis of the model without boundary. With a total of 1000 time steps, a large window of 999 steps (Figure 4.3a) clearly shows a horizontal line, indicating the system's excitation. In contrast, a shorter window of 40 time steps (Figure 4.3b) reveals additional excitations, particularly more transient vibrations within the first two seconds. However, the response remains relatively constant, without significant excitation of different frequencies.

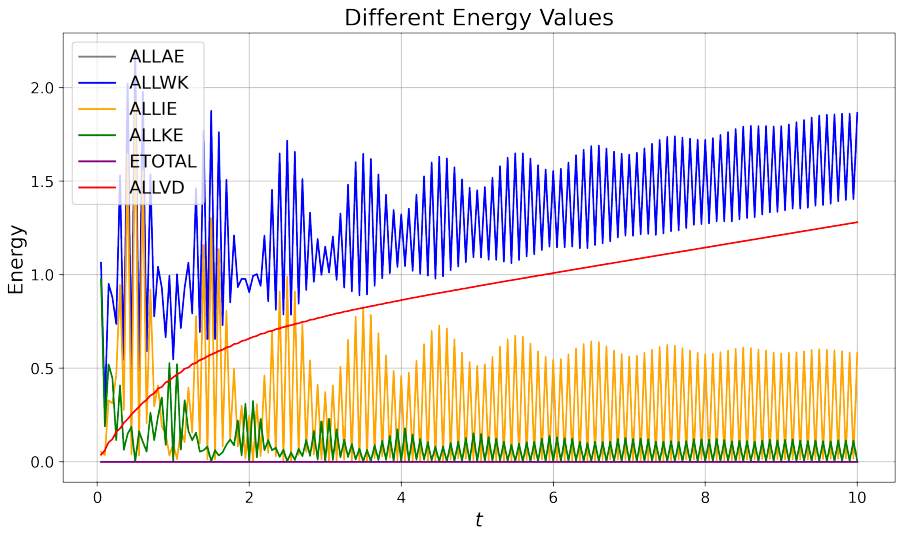

Figure 4.2: Energy plot model without rigid boundary

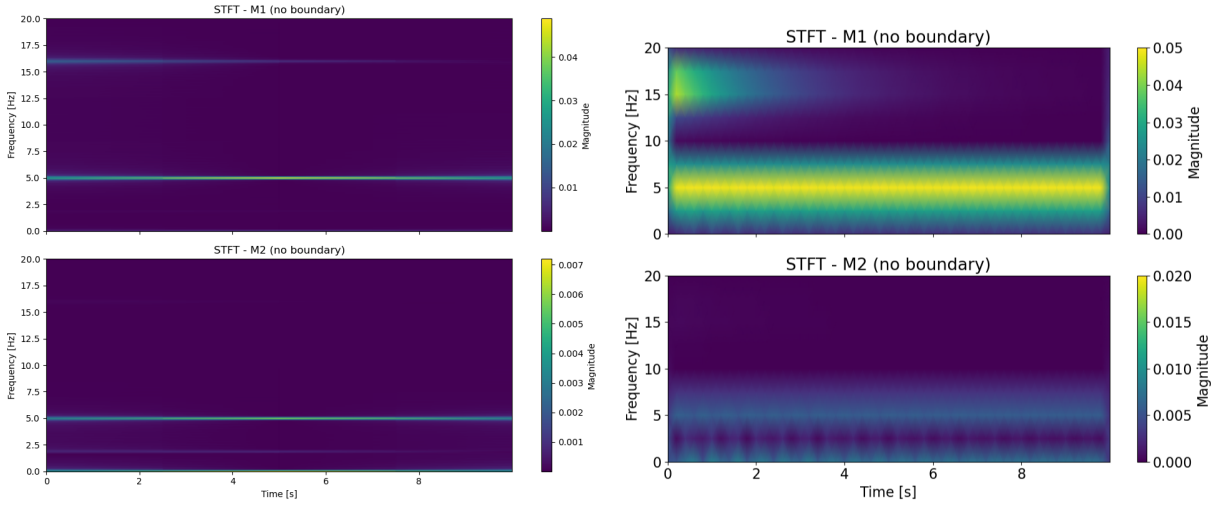

(a) Model without boundary, large time window

(b) Model without boundary, short time window

Figure 4.3: Time-frequency analyses with large and small window

4.2.2 Baseline model

This model was developed using the parameters detailed in Table 4.1. The resulting energy plot, depicted in Figure 4.4, indicates an increase of total work over time. The presence of viscous damping leads to a gradual increase in external work over time, along with a small contribution to the kinetic energy. Due to the contact, higher frequencies are excited, which contribute to higher energy dissipation via viscous damping. In this case, this leads to an increase of 20 percent.

The time-frequency analysis (Figure 4.5) provides insight into the dynamic response of the model with boundary conditions. Compared to the case without boundary, the analysis shows that neither mass 1 nor mass 2 exhibits a single, constant frequency component. At the moment of impact, the frequencies in the time-frequency response of mass 2 increase noticeably, which may contribute to greater energy dissipation through viscous damping. Furthermore, the initially excited frequencies, in the range of approximately 15–20 Hz, appear to persist and propagate further in time than in the case without boundary.

Since only a single parameter set is chosen, it is possible that the system's behavior — and thus the amount of viscous energy dissipation — changes when the parameters are varied. As this

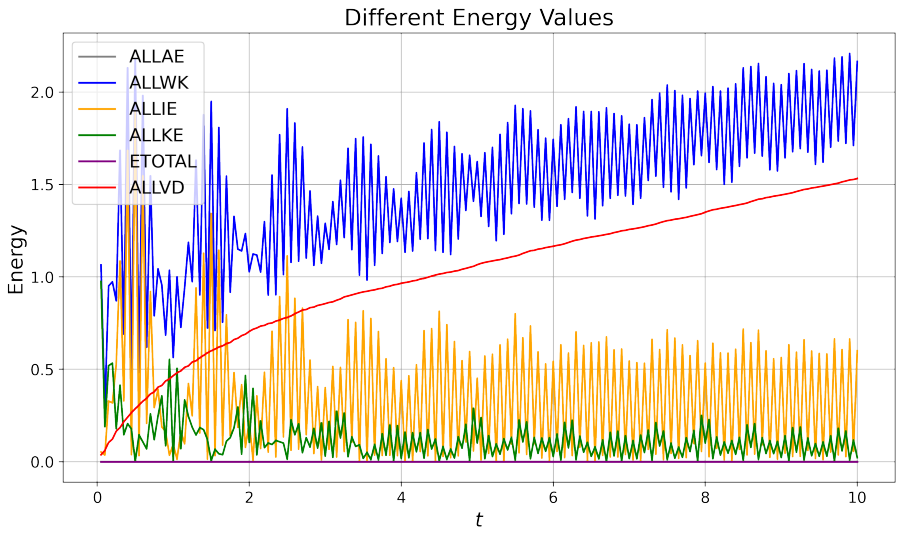

Figure 4.4: Energy plot baseline model

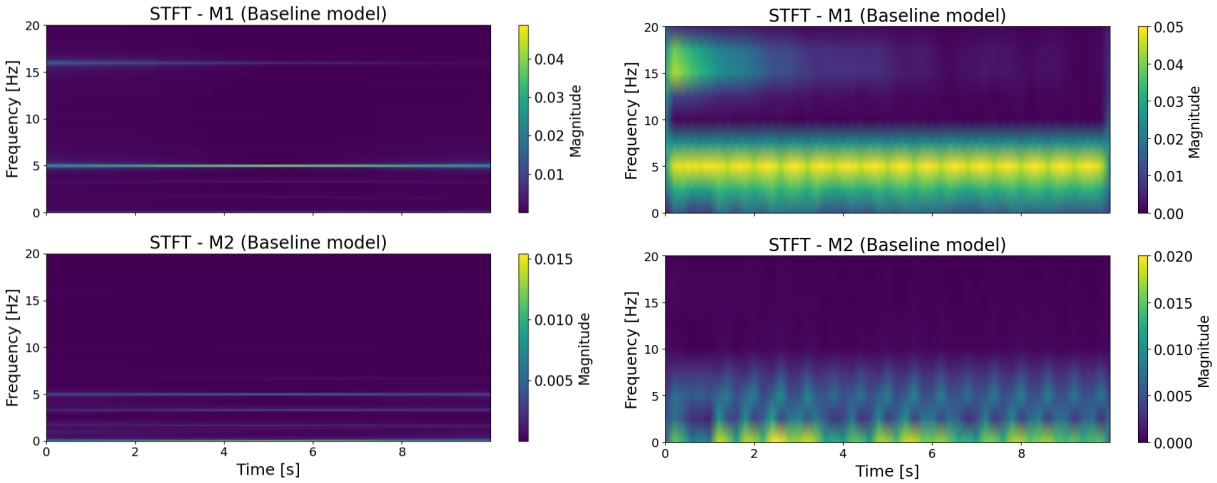

(a) Model without boundary, large time window

(b) Model without boundary, short time window

Figure 4.5: Time-frequency analyses with large and small window

report presents a preliminary investigation of the impact-based resonator, a limited parametric analysis has been carried out for a few selected cases. A full parametric numerical analysis is not feasible within the current Abaqus model.

4.2.3 Changing stiffness

In order to increase energy dissipation via viscous damping, the stiffness parameters were varied in different cases to assess their potential effect on improving viscous damping.

In a linear 2DOF system, the most energy is extracted when the input frequency matches the eigenfrequency of the system. To assess whether this still holds for the nonlinear system, the stiffnesses have been set such that the resonance frequency of the system is at $\omega_n = 5$ Hz. This is done by setting $k_1 = 200$ N/m and $k_2 = 262.8$ N/m.
Examining the energy graph in Figure 4.6 shows that both the total work and the energy dissipated through viscous damping decrease. This effect may be related to the introduction of the boundary, as the resonance frequency appears to have little influence. In this configuration, k_2 is stiffer than k_1.

Since changing the stiffness parameters can have a significant effect on the energy dissipation,

a fair comparison can be made by leaving the stiffness parameters the same as in the Baseline model, but changing the excitation frequency to the eigenfrequency of the system - which is $\omega_n = 2.17$ Hz. Figure 4.7 shows that there is definitely an increase viscous damping at the impact, but since there are not a lot of impacts due to the low excitation the amount of energy dissipation is not increased significantly.

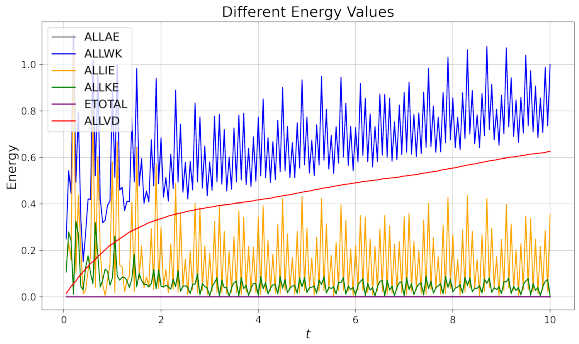

Figure 4.6: Energy plot resonance case, stiffnesses tuned such that $\omega_n = 5$ Hz

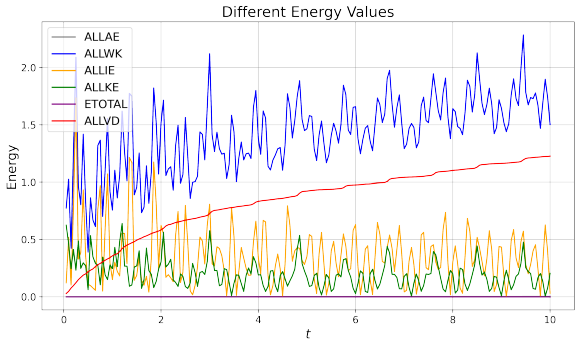

Figure 4.7: Energy plot resonance case, excitation frequency = 2.17 Hz

In addition to analyzing the system at its resonance frequency, different stiffness configurations were tested. In the resonance case, $k_1 < k_2$. In the following sections, the cases $k_1 > k_2$ and $k_1 = k_2$ are examined.

Specifically, the stiffness of k_1 was increased beyond its baseline value, from 100 N/m to 200 N/m, resulting in a parameter set where $k_1 > k_2$. The results, shown in Figure 4.8, indicate that increasing the stiffness of k_1 yields outcomes that are very similar to those observed in the resonance case. This does not lead to higher values of the viscous dissipation.

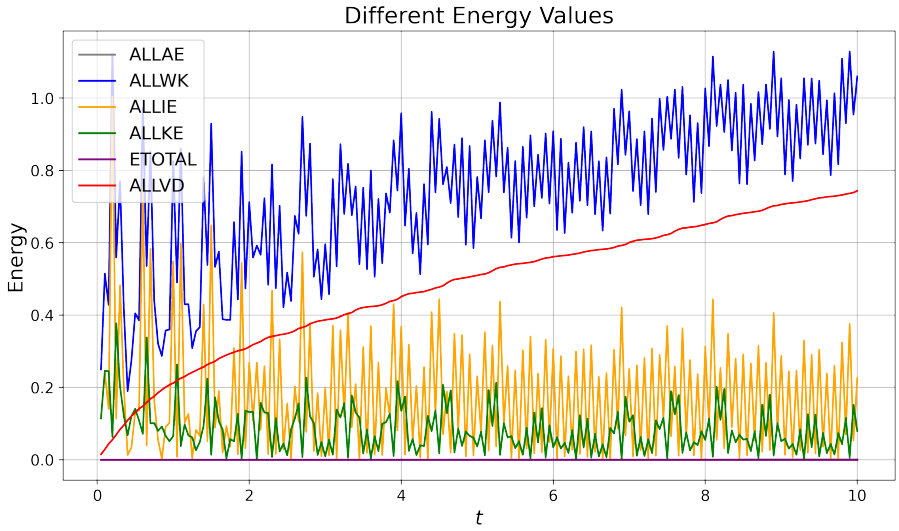

Figure 4.8: Energy plot increased stiffness $k_1 > k_2$, $k_2 = 200$ N/m

The following case is $k_1 = k_2$, and the parameters are set equal at 100 N/m. Figure 4.9 leads to a significant increase of total work and viscous damping. In this case, the viscous damping reaches an even higher value than in the baseline case. The time-frequency analysis shows that there are more frequencies excited in this analysis, as can be seen in Figure 4.10. The system exhibits excited frequencies around 5 Hz, as well as additional components in the range of 15–20 Hz.

From the preliminary parametric study on varying the stiffness parameters, it appears that setting the stiffnesses k_1 and k_2 equal, with a value around 100 N/m, is beneficial for this case.

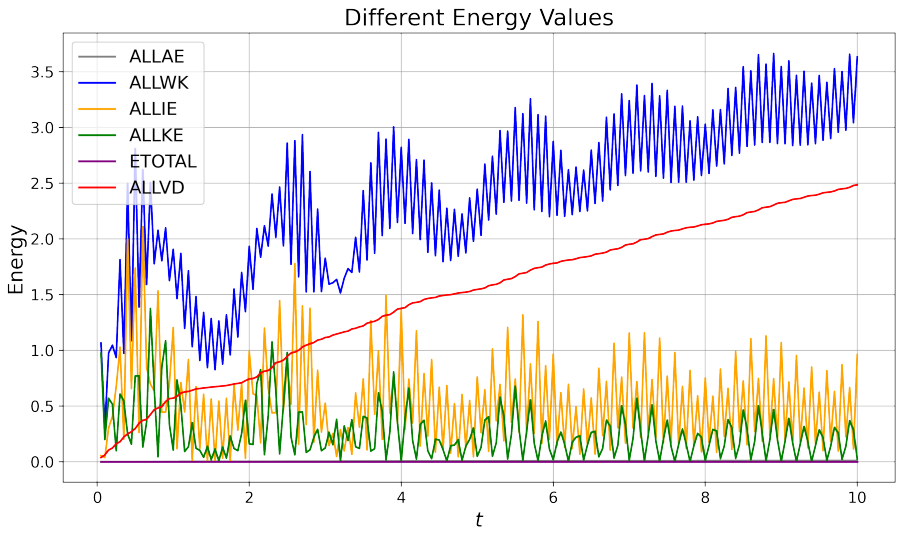

Figure 4.9: Energy plot, $k_1 = k_2 = 100$ N/m

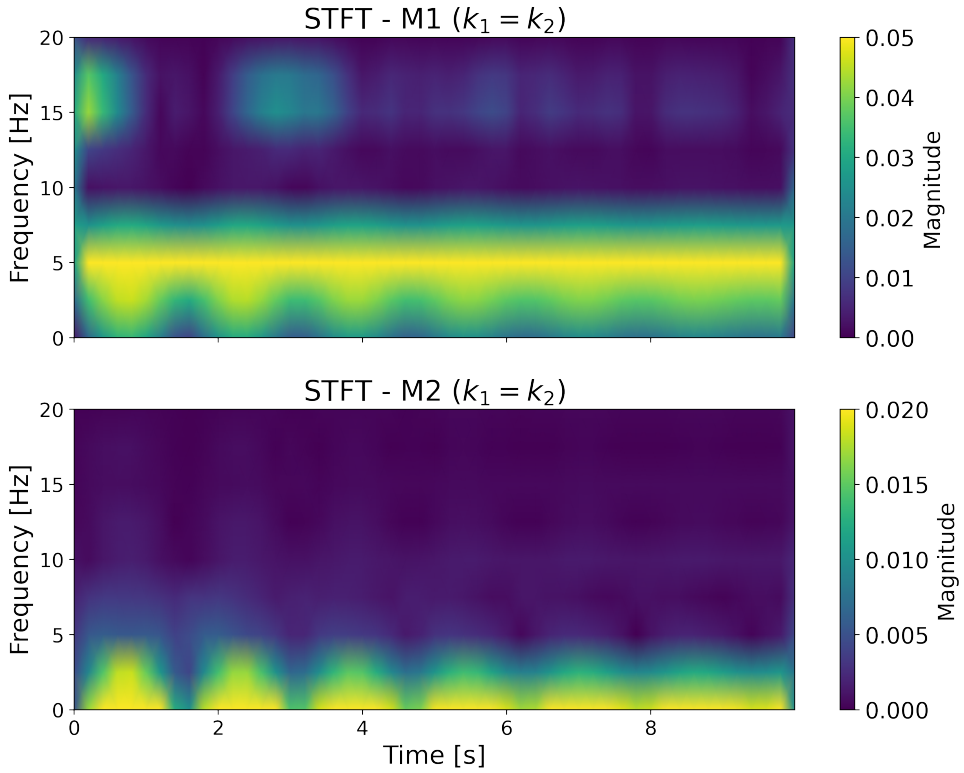

Figure 4.10: Energy plot, $k_2 = k_2 = 100$ N/m

This configuration results in a significant increase in viscous energy dissipation.

4.2.4 Changing Mass 2

To see whether changes in m_2 contribute to a higher viscous damping, there is a strong indication that also when increasing the mass, there is an optimum. When the mass is too small, it is not capable of transferring enough energy to the boundary. When the mass is too large, it takes a lot of energy to get it moving with a low velocity. This leads to a very weak moment of contact, so the energy transfer is also not optimal.

Figure 4.11 shows this optimum. The total amount of viscous damping after 10 seconds is tested

for different values of m_2 and plotted.

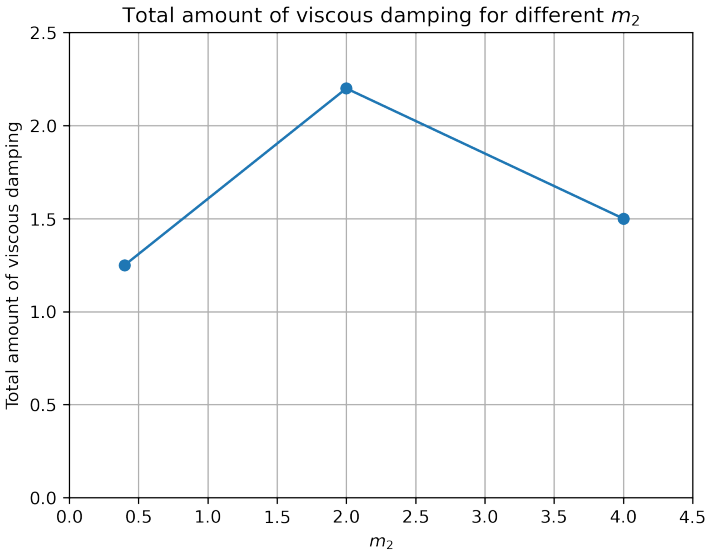

Figure 4.11: Total viscous damping for different m_2 at $t = 10$ seconds

4.2.5 Changing distance to boundary

When increasing the distance to the boundary, the impacts are less powerfull. In the case where m_1 and m_2 are moving in the same direction, but the displacement m_1 is a little more, the masses have contact, but the energy transfer is very low. Therefor, placing the boundary close to the mass at rest is beneficial.

4.3 Impact-based resonator on soil

The results of the analysis in chapter 4.2 look promising, so this paragraph presents the results when modelling the impact-based resonator on a soil domain. The soil domain used is the same as in chapter 3 from this thesis (Figure 3.1).

The resonator is designed with an eigenfrequency of 10 Hz, because then the most movement can be expected. For the first model with impact-based resonators, the parameters stated in Table 4.2 are used.

Parameter	**Value**
Amount of resonators	20
Excitation frequency	10 Hz
Running time	2.5 s
Eigenfrequency	10 Hz
Stiffness k	790000 N/m
Viscous damping c	1 Ns/m
Mass m	200 kg
Distance to boundary e	0.0025 m

Table 4.2: System parameters

4.3.1 Subject to harmonic excitation

This thesis presents preliminary research into an impact-based resonator on a soil domain subjected to a harmonic excitation. Three distinct models are analyzed and compared: a reference case without metamaterial, a case incorporating uniform metawedge without impact

(i.e., no rigid boundary), and a case with uniform metamaterial including impact with a rigid boundary, which leads to contact between the mass-spring system and the boundary. The boundary is connected to the soil, at the node at which the spring of the mass is attached.

A dedicated energy graph is presented to highlight the energy distribution between the two metamaterial models. The energy balance equation for these models features an additional term, ALLQB, which quantifies the energy dissipated via the infinite 'quiet' boundaries at all sides of the soil domain.

Upon examination of the energy graphs (Figure 4.12), it becomes evident that the introduction of a boundary results in an increase in total work, probably done by the boundary. This augmented work is accommodated, in part, by slightly enhanced viscous damping, alongside an observable increase in internal energy, which mostly consist of an increase of the energy in the artificial springs, which is the penalty contact.

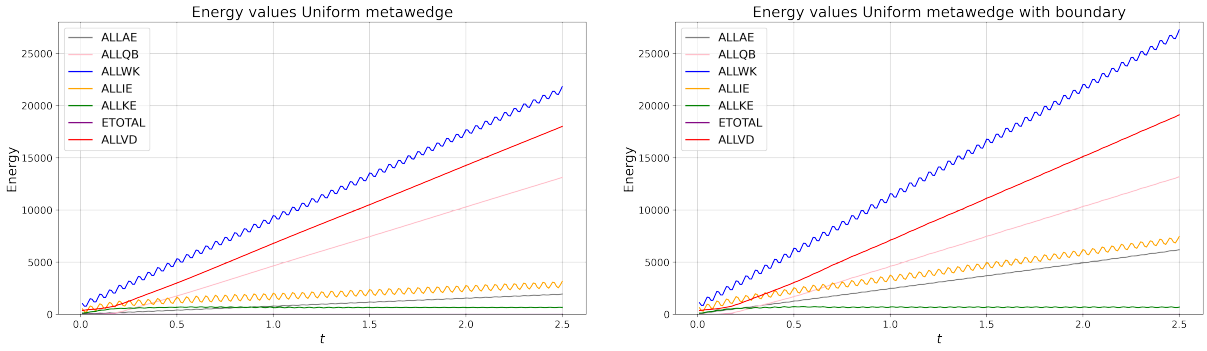

(a) Uniform metawedge

(b) Uniform metawedge with boundary

Figure 4.12: Energy balances of a metamaterial on soil

The time-frequency analysis of the mass of the first resonator tells that there are indeed multiple frequencies excited at the moments of contact. The frequencies excited seem more strongly across a broader range of different frequencies in the case of contact (Figure 4.13b) then in the case without contact (Figure 4.13a).

An analysis of the surface response behind the metawedges reveals some unexpected results. The displacements of the nodes behind the metamaterial increase to nearly twice the level observed without any metamaterial. Figure 4.14a illustrates the maximum displacements at the surface nodes. The frequency response of the displacements (Figure 4.14b) shows that the contact broadens the spectrum, exciting additional frequencies and introducing a new peak near 20 Hz. This indicates that the contact mechanism indeed broadens the range of excited frequencies. However, in this case, the introduction of the boundary also results in significantly higher surface displacements behind the soil.

Since the surface displacements are even higher than in the case without a metamaterial, this outcome is clearly unexpected. Although the choice of parameters can influence the amount of energy dissipated, it remains questionable whether parameter selection alone could explain such an adverse effect on the surface displacements.

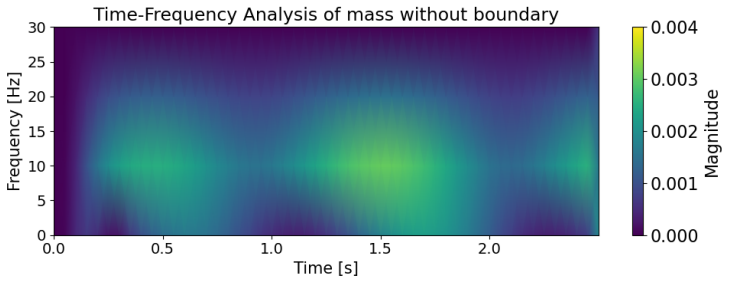

(a) Resonator mass without boundary

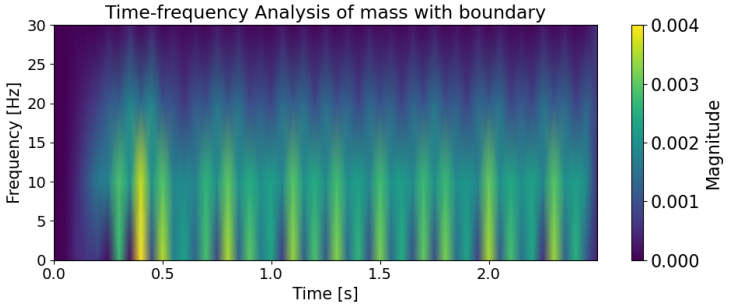

(b) Resonator mass with boundary

Figure 4.13: Time-frequency analysis of the mass of the resonator in two cases

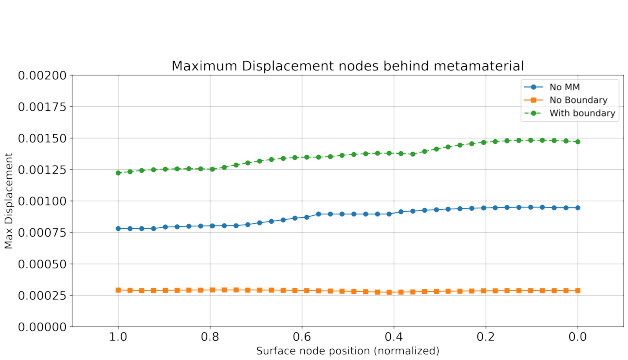

(a) Maximum displacement

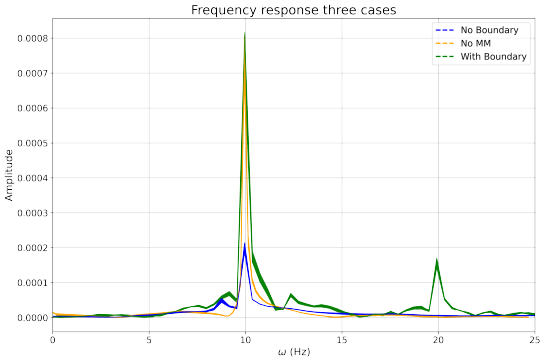

(b) Frequency response

Figure 4.14: Behavior surface nodes behind metamaterial

Several hypotheses may explain why the impact-based resonator, in its current configuration, does not reduce surface displacements effectively:

- Energy is transferred from the mass, through the contact, back into the soil.
- Also frequencies lower than the excitation frequency are excited, leading to a performance decrease of the viscous energy dissipation.
- The chosen parameter set negatively affects the reduction of surface displacements.

To investigate these possibilities, several additional cases were analyzed to better understand the observed behavior.

First, to test whether energy is transferred from the boundary back into the soil, the boundary was disconnected from the soil and fixed at a position above the mass. However, this configuration introduced a different phenomenon that still adversely affected the displacement of the soil surface. As shown in Figure 4.15a, the soil displacement gradually increases downward over time, as the boundary restricts the upward motion of the mass and thus exerts an increasing downward pull on the soil. This is evident when looking at the frequency response of the surface nodes

in Figure 4.15b, which shows a pronounced peak at very low frequencies — consistent with the slow sinking of the soil — while the 10 Hz peak remains unchanged. These observations suggest that this configuration does not mitigate vibrations effectively, and the amplified response at the surface does not appear to be primarily caused by feedback of the impact energy from the boundary into the soil.

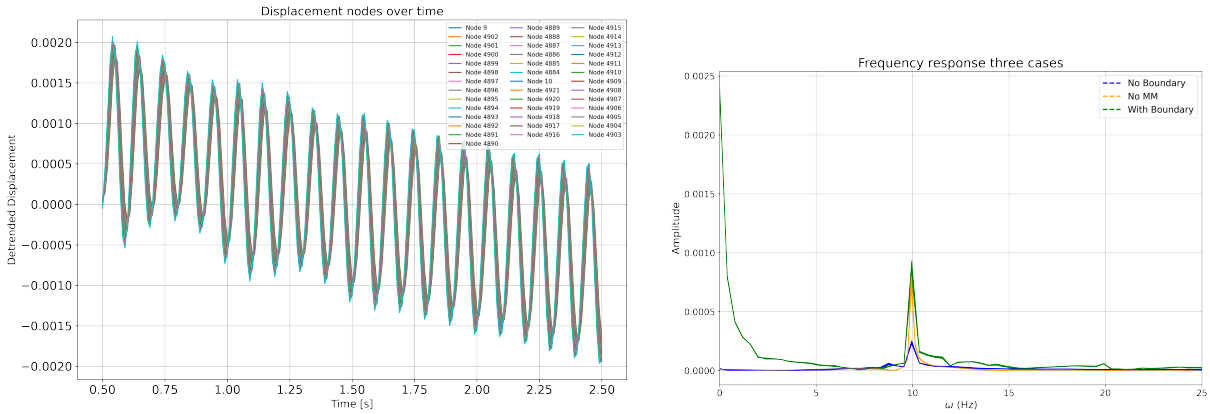

(a) Displacements surface nodes over time

(b) Frequency response

Figure 4.15: Behavior surface nodes behind metamaterial with fixed boundary

To investigate the cause of the high displacement levels observed at the receiver, three parameters were modified in the model with impact-based resonators, shown in Figure 4.16. However, introducing the rigid boundary led in all cases to a higher displacement then when there is no metamaterial placed. The maximum displacements in these cases as well as the frequency response of the surface nodes can be found in Figure 4.17.

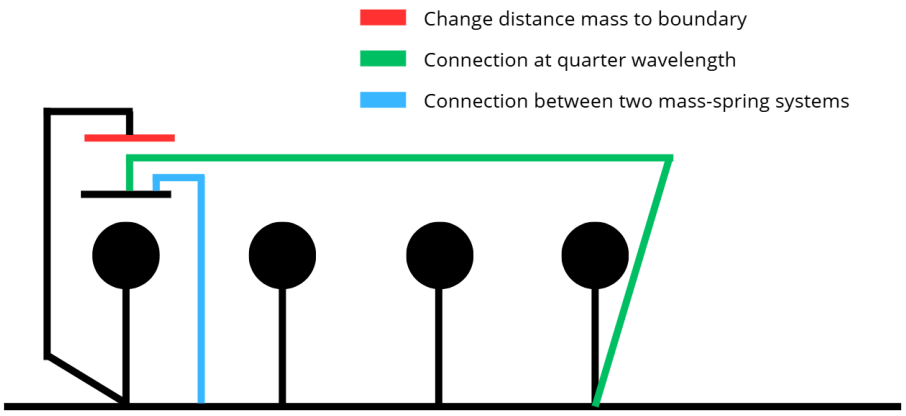

Figure 4.16: 3 changes made in the model

In the first case, the distance between the mass and the boundary was increased, reducing the intensity of their interaction. As a result, the frequency response of the nodes showed a slightly lower peak at 10 Hz, while maintaining a noticeable peak around 20 Hz. For the surface nodes behind the metamaterial, this adjustment led to a modest decrease in displacement compared to the case where the boundary was closer. Nevertheless, the displacements remained relatively high.

In the second case, the way the boundary was connected to the soil was modified. In the initial configuration, the boundary was attached to the same node as the spring. By connecting the boundary to the soil at a quarter wavelength, the phase difference will change. The expectation was to have more impact and thus higher energy dissipation via viscous damping. To investigate

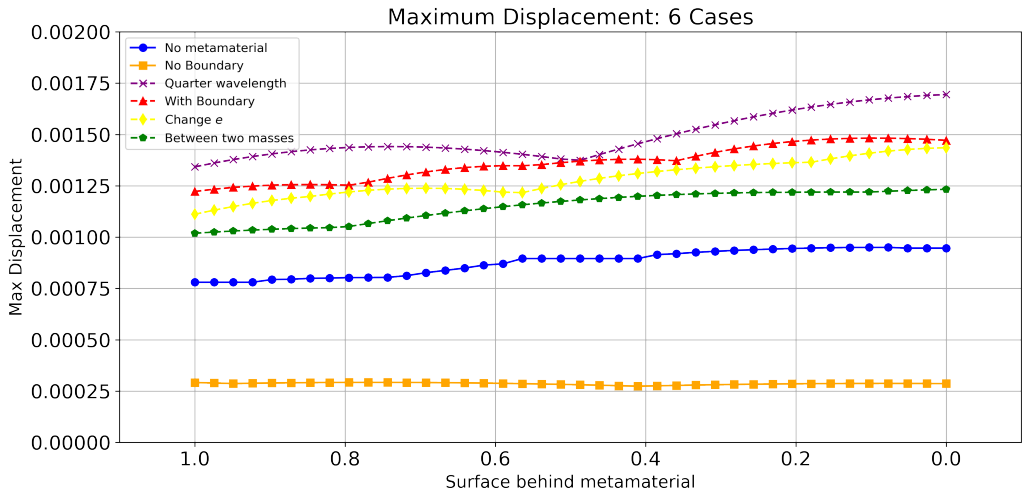

(a) Displacements surface nodes over time

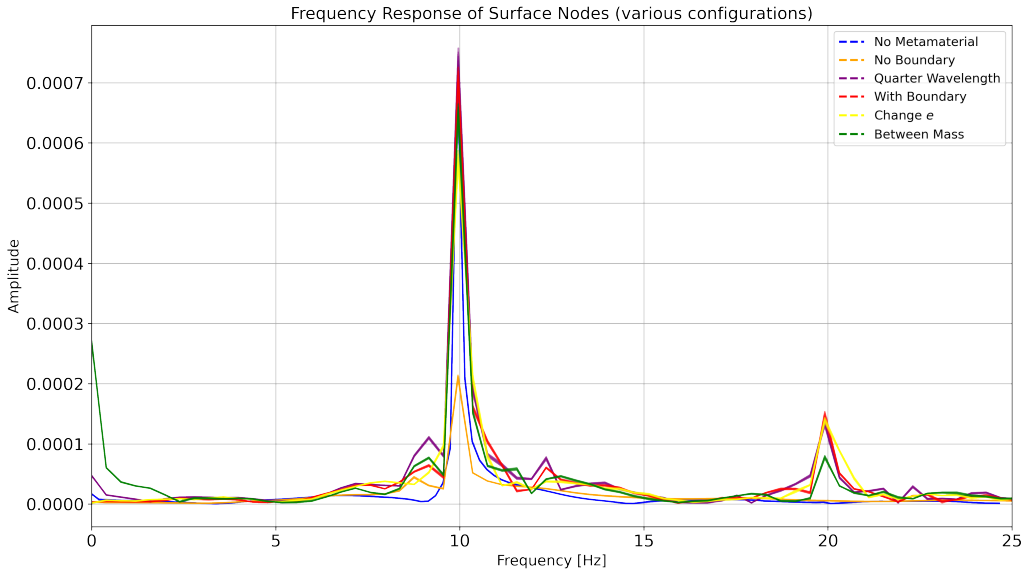

(b) Frequency response

Figure 4.17: Behavior surface nodes behind metamaterial for three different cases

potential improvements, the boundary was connected 2 m to the right of the mass contact point—approximately a quarter wavelength. This new connection was still to a node linked to a spring and therefore subject to significant motion. This change in the model led to even higher displacements at the receiver. At the start of the simulation, the mass and boundary move out of phase, but the moments of impact cause the boundary to move. Since the boundary is attached to the soil, the results differ from the results of a decoupled system. As a result, maintaining an out-of-phase relationship throughout the event proved difficult and the contact did not increase significantly.

It is possible that some energy was redirected from the boundary into the soil due to this connection, passing again through previously excited mass–spring systems. While this was expected to increase viscous damping—as confirmed by the energy graph in Figure 4.18—it unexpectedly resulted in even higher displacements of the surface nodes behind the metamaterial.

The third case that was tested also concerned the connection of the boundary to the soil. Instead of connecting the boundary at a node to which a spring is attached, the connection was made exactly in the middle between two masses. In this configuration, the soil absorbs the first part of the energy transferred back to it, instead of the energy being directly transmitted to the

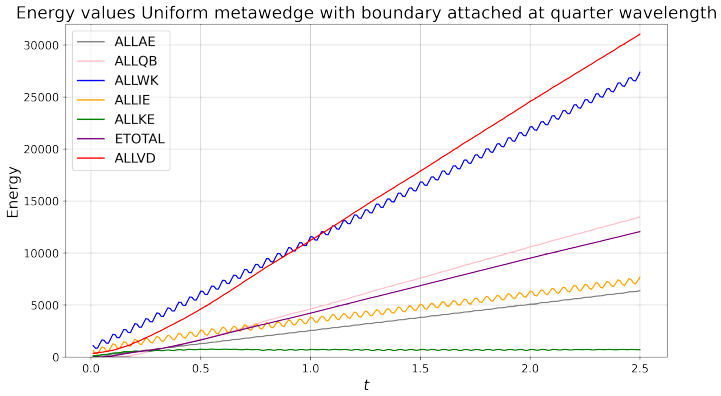

Figure 4.18: Energy plot of system with boundary attached at quarter wavelength to the right

mass–spring system.
The energy graph (Figure 4.19) shows that in this case, the viscous energy dissipation is also significantly increased. The displacements (Figure 4.17) of the nodes behind the metamaterial are lower than in the first case with boundary, but still larger than the scenario without mitigation. In the frequency response graph of the nodes behind the metamaterial, a peak appears at very low frequencies. This corresponds to the soil being gradually pushed down. In this case, the boundary does not respond as strongly as in the other configurations, and can therefore be considered semi-fixed. The same phenomenon is observed here: the soil is pushed down due to a (semi-)fixed boundary.

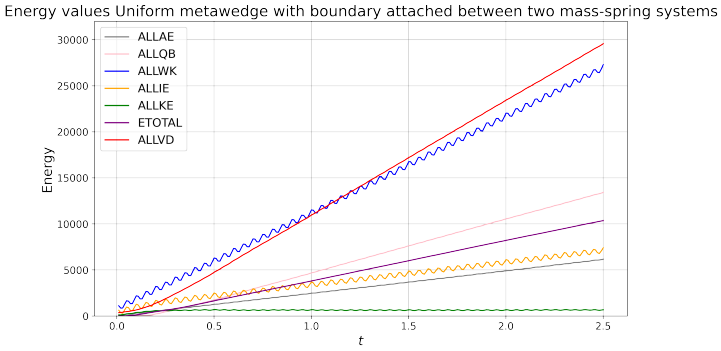

Figure 4.19: Energy plot of system with boundary attached between two mass-spring systems

With these changes, there is still no conclusive explanation as to why the impact-based resonator on soil results in an increase of the displacements of the surface nodes. Regarding the initial hypotheses: it is most likely not due to energy being transferred back to the soil via the boundary, nor due to lower frequencies being excited that would cause this counterintuitive behavior. A full parametric study could not be conducted within the scope of this preliminary research. Nevertheless, it remains puzzling that even with suboptimal parameter choices, the displacements of the surface nodes increase compared to the case without the metamaterial — and without viscous damping.

Although the 2-DOF system demonstrated promising results for an impact-based resonator, its application to a soil domain produced results that cannot yet be satisfactorily explained. Due to time constraints, a full explanation could not be developed. However, based on the results obtained so far, several design requirements and lessons have been identified. These will be discussed in the next chapter.

5 Limitations and design requirements

This chapter provides an overview of the research, outlining the study's limitations. It also presents the practical implications of the findings as design requirements for engineers.

5.1 Limitations of thesis

Before addressing the research questions, a general evaluation of the research will be conducted, examining some critical assumptions or parts of the analysis within the study. This evaluation will first discuss limitations within the model of the soil domain, followed by a discussion about the assessment of the metawedges. After that, the limitations on the study of the impact-based damper are discussed.

The soil model employed in this research is highly simplified. Only density, Young's modulus, and the Poisson ratio are taken into account in the soil domain, and the entire analysis is performed in 2D. Incorporating a specific amount of damping, adding soil layers, or conducting the analysis in 2.5D or 3D would introduce greater complexity to the research and could introduce some other mechanisms, but it would contribute to making it more realistic.

The amplitude of the harmonic forcing applied to the soil domain is not based on a realistic value. Consequently, the numerical results might yield absolute values that are not representative of real-life scenarios. However, the general behavior and comparisons between different metawedges and designs are not affected by a non-realistic amplitude and can be considered correct, even in reality.
The amplitude in the case study needed amplification to be used as an input parameter. A factor of 1000 was used, but a factor of 200 would have been more appropriate to achieve the same ground velocity at the nodes behind the metamaterial as observed in the measurements. Still, in this case, the comparisons and behavior are not affected, only the numerical absolute values.

When considering the assessment for metawedges at different frequencies, the results are compared to the case without metamaterial with a harmonic frequency of 10 Hz. Exciting the soil with another frequency at the same amplitude would lead to a different energy flux in the case without a metamaterial. The frequencies compared to the 10 Hz case do not differ substantially, so the results are usable but not entirely fair.

Then, throughout the whole report, the damping coefficient is chosen as a low value $\zeta = 0.001$. However, this means that the damping coefficient is dependent on the mass. The amount of damping can change the mechanism, and with that the performance of the metamaterial, while resonators can be designed such that the damping coefficient is independent of the mass. Therefor, adviced is to use the same amount of viscous damping per meter in follow-up research.

This report explores the efficacy of an impact-based damper, used as a resonator, in contrast to a traditional uniform metawedge, specifically under harmonic excitation. While the impact-based damper holds significant promise for large, transient impacts, further investigation into these transient vibration scenarios was not feasible within the scope of this research due to time and numerical running time limitations.

5.2 Design requirements for engineers

This section offers practical guidance on applying metamaterials, drawing from the insights gained in this research.

Locally resonant metamaterials

To determine if a metamaterial is suitable for a given scenario, the input force needs to be analyzed first. If the input force exhibits a largely harmonic behavior with a significant amplitude

for a sufficient amount of time, the metamaterial will have enough time to respond and resonate, leading to large displacements. This differs for every scenario, depending on how much viscous damping there is applied. If the signal is more transient, a locally resonant metamaterial might not be the best option for mitigating those vibrations.

If a metamaterial is deemed suitable, the next step is to identify the target frequencies. If there's only one target frequency, a uniform metawedge will perform optimally. The parameters of the mass-spring systems should be adjusted so that their eigenfrequency matches the target frequency.

If dealing with multiple target frequencies, it's crucial to consider the metamaterial's surrounding environment. If the environment can tolerate an amplification of energy levels related to the input force, a wave conversion metawedge will be most effective. Conversely, if the surrounding environment is sensitive to increased energy levels, the rainbow trapping metawedge is the right choice for that application.

The parameters of both the wave-conversion metawedge and the rainbow-trapping metawedge can be determined based on the design criteria detailed in section 3.5 of this thesis.
The first design principle states that the resonators can be placed very close to each other, as the spacing between them has little impact on the metawedge's performance.
The second design principle focuses on the resonator bandwidth, which is quantified using the coefficient of relative resonator bandwidth:

$$0.025 < RRBN = \frac{f_{high} - f_{low}}{f_{center} \cdot N} < 0.030 \tag{5.1}$$

This formula accounts for the highest, lowest, and central eigenfrequencies of the resonators, as well as the total number of resonators. Assuming a linear gradient, it determines the parameters of the resonators.
The third design criterion offers guidance on selecting appropriate masses. To maintain good performance while considering cost and resource constraints, masses in the range of 100–200 kg are recommended.

Impact-based resonator on soil

While a blueprint for success is not available yet, some important lessons were learned about what does not work. It seems that attaching a boundary to the same node as the spring, especially with a fixed boundary, does not help in decreasing the surface displacement of the soil.

Even more surprisingly, placing this boundary connection closer to the input force than where the boundary itself is located actually led to even larger amount of contact, more potential energy redirection through the resonators and eventually greater soil displacements. This highlights that the behavior of this system cannot be explained yet.

A more promising avenue involved placing the connection between the boundary and the soil between two mass-spring systems. This arrangement seems to allow the soil to absorb vibrations from the boundary more effectively before they reach the mass-spring system, which in turn means the boundary itself doesn't vibrate as much.

Lastly, adjusting the gap between the mass and the boundary did not significantly alter how the system behaved.

6 Conclusion

The conclusion will address all three research questions and provide corresponding answers.

Which metawedge design provides the most effective solution for mitigating ground-borne vibrations?

Given that ground-borne vibrations exhibit their highest energy content near 10 Hz, this frequency became the central focus of the research. To address the sub-question concerning the influence of mass, stiffness, and damping variations on vibration mitigation, the metamaterial was positioned on a beam, limiting the mitigation mechanism to dissipation. Findings indicate that increasing the metamaterial's mass directly improves performance by augmenting its capacity to draw energy from the vibrating system. Adjustments to stiffness were made in tandem with mass changes to ensure the metamaterial's eigenfrequency remained tuned to the 10 Hz target. While greater viscous damping extends the mitigation frequency range, it leads to lower overall performance. The introduction of an inerter leads to a shift of the metamaterial's eigenfrequency downwards, but also results in reduced bandgap and performance.

To assess the most effective design, the metamaterial was tested as a metawedge on a soil domain with a harmonic frequency. Three distinct designs were evaluated in this research. The Uniform metawedge was found to be tuned for mitigating a specific, single frequency. The rainbow trapping metawedge functions by slowing and trapping waves using "elastic rainbow trapping." The third design, the wave conversion metawedge, works by speeding up waves, which converts surface waves into body waves that are subsequently redirected from the surface.

The wave conversion metawedge proves most effective for energy mitigation at the surface, though its wave redirection mechanism could result in elevated energy levels in the surrounding environment.
In contrast, the rainbow trapping metawedge achieves less surface energy flux mitigation directly behind the metamaterial, but it ultimately reduces the total energy flux due to its dissipating nature.

For both the wave conversion and rainbow trapping metawedges, energy mitigation performance decreases when the excitation frequency matches the eigenfrequencies of the resonators at the metamaterial's edges.

How do design parameters such as number of resonators, target frequency, resonator spacing and resonator mass influence the effectiveness of metamaterials in mitigating ground-borne vibrations? Can these components be captured in design criteria?

To identify the minimum number of resonators needed for an effective wave conversion or rainbow trapping metawedge, this study introduces an improved evaluation criterion: the relative resonator bandwidth coefficient (RRBN). The RRBN is defined based on the highest, lowest, and center eigenfrequencies of the metawedge (f_{high}, f_{low}, f_{center}) along with the number of resonators (N), and it indicates the range of frequencies that can be effectively targeted.

$$0.025 < RRBN = \frac{f_{high} - f_{low}}{f_{center} \cdot N} < 0.030 \tag{6.1}$$

This formula is based on the principle that lower frequencies are more challenging to mitigate than higher ones. Consequently, mitigating a band of low frequencies requires a smaller gap between the eigenfrequencies of the resonators, which in turn means more resonators are needed.

Increasing the number of resonators (N) can lead to the coefficient dropping below 0.025. Generally, a higher number of resonators results in greater energy dissipation through them. As

the gap between the eigenfrequencies of the resonators becomes quite small, the mechanism of the uniform metawedge will be utilized more.

Results indicate that frequencies in the middle of a resonator's bandwidth achieve optimal mitigation. Therefore, the target frequency should be located within the middle third of the resonators' eigenfrequency bandwidth. It's worth noting that if the target frequency falls on the higher side of this middle third, the mitigation of energy flux will see a slight increase compared to the lower side of the middle third.

The target frequency of 10 Hz corresponds to relatively large wavelengths. In this study, locally resonant metamaterials were chosen over those relying on Bragg scattering. Locally resonant metamaterials operate based on the semi-wavelength. When the resonators are spaced with respect to the wavelength, the distance between them has little influence on the metamaterial's performance, allowing the mitigation device to be made very compact without significant loss of effectiveness.

A higher resonator mass generally leads to better mitigation. When the mass becomes excessively high, the metamaterial's unique mechanism is superseded by simple wave blocking, akin to conventional methods. However, when looking at resources and the effect of adding mass, the optimum mass lays between 100 and 200 kg.

What is the effect of an impact-based resonator and how does incorporating an impact-based resonator influence the performance of a metawedge for wave mitigation?

The performance of an impact-based resonator was evaluated using two methods: a simple 2-degree-of-freedom (2DOF) system and a series of resonators placed on a soil domain, both subjected to harmonic frequency excitation.

The primary damping mechanism considered in this analysis is the redistribution of frequencies that occurs during contact. The amount of energy dissipated through viscous damping is dependent on the excited frequency, and contact itself leads to an increase in this viscous damping.

The 2DOF system showed that, in certain configurations, viscous damping indeed increases. However, when implementing the impact-based resonator in series on a soil domain, this resulted in a significant increase in surface displacement beyond the metamaterial. Several modifications to the model were explored, but no conclusive explanation has yet been identified for the mechanism responsible for these high energy levels.

The analysis did not account for damping from the contact itself, which includes energy dissipated as heat, sound, and deformation; considering this could show an even greater increase in dissipated energy. Additionally, due to its nonlinear nature, the resonator's full potential may be in dissipating multiple frequencies, such as transient vibrations. In these scenarios, it could potentially outperform the traditional metawedges discussed in this report.

6.1 Recommendations

This study serves as a foundational step for designing various metawedges. To enhance their effectiveness, two promising methods warrant further investigation.

Currently, a linear relationship is assumed for the eigenfrequencies of the resonators. However, given that lower frequencies are inherently more challenging to mitigate than higher frequencies, future research could explore alternative relationships. Specifically, resonators with lower natural frequencies could be placed closer together (in terms of their eigenfrequencies), while those with higher natural frequencies are spaced further apart. This strategic arrangement could potentially broaden the bandgap without increasing the total number of resonators. Additionally, while

Rayleigh waves primarily exhibit a strong vertical motion along the surface, they also possess a horizontal component. To achieve comprehensive motion mitigation, it would be advantageous to research resonators capable of movement in both vertical and horizontal directions.

The second part of this research investigated the potential of an impact-based damper as a resonator. Initial findings from the 2DOF system suggest it holds promise. Further research could delve into the potential of impact-based resonators when exposed to more transient signals. Real-world signals often comprise both transient and harmonic vibrations. Therefore, future studies could explore a combined approach, which utilizes an impact-based damper to absorb the initial, high-impact transient vibrations, and then employs a traditional metawedge to damp out the subsequent harmonic vibrations. To understand more of the reason why the soil displacement increases when conducting an impact-based resonator on soil, more research should be conducted on the parameters of the impact-based damper. This could potentially lead to the implementation Targeted Energy Transfer in the form of a Nonlinear Energy Sink. In this case, the energy extracted from the soil is not transferred back to the surface. Lastly, to reduce the reaction time within the metamaterial, further research could focus on unstable resonators. Their capacity for exponential amplitude growth might prove beneficial in accelerating the material's response.

During this thesis, two other promising approaches to enhancing the performance of the metamaterial emerged. The first involves the use of particle dampers. Unlike a single point of contact, particle dampers consist of many particles interacting with each other, resulting in more contact moments, and thus significantly higher damping.
The second approach is to widen the bandgap by employing a two-degree-of-freedom resonator, which can be modelled as two mass–spring systems stacked on top of each other. This configuration has two eigenfrequencies and can therefore attenuate a broader frequency range.

As the complexity of the soil model increases to 2.5D or 3D, the placement of resonators can be further optimized. Considering that the precise distance between resonators may not be critically important, exploring their arrangement in a chessboard pattern could be a valuable avenue.

Bibliography

Bracci, A. (2021). *Assessment of Stiff Trench and Metawedge as Mitigation Measures for Railway Induced Ground Vibration*. URL: https://www.politesi.polimi.it/retrieve/93ba0b4a-be0c-4343-b140-dc647418f11c/2022_4_Bracci_01.pdf.

Bracci, A., A. Fărăgău, A.V. Metrikine, K. van Dalen, R. Corradi, and E. Vlijm (2023). "On the effectiveness of periodic structures in the mitigation of ground vibrations induced by surface sources". In: *Journal of Physics: Conference Series* 2647. URL: https://doi.org/10.1088/1742-6596/2647/20/202003.

Cao, Y., Q. Xiang, B. Li, and Z. Li (2023). "Field measurement and energy analysis of ground-borne vibration around high-speed railway viaduct". In: URL: https://onlinelibrary.wiley.com/doi/10.1155/2023/4640726.

Colombi, A., P. Roux, S. Guenneau, D. Colquitt, and R. V. Craster (2016). "A seismic metamaterial: The resonant metawedge". In: URL: https://www.nature.com/articles/srep27717.

Contreras N. Zhang, X., H. Hao, and F. Hernández (2024). "Application of elastic metamaterials/meta-structures in civil engineering: A review". In: *Engineering Structures*. URL: https://www.sciencedirect.com/science/article/pii/S0263822323010097?via%3Dihub.

Dalen, K. N. van and A. V. Metrikine (2008). "Transition radiation of elastic waves at the interface of two elastic half-planes". In: *Journal of Sound and Vibration* 310, pp. 702–717. URL: https://doi.org/10.1016/j.jsv.2007.06.007.

Ding, H. and L. Chen (2020). "Designs, analysis, and applications of nonlinear energy sinks". In: *Nonlinear Dynamics*. URL: https://doi.org/10.1007/s11071-020-05724-1.

Elmadih, W., D. Chronopoulos, W. P. Syam, I. Maskery, H. Meng, and R.K. Leach (2019). "Three-dimensional resonating metamaterials for low-frequency vibration attenuation". In: URL: https://doi.org/10.1038/s41598-019-47644-0.

Euphonics (n.d.). *Sources of nonlinearity: smooth and non-smooth*. Accessed 2024. URL: https://euphonics.org/8-2-2-duffings-equation-and-harmonic-balance/.

Eurostat (2024). *Urban–rural Europe – demographic developments in cities*. Statistics Explained, European Commission. URL: https://ec.europa.eu/eurostat/statistics-explained/index.php?title=Urban-rural_Europe_-_demographic_developments_in_cities.

Fărăgău, A., S. van Gaal, E. Vlijm, A.V. Metrikine, A. Tsouvalas, and K. van Dalen (2024a). "Mitigating Ground-borne Vibration Induced by Railway Traffic Using Metamaterials". In: *International Congress on Sound and Vibration*. URL: https://iiav.org/content/archives_icsv_last/2024_icsv30/content/papers/papers/full_paper_776_20240416163757373.pdf.

Fărăgău, A. B., S. van Gaal, E. Vlijm, A. Metrikine, A. Tsouvalas, and K. N. van Dalen (2024b). "Performance Comparison of the Forward and Inverse Metawedge for Ground-Borne Vibration Mitigation". In: *Canadian Congress of Computational Mechanics*. URL: https://doi.org/10.4203/ccc.7.13.8.

Gaal, S. van (2024). *The Mitigation of Train-Induced Ground-Borne Vibrations: A Metamaterial-Based Solution*. https://repository.tudelft.nl/record/uuid:eddec6fb-89e8-490a-ab10-0f804e555c78. Accessed 2024.

Georgiadis, P. and A. Hancock (2024). *Can Europe's trains compete with low-cost airlines?* Financial Times. URL: https://www.ft.com/content/b5591361-7e10-4926-ae90-851fb5c1520d.

Goldstein, H. (2002). *Classical Mechanics (3rd Edition)*. Addison-Wesley.

Hussein, M. I., M. J. Leamy, and M. Ruzzene (2014). "Dynamics of phononic materials and structures: historical origins, recent progress, and future outlook". In: URL: https://doi.org/10.1115/1.4026911.

Kaláb, Z., M. Lednická, R. Korínek, and E. Hrubesová (2011). "Influence of local geological pattern on values of vibrations induced by road traffic". In: *Procedia Engineering*. URL: https:

//www.researchgate.net/publication/257908313_Influence_of_local_geological_pattern_on_values_of_vibrations_induced_by_road_traffic.

Kanellopoulos, C., N. Psycharis, H. Yang, B. Jeremić, I. Anastasopoulos, and B. Stojadinović (2022). "Seismic resonant metamaterials for the protection of an elastic-plastic SDOF system against vertically propagating seismic shear waves (SH) in nonlinear soil". In: *Soil Dynamics and Earthquake Engineering* 162. URL: https://doi.org/10.1016/j.soildyn.2022.107366.

Kempen, E. van, J. Hoekstra, S. Simon, A. Kok, J. van de Kassteele, and H. van Wijnen (2024). *Annoyance and sleep disturbance due to vibrations from trains*. Accessed 2024. URL: https://rivm.openrepository.com/handle/10029/628235.

Landau, L. D. and E. M. Lifshitz (1976). *Mechanics (3rd ed., Vol. 1)*. Pergamon Press.

Li, W., N.E. Wierschem, X. Li, and T. Yang (2018). "On the energy transfer mechanism of the single-sided vibro-impact nonlinear energy sink". In: *Journal of Sound and Vibration* 437. URL: https://www.sciencedirect.com/science/article/pii/S0022460X18305716?via%3Dihub.

Li, Z., Y. Cao, M. Ma, and Q. Xiang (2023). "Prediction of ground-borne vibration from random traffic flow and road roughness: Theoretical model and experimental validation". In: *Engineering Structures* 285. URL: https://www.sciencedirect.com/science/article/abs/pii/S0141029623004741.

Lou, J., S. Zhang, H. Fan, X. Fang, and J. Du (2025). "Ultra-low frequency and broadband flexural wave attenuation using an inertant nonlinear metamaterial beam". In: *Engineering Structures* 323. URL: https://doi.org/10.1016/j.engstruct.2024.119169.

Muhammed, A., C.W. Lim, and K.K. Zúr (2021). "Wide Rayleigh waves bandgap engineered metabarriers for ground borne vibration attenuation". In: *Engineering Structures* 246. URL: https://doi.org/10.1016/j.engstruct.2021.113019.

Saeed, A. S., R. A. Nasar, and M. A. Sl-Shudeifat (2023). "A review on nonlinear energy sinks: designs, analysis and applications of impact and rotary types". In: *Nonlinear Dynamics*. URL: https://doi.org/10.1007/s11071-022-08094-y.

Selvadurai, A. P. S. (1999). "On Boussinesq's problem". In: URL: https://www.researchgate.net/publication/256732359_On_Boussinesq's_problem.

Smith, M. C. (2020). "The Inerter: A Retrospective". In: *Annual Review of Control, Robotics, and Autonomous Systems* 3, pp. 361–391. URL: https://doi.org/10.1146/annurev-control-053018-023917.

Suhairy, S. Al (2000). *Prediction of ground vibration from railways*. URL: https://www.schiu.com/utilidades/artigos/Artigo-MetodoSuecoPrevisaoVibracao.pdf.

Sun, Xiaojing (2021). "Ground vibration from freight railway: environmental impact and potential mitigation measure at propagation path". In: *Environmental Science and Pollution Research* 29. URL: https://link.springer.com/article/10.1007/s11356-022-18955-z.

Vakakis, A. F., O.V. Gendelman, L.A. Bergman, D.M. McFarland, G. Kerschen, and Y.S. Lee (2008). *Nonlinear Targeted Energy Transfer in Mechanical and Structural Systems I*. Springer.

Vos, P. de (2017). *Railway Induced Vibration: state of the art report*. Accessed 2024. URL: https://uic.org/IMG/pdf/uic-railway-induced-vibration-report-2017.pdf.

Xiao, L., Z. Cao, Y. Xu, X. Pu, and Y. Cai (2025). "Resonant topological metasurface for Rayleigh wave attenuation and energy localization in homogeneous and layered elastic half-spaces". In: *Journal of Sound and Vibration* 609. URL: https://doi.org/10.1016/j.jsv.2025.119112.

Appendices

Appendix A: Frequency spectra coming from moving loads

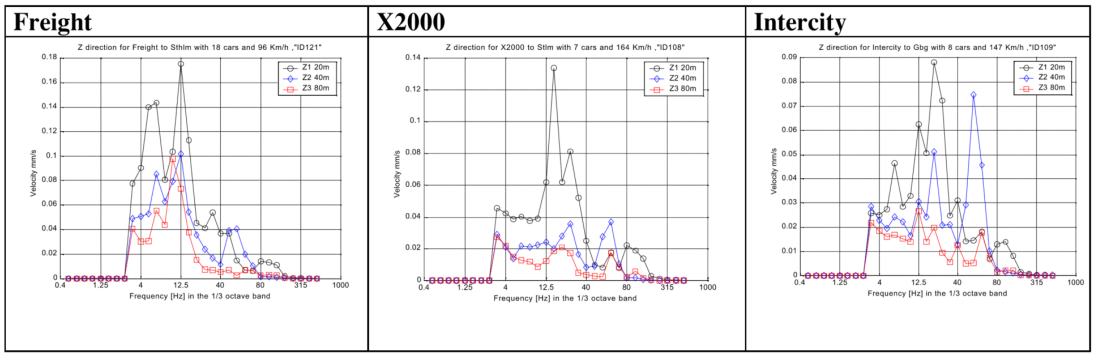

Figure 1: Frequency spectra at different measurement points [28]

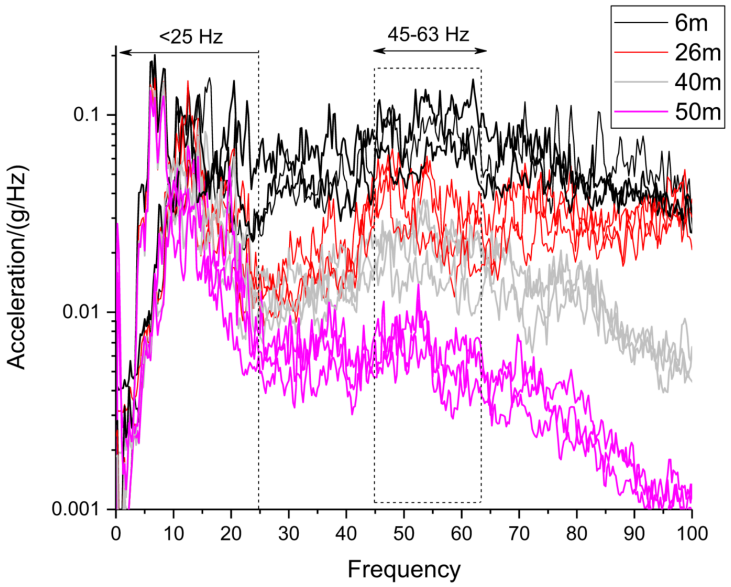

Figure 2: Frequency spectra for freight trains at different measurement points [29]

Vehicle Speed	40 kph	80 kph	160 kph
Moving load (axle spacing approx. 1.8 m)	3 Hz	5 Hz	11 Hz
Track unevenness	≥ 1 Hz ≤ 100 Hz	≥ 2 Hz ≤ 200 Hz	≥ 4 Hz ≤ 400 Hz
Rail corrugation	Approx. 500 Hz	Approx. 1000 Hz	Approx. 2000 Hz
Wheel unevenness	≥ 4 Hz	≥ 8 Hz	≥ 15 Hz
Wheel polygonisation (here assuming a wavelength of 0.1 m)	Approx. 100 Hz	Approx. 200 Hz	Approx. 400 Hz
Inter bogie spacing (assuming approx. 8 m)	Approx. 1 Hz	Approx. 3 Hz	Approx. 5 Hz
Sleeper spacing (0.6 m)	Multitudes of 16 Hz	Multitudes of 32 Hz	Multitudes of 64 Hz

Figure 3: Different causes of vibrations coming from the railway track [31]

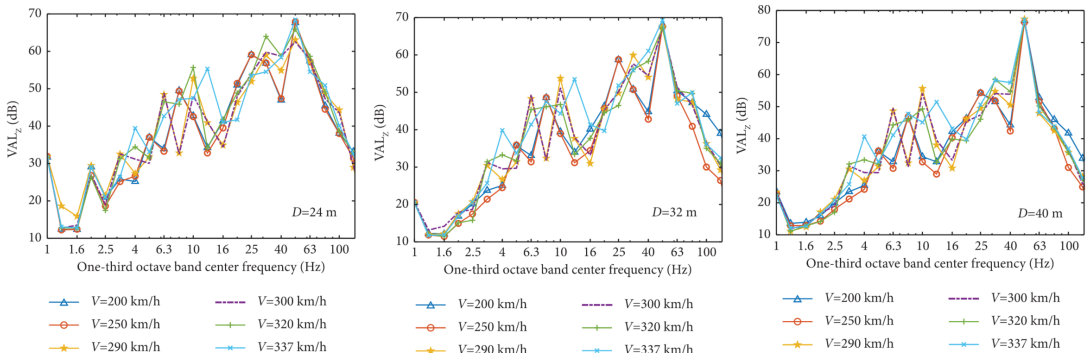

Figure 4: Frequency spectra of trains at different speeds, at different measurement locations [3]

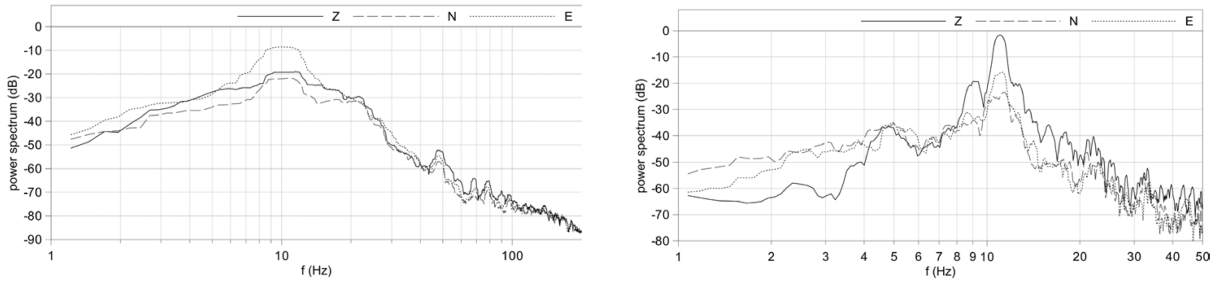

(a) First measurement location

(b) Second measurement location

Figure 5: Frequency spectra (road) coming from the research of Kaláb [17]

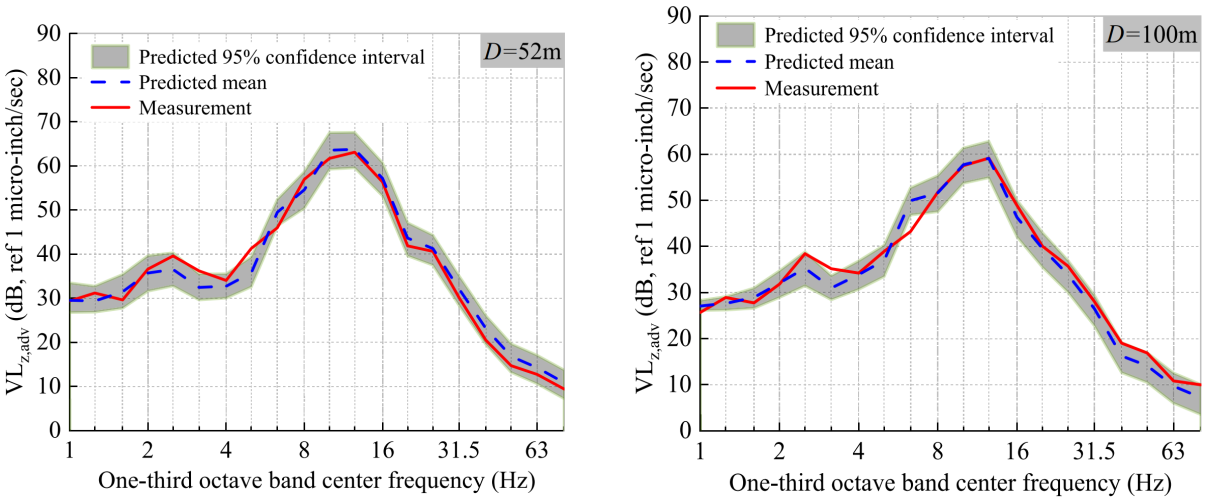

(a) Measurements at 52 meters distance

(b) Measurements at 100 meter distance

Figure 6: Frequency spectra (road) from measurements research Zhe Li [22]

Appendix B: parameters resonators rainbow trapping metawedge

Resonator	Eigenfreq (Hz)	M (kg)	k (N/m)	c (Ns/m)
1	14.00	50	386888	9
2	13.68	50	369632	9
3	13.37	50	352769	8
4	13.05	50	336299	8
5	12.74	100	640447	16
6	12.42	100	609083	16
7	12.11	100	578506	15
8	11.79	100	548717	15
9	11.47	100	519715	14
10	11.16	100	491501	14
11	10.84	100	464074	14
12	10.53	100	437434	13
13	10.21	150	617372	19
14	9.89	150	579775	19
15	9.58	150	543359	18
16	9.26	150	508123	17
17	8.95	200	632092	22
18	8.63	200	588261	22
19	8.32	200	546005	21
20	8.00	200	505324	20

Table 1: Parameters for resonators in Version 1

Resonator	Eigenfreq (Hz)	M (kg)	k (N/m)	c (Ns/m)
1	12.00	100	568489	15
2	11.68	100	538962	15
3	11.37	100	510223	14
4	11.05	100	482271	14
5	10.74	100	455106	13
6	10.42	100	428729	13
7	10.11	100	403139	13
8	9.79	100	378337	12
9	9.47	100	354322	12
10	9.16	100	331094	12
11	8.84	100	308653	11
12	8.53	100	287000	11
13	8.21	150	399202	15
14	7.89	150	369085	15
15	7.58	150	340149	14
16	7.26	150	312393	14
17	6.95	200	381092	17
18	6.63	200	347235	17
19	6.32	200	314952	16
20	6.00	200	284245	15

Table 2: Parameters for resonators in Version 2

Appendix C: parameters resonators wave conversion metawedge

Resonator	Eigenfreq (Hz)	M (kg)	k (N/m)	c (Ns/m)
1	15.00	100	888264	19
2	14.63	100	845166	18
3	14.26	100	803140	18
4	13.89	100	762185	17
5	13.53	100	722302	17
6	13.16	100	683491	17
7	12.79	100	645751	16
8	12.42	100	609083	16
9	12.05	100	573487	15
10	11.68	100	538962	15
11	11.32	100	505510	14
12	10.95	100	473129	14
13	10.58	150	662729	20
14	10.21	150	617372	19
15	9.84	150	573624	19
16	9.47	150	531482	18
17	9.11	200	654598	23
18	8.74	200	602697	22
19	8.37	200	552938	21
20	8.00	200	505324	20

Table 3: Parameters for resonators in Version 3

Resonator	Eigenfreq (Hz)	M (kg)	k (N/m)	c (Ns/m)
1	9.00	200.0	639550	23
2	9.21	200.0	669821	23
3	9.42	200.0	700791	24
4	9.63	200.0	732461	24
5	9.84	150.0	573624	19
6	10.05	150.0	598426	19
7	10.26	150.0	623754	19
8	10.47	150.0	649606	20
9	10.68	100.0	450655	13
10	10.89	100.0	468590	14
11	11.11	100.0	486875	14
12	11.32	100.0	505510	14
13	11.53	100.0	524494	14
14	11.74	100.0	543829	15
15	11.95	100.0	563513	15
16	12.16	100.0	583548	15
17	12.37	50.0	301966	8
18	12.58	50.0	312333	8
19	12.79	50.0	322876	8
20	13.00	50.0	333593	8

Table 4: Parameters for resonators in Version 1

Resonator	Eigenfreq (Hz)	M (kg)	k (N/m)	c (Ns/m)
1	8.00	200	505324	20
2	8.32	200	546005	21
3	8.63	200	588261	22
4	8.95	200	632092	22
5	9.26	150	508123	17
6	9.58	150	543359	18
7	9.89	150	579775	19
8	10.21	150	617372	19
9	10.53	100	437434	13
10	10.84	100	464074	14
11	11.16	100	491501	14
12	11.47	100	519715	14
13	11.79	100	548717	15
14	12.11	100	578506	15
15	12.42	100	609083	16
16	12.74	100	640447	16
17	13.05	50	336299	8
18	13.37	50	352769	8
19	13.68	50	369632	9
20	14.00	50	386888	9

Table 5: Parameters for resonators in Version 2